



UNIVERSITÀ DEGLI STUDI DI SALERNO



UNIVERSITÀ DEGLI STUDI DI SALERNO
Dipartimento di Farmacia

Dottorato di ricerca
in Scienze Farmaceutiche
Ciclo XII NS — Anno di discussione 2014

Coordinatore: Chiar.mo Prof. *Gianluca Sbardella*

***DESIGN AND SYNTHESIS OF PEPTIDES THAT
MODULATE APOPTOTIC PROCESS***

settore scientifico disciplinare di afferenza: CHIM/08

Dottorando

Dott. *Ermelinda Vernieri*

Tutore

Chiar.mo Prof. *Pietro Campiglia*

INDEX

Chapter 1: Programmed cell death pathways in cancer governed by the balanced action of PTKs and PTPs.....	1-26
Chapter 2: Synthesis, characterization and biological evaluation of PTPRJ (protein tyrosine phosphatase receptor like-j) agonists.....	27-79
Chapter 3: SAR studies and conformational analysis of a series of novel peptides G protein-coupled receptor kinase 2 (GRK2) inhibitors.....	80-127
Chapter 4: Characterization of a selective CaMKII peptide inhibitor.....	128-159
Appendix A: Automated Peptide Synthesizers.....	160-166
Appendix B: An Optimized Fmoc Synthesis of Human Defensin	167-179

CHAPTER 1

**Programmed cell death pathways in cancer governed by the
balanced action of PTKs and PTPs**

Abstract Oncogenic activation of tyrosine kinases is a common feature in cancer, and its regulation represents an excellent antitumoral target. Tyrosine phosphorylation is also controlled by protein-tyrosine phosphatases (PTPs). Recent evidence has shown that PTPs can function as tumour suppressors. An improved understanding of how these enzymes function and how they are regulated might aid the development of new anticancer agents.

It has been shown that cross-regulation of kinases/phosphatases and caspases allows for fine-tuning of the apoptotic threshold, as well as the opportunity to amplify apoptotic signals. The signaling pathways involved in the control of cell proliferation, adhesion and migration are governed by the balanced action of protein tyrosine kinases (PTKs) and protein-tyrosine phosphatases (PTPs).

Keywords caspases, pathway, kinases, phosphatases.

Abbreviations IAPs, Inhibitor of Apoptosis Proteins; TRADD, TNF receptor-associated death domain; FADD, Fas-associated death domain; DISC, death-inducing signaling complex; AIF, apoptosis inducing factor; Smac, second mitochondria-derived activator of caspase; TRAF2, TNF receptor associated factor 2; Erk, extracellular signal-regulated kinase; Cdk1, cyclin-dependent kinase; PTKs, protein tyrosine kinases; PTPs, protein-tyrosine phosphatases; PTPRJ, Protein Tyrosine Phosphatase receptor like-j; CaMKII, Ca^{2+} /Calmodulin-dependent protein kinase II; GRK2, G-protein-coupled receptor kinase 2; FasL, Fas ligand; LOH, loss of heterozygosity; S2ED, heparin sulfate proteoglycan Syndecan-2; TSP1, Thrombospondin- 1; GPCRs, G protein coupled receptors; $\beta_2\text{AR}$, β_2 -adrenergic receptor.

1. Introduction

Cancer can be viewed as the result of a succession of genetic changes during which a normal cell is transformed into a malignant one while evasion of cell death is one of the essential changes in a cell that cause this malignant transformation.^{1,2} As early as the 1970's, Kerr et al. had linked apoptosis to the elimination of potentially malignant cells, hyperplasia and tumour

progression.³ Hence, reduced apoptosis or its resistance plays a vital role in carcinogenesis.

Apoptosis is a form of programmed cell death that eliminates individual cells within an organism while preserving the overall structure of surrounding tissue.⁴

However, it was not until the mid-1990s that apoptosis was linked to the activation of the cysteine-dependent aspartate driven proteases (caspases),^{5,6} which cleave key intracellular substrates to promote cell death. Given the critical role that caspases play in dismantling the cell during apoptosis, their activation and subsequent activity are highly regulated. Failure of a cell to properly modulate caspase activity can cause aberrant or untimely apoptotic cell death, potentially leading to carcinogenesis, autoimmunity, neurodegeneration, and immunodeficiency.^{7,8}

There are many ways through which a malignant cell can acquire reduction in apoptosis or apoptosis resistance. Generally, the mechanisms of the evasion of apoptosis can be broadly divided into: 1) disrupted balance of pro-apoptotic and anti-apoptotic proteins (like Bcl-2 family, p53 and Inhibitor of Apoptosis Proteins (IAPs)); 2) reduced caspase function and 3) impaired death receptor signaling.

1.1 Caspases, a family of cysteine proteases

The caspases are a family of cysteine proteases that are constitutively present in most mammalian cells, and they reside in the cytosol as single chain proenzymes.

The primary structure of a caspase is an amino-terminal prodomain and a carboxy-terminal protease domain, which contains the key catalytic cysteine residue. Caspases are categorized as initiator or effector caspases, based on their position in apoptotic signaling cascades. The initiator caspases (caspase-2, -8, -9, and -10) act apically in cell death pathways and all share long, structurally similar prodomains.^{9,10} This group of enzymes is activated through “induced proximity” when adaptor proteins interact with the prodomains and promote caspase dimerization.^{11, 12} In contrast, the effector caspases

(caspase-3, -6, and -7) have shorter prodomains and exist in the cell as preformed, but inactive, homodimers. Following cleavage mediated by an initiator caspase, effector caspases act directly on specific cellular substrates to dismantle the cell. Although many individual caspase substrates have been implicated in specific aspects of cellular destruction (e.g., lamin cleavage is required for the efficient packaging of nuclei into small membrane-bound vesicles), recent proteomic approaches have greatly expanded the known repertoire of proteolytic products generated during apoptosis.¹³ Further work will be needed to confirm these findings and to determine how (or if) all of these substrates participate in the apoptotic process,¹⁴ especially as new details emerge on the relationship between posttranslational modifications, like phosphorylation, and caspase cleavage.¹⁵

1.2 Apoptotic pathways

There are three pathways by which caspases can be activated. The two commonly described initiation pathways are the intrinsic (or mitochondrial) and extrinsic (or death receptor) pathways of apoptosis (Figure 1). Both pathways eventually lead to a common pathway or the execution phase of apoptosis. A third less well-known initiation pathway is the intrinsic endoplasmic reticulum pathway.¹⁶

1.2.1 The extrinsic death receptor pathway

The extrinsic death receptor pathway, as its name implies, begins when death ligands bind to a death receptor. Although several death receptors have been described, the best known death receptors is the type 1 TNF receptor (TNFR1) and a related protein called Fas (CD95) and their ligands are called TNF and Fas ligand (FasL) respectively.¹⁷ These death receptors have an intracellular death domain that recruits adapter proteins such as TNF receptor-associated death domain (TRADD) and Fas-associated death domain (FADD), as well as cysteine proteases like caspase 8.¹⁸ Binding of the death ligand to the death receptor results in the formation of a binding site for an adaptor protein and the whole ligand-receptor-adaptor protein complex is known as the death-inducing signaling complex (DISC). DISC then initiates the assembly and activation of pro-caspase 8. The activated form of the enzyme, caspase 8

is an initiator caspase, which initiates apoptosis by cleaving other downstream or executioner caspases.

1.2.2 The intrinsic mitochondrial pathway

As its name implies, the intrinsic pathway is initiated within the cell. Internal stimuli such as irreparable genetic damage, hypoxia, extremely high concentrations of cytosolic Ca^{2+} and severe oxidative stress are some triggers of the initiation of the intrinsic mitochondrial pathway. Regardless of the stimuli, this pathway is the result of increased mitochondrial permeability and the release of pro-apoptotic molecules such as cytochrome-c into the cytoplasm.¹⁹ The intrinsic pathway is closely regulated by a group of proteins belonging to the Bcl-2 family, named after the BCL2 gene originally observed at the chromosomal breakpoint of the translocation of chromosome 18 to 14 in follicular non-Hodgkin lymphoma. There are two main groups of the Bcl-2 proteins, namely the pro-apoptotic proteins (e.g. Bax, Bak, Bad, Bcl-Xs, Bid, Bik, Bim and Hrk) and the anti-apoptotic proteins (e.g. Bcl-2, Bcl-XL, Bcl-W, Bfl-1 and Mcl-1).²⁰ While the anti-apoptotic proteins regulate apoptosis by blocking the mitochondrial release of cytochrome-c, the pro-apoptotic proteins act by promoting such release. It is not the absolute quantity but rather the balance between the pro- and anti-apoptotic proteins that determines whether apoptosis would be initiated. Other apoptotic factors that are released from the mitochondrial intermembrane space into the cytoplasm include apoptosis inducing factor (AIF), second mitochondria-derived activator of caspase (Smac), direct IAP Binding protein with low pI (DIABLO) and Omi/high temperature requirement protein A (HtrA2). Cytoplasmic release of cytochrome c activates caspase 3 via the formation of a complex known as apoptosome which is made up of cytochrome c, Apaf-1 and caspase 9.²¹ On the other hand, Smac/DIABLO or Omi/HtrA2 promotes caspase activation by binding to inhibitor of apoptosis proteins (IAPs) which subsequently leads to disruption in the interaction of IAPs with caspase-3 or -9.²²

1.2.3 The common pathway

The execution phase of apoptosis involves the activation of a series of caspases. The upstream caspase for the intrinsic pathway is caspase 9 while that of the extrinsic pathway is caspase 8. The intrinsic and extrinsic pathways converge to caspase 3. Caspase 3 then cleaves the inhibitor of the caspase-activated deoxyribonuclease, which is responsible for nuclear apoptosis. In addition, downstream caspases induce cleavage of protein kinases, cytoskeletal proteins, DNA repair proteins and inhibitory subunits of endonucleases family. They also have an effect on the cytoskeleton, cell cycle and signaling pathways, which together contribute to the typical morphological changes in apoptosis.²³

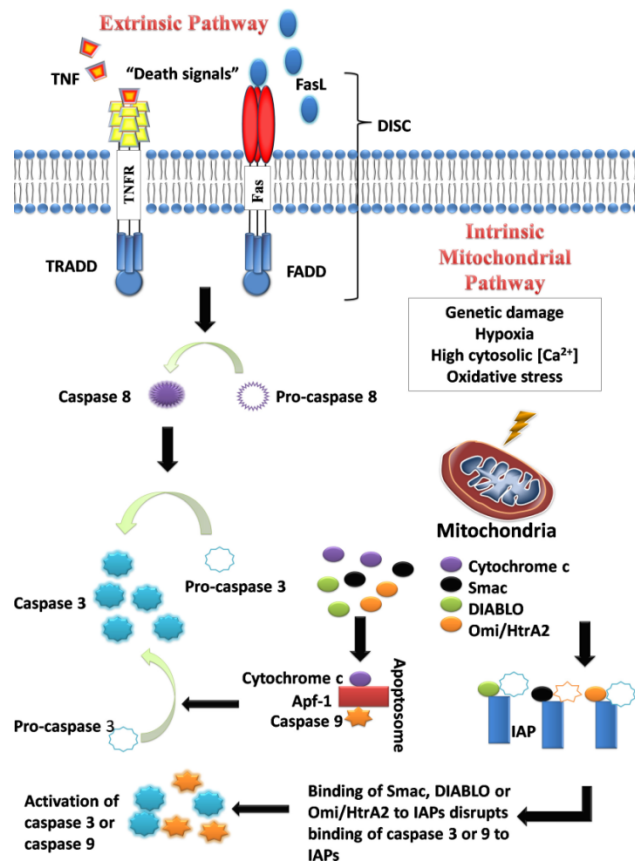


Figure 1. The intrinsic and extrinsic pathways of apoptosis.

1.2.4 The intrinsic endoplasmic reticulum pathway

This intrinsic endoplasmic reticulum (ER) pathway is a third pathway and is less well known. It is believed to be caspase 12-dependent and mitochondria-independent.²⁴ When the ER is injured by cellular stresses like hypoxia, free radicals or glucose starvation, there is unfolding of proteins and reduced protein synthesis in the cell, and an adaptor protein known as TNF receptor associated factor 2 (TRAF2) dissociates from procaspase-12, resulting in the activation of the latter.

1.3 The bidirectional communication between caspases and kinases/phosphatases

Although the cleavage of many caspase substrates is required for the structural packaging of cellular contents during apoptosis, a subset of caspase substrates are signaling molecules whose cleavage alters their signaling properties to affect the internal environment of the dying cell. In turn, signaling molecules can modulate caspase function to positively or negatively alter the trajectory of the cell death program. Given the millions of reversible phosphorylation events necessary to maintain cellular homeostasis and to allow cells to adapt nimbly to changing internal and external environments, the bidirectional communication between caspases and the kinases/phosphatases that control the cellular phosphoproteome is of particular interest.²⁵

With respect to phosphorylation, both the caspase activation process and intrinsic enzymatic activity are under the control of modifying kinases and phosphatases. This permits cellular flexibility in setting a threshold for the induction of apoptosis in response to alterations in the cellular environment (for example, after growth factor stimulation or changes in cellular metabolism) through changes in the activity of pro- or antiapoptotic kinases and phosphatases. Phosphorylation may also control caspase activity indirectly by controlling other apoptotic modulators (including caspase binding partners). If we consider that the control of caspases can be exerted via their direct phosphorylation, focused on caspase 9 we find that of caspase 9 may result in the failure of apoptotic induction. In particular the phosphorylation of caspase 9 by both Erk (extracellular signal-regulated kinase) and Cdk1

(cyclin-dependent kinase 1) suppresses caspase 9 activation.²⁶ Given that the Erk pathway is upregulated in a variety of cancers, this inhibitory phosphorylation of caspase 9 may contribute to apoptotic (and therefore chemotherapeutic) resistance. It's note that phosphorylation and inhibition of caspase 9 by ERK promotes cell survival during development and tissue homeostasis suggesting that phosphorylation of Thr 125 on caspase 9 may be an important mechanism through which growth factor and survival signals that activate the ERK-MAPK pathway can inhibit apoptosis.

Therefore the apoptosis pathway could be regulated by a phosphorylation and a dephosphorylation event of apoptotic effectors.

Cross-regulation of kinases/phosphatases and caspases allows for fine tuning of the apoptotic threshold, as well as the opportunity to amplify apoptotic signals.

In the apoptotic process, the regulatory role of protein kinases is clearly established instead of the regulatory role of protein phosphatases is not clear. For this reason we are interested in the regulation of signaling responses of phosphatases.

However, it has recently become apparent that protein phosphatases can no longer be viewed as passive housekeeping enzymes, but they partner with kinases in the regulation of signaling responses. The distinct but complementary function of these enzymes is emphasized by recent studies, in which kinases have been implicated in controlling the amplitude of signaling responses, whereas phosphatases are thought to have an important role in controlling the rate and duration of the response.^{27,28}

In base to these considerations, my doctoral thesis aimed to identify chemical entities able to regulate the apoptotic process through the modulation of phosphatase and kinase activities. Therefore, I studied 1) PTPRJ, a protein tyrosine phosphatase receptor like j; 2) GRK2, G protein-coupled receptor kinase 2; and 3) CaMKII, Ca²⁺/Calmodulin-dependent protein kinase II.

1.4 Protein Phosphatases

The first PTP was purified in 1988, approximately 10 years after the discovery of tyrosine kinases. It is now known that PTPs constitute a large, structurally diverse family of tightly regulated, highly specific enzymes with important regulatory roles.^{29,30}

It is also clear that PTPs have both inhibitory and stimulatory effects on cancer associated signaling processes, and that deregulation of PTP function is associated with tumorigenesis in different types of human cancer.

Among all protein tyrosine phosphatases, PTPRJ is of particular interest for its role in human and experimental tumorigenesis.³¹ In fact, after its discovery,³² a consistent body of literature supports its tumor suppressor activity in several models. PTPRJ (also named DEP-1, HPTP η , or CD148) is down-regulated in mammary cancer cells, and its restoration blocks their proliferation; a similar behavior was described in both human and experimental models of thyroid tumorigenesis, where PTPRJ overexpression was able to interfere with cancer cells malignant phenotype both in vitro and in vivo.³³ Moreover, down-regulation of PTPRJ expression operated by miR-328 increases cell proliferation in HeLa and SKBr3 cell lines.³⁴

PTPRJ has been successfully used as a therapeutic gene in cancer gene therapy preclinical models of thyroid and pancreatic cancer.³⁵ The role of PTPRJ in human tumorigenesis was also highlighted by Ruivenkamp et al.,³⁶ who demonstrated that PTPRJ was affected by loss of heterozygosity (LOH) in colon, lung, and mammary tumors; a significant percentage of LOH was also described in human thyroid tumors.³⁷ Moreover, a polymorphism in the mouse *PtpRJ* locus (*Scc1*) is associated with colon cancer development, although *PtpRJ* genetic ablation did not induce spontaneous tumors in mice.^{38,39}

The biochemical pathways negatively regulated by PTPRJ have been partly elucidated. Various reports indicate an inhibitory effect of PTPRJ on several players of the mitogenic signals in both normal and cancer cells. In fact, CD148 interacts with and dephosphorylates numerous receptor tyrosine kinases (RTKs) including PDGFR, HGFR,^{40,41} RET, and EGFR^{42,43} whose aberration in cancer cells is responsible for self sufficiency cell growth.⁴⁴ PTPRJ is also a negative modulator of the signaling mediated by cytosolic transducers, including phospholipase C γ 1 (PLC γ 1), LAT, PKB/Akt,⁴⁵ and PI3K.^{46,47} Noteworthy, the role of PTPRJ on the inhibition of RTKs was also extended to VEGFR-2,^{48,49} whose activity is required for the formation of new vessels in tumor progression. Lately, PTPRJ ligands have been discovered, they include the heparin sulfate proteoglycan Syndecan-2 (S2ED)⁵⁰ and Thrombospondin-1 (TSP1).⁵¹ CD148 acts as key intermediary in S2ED mediated cell adhesion, by modulating downstream β 1 integrin mediated adhesion and cytoskeletal organization, whereas TSP1, a glycoprotein that

mediates cell-cell and cell-matrix interactions, increases PTPRJ activity, influencing the dephosphorylation of its substrates. These findings make PTPRJ an interesting candidate for the generation of novel therapeutic strategies.

1.4.1 PTPRJ regulates cell growth and cell cycle

The tumor-suppressive role of PTPRJ was clearly displayed in experiments where highly malignant thyroid cells, after transduction by a retrovirus carrying CD148, appeared to acquire a normal phenotype and showed increased adhesion, restoration of differentiation, reduced proliferation and decreased tumorigenicity. The same report established that PTPRJ induced a G1 growth arrest by suppressing the degradation of the cyclin-dependent kinase inhibitor p27kip1 protein.

Therefore, synthesizing PTPRJ agonists could be one of a possible approach in cancer therapy.

The receptor-like PTP phosphatase DEP-1 opposes various oncogenic receptor tyrosine kinases. Recently, DEP-1 agonists were isolated from a random peptide phage-display library.⁵²

Intriguingly, these agonists circularize in vitro via an intramolecular disulfide bridge and form stable dimers that induce the dimerization-mediated activation of DEP-1 (Figure 2). Consistent with the activation of DEP-1 as a tumor suppressor, these peptides reduced proliferation and triggered apoptosis of cancer cells.

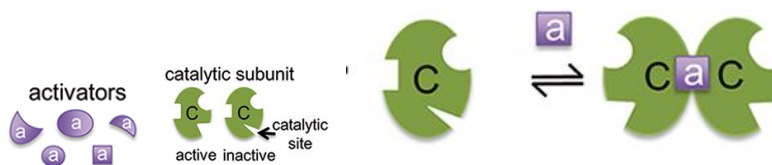


Figure 2. Small-molecule activators of protein phosphatases.

Starting from these observations during my PhD I focused the attention on two peptides, recently identified by means of a phage display library, able to bind and activate PTPRJ ([Cys-His-His-Asn-Leu-Thr-His-Ala-Cys]-OH and [Cys-Leu-His-His-Tyr-His-Gly-Ser-Cys]-OH) designing and synthesizing new PTPRJ agonists with the aim to identify a more stable and active peptide

sequence.⁵³ These informations could help the design of peptidomimetics with PTPRJ agonistic properties.

1.5 Protein kinases as drug targets

Nearly every cellular process is controlled by phosphorylation of key regulatory proteins on specific serine (Ser), threonine (Thr), or tyrosine (Tyr) residues. The covalent attachment of a bulky and negatively charged phosphate group by a kinase usually induces a conformational change that affects protein function. Mammalian genomes harbor more than 500 genes that encode protein kinases. Almost all of these belong to the same protein kinase superfamily and have a highly similar catalytic core and mechanism, implying that they originate from a common ancestor. In recent years protein kinases have become one of the most popular drug targets.⁵⁴

There are more than 518 human protein kinases recognized through their conserved sequence motifs. These constitute the third most populous protein family and represent <1.7% of the human genome. Of the total, 478 protein kinases are typical kinases, and 40 are atypical. The typical kinases are divided into those that phosphorylate serine or threonine residues (388 kinases) and those that phosphorylate tyrosine residues (90 kinases). These proteins have biochemical kinase activity but lack sequence similarity to the conventional eukaryotic kinases.

A distinguishing feature of the protein kinase family is the different structures that they adopt between the active and inactive states. This family characteristic was first appreciated following the determination of the first protein kinase structures of protein kinase A (PKA) [Protein Data Bank (PDB) code 1ATP] in the active conformation and cyclin-dependent protein kinase 2 (Cdk2) (PDB code 1HCK) in an inactive conformation.

Deregulation of protein kinase activity through mutation to constitutively active forms, loss of negative regulators, and chromosomal rearrangements that lead to the formation of active fusion proteins are associated with a number of disorders. Protein kinases have become major targets for therapy, and protein kinase structures have had a significant impact on the development of selective and specific targeted therapy. Phosphorylation of protein substrates can have profound effects. Phosphorylation can result in enzyme activation, enzyme inhibition, the creation of recognition sites for recruitment

of other proteins, and transitions in protein state from order to disorder or disorder to order.

1.5.1 Protein kinases in cancer

During my PhD I studied two different protein kinases: Ca²⁺/Calmodulin-dependent protein kinase II and GRK2, G-protein coupled receptor kinase 2.

Aberrant protein kinase activity is linked to a range of diseases, most notably cancer.⁵⁵ Recent large scale sequencing projects revealed that kinases are indeed the most frequently mutated proteins in tumors.^{56,57}

Why is that? Cancer is the malignant growth of cells and tissues, a development that requires independence from organism control in a spectrum of processes; as for example the proliferation, survival and migration of cells. All these functions are orchestrated by protein kinase signaling networks, making kinases a likely starting point for dysregulation. This can be achieved by alteration of expression levels, but also by introducing activity modulating mutations in the kinase domain. Hence it appears logical to fight cancer with kinase activity modulating drugs.

The general structure of CaMKs includes an N-terminal kinase domain, an autoregulatory domain, an overlapping CaM-binding domain and, in phosphorylase kinase and CaMKII, a C-terminal association domain that is essential for multimerization and targeting.⁵⁸ The best characterized CaM Kinase is CaMKII.

1.5.1.1 CaMKII, Ca²⁺/Calmodulin-dependent protein kinase II

CaMKII is a serine/threonine protein kinase which plays an essential role in central nervous system function.^{59,60} There are many types of CaMKII molecules and each tissue expresses at least one type of CaMKII.^{61,62} Therefore, CaMKII plays a variety of functions in different cell types.⁶³

One of the functions CaMKII plays is the control of apoptosis.^{64,65}

However, the mechanism by which CaMKII controls apoptosis remains to be determined. p27 was first identified as a cell cycle inhibitor and it was later revealed that p27 also functions as a positive cell cycle controller. Phosphorylation of serine 10 of p27 induces the translocation of p27 from

nucleus to cytoplasm.^{66, 67} Cytoplasmic p27 may control apoptosis.⁶⁸ In particular CaMKII can directly bind to MEK1, activate the kinase activity of MEK/ERK, and enhance the phosphorylation of p27 protein, therefore promoting the S-G2/M transition of the cell cycle progression and then the tumor cell growth (Figure 3).

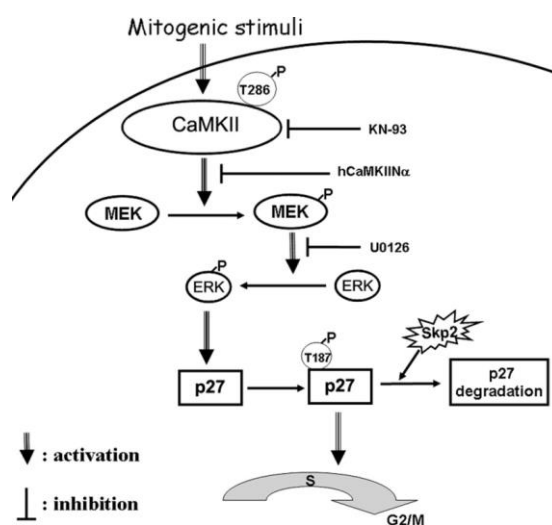


Figure 3. Models depicting the roles of MEK/ERK signaling in CaMKII induced promotion of cell cycle progression.

CaMKII also regulates apoptosis by inactivating Bad. One phosphorylation site on Bad, Ser170, is a potential CaMKII target, raising the possibility that CaMKII phosphorylates Bad directly.

The mechanism by which CaMKII inactivates Bad involves multiple signaling pathways, and differs among cell types. CaMKII also suppresses nuclear translocation of histone deacetylase, thereby promoting neuronal survival.⁶⁹ Indeed, CaMKII has been shown to activate the pro-survival transcriptional regulator NF-κB in T lymphocytes and in neurons.⁷⁰ Because dominant-negative CREB constructs do not reduce the pro-survival effect of CaMKII, it is unlikely that CREB is the nuclear target of CaMKII.

Starting from these observations synthesizing CaMKII antagonists could be one of a possible approach in cancer therapy.⁷¹

1.5.1.2 GRK2, G-protein coupled receptor kinase 2

Different functions of G-protein coupled receptor kinase 2. Cellular proliferation is regulated by specific membrane receptors, including receptor-tyrosine kinases and G protein coupled receptors (GPCRs), among others. GPCRs initiate a variety of intracellular signaling cascades that can modulate cell division involving both G protein-dependent and independent mechanisms.⁷² Regarding the latter, G protein-coupled receptor kinases (GRKs) and β -arrestins, first identified as key molecules involved in the agonist-induced desensitization of multiple GPCRs, are emerging as alternative signal transducers with a direct or potential impact on cell growth and proliferation.

Whereas β -arrestins can bring different signaling molecules into the receptor complex,⁷³ a growing number of non-GPCR substrates and interacting proteins are being identified for GRKs, particularly for the ubiquitous GRK2 isoform.

These include PDGF and EGF receptors, and a variety of proteins involved in pathways controlling cell migration and proliferation, such as p110-PI3K, p38Mapk, GIT, MEK, or AKT.⁷⁴

Consistently, GRK2 expression has been reported to have distinct impacts on cell proliferation, depending on both the cell type and the mitogenic stimuli analyzed.

Such canonical role of GRK2 are to inhibit TGF mediated cell growth arrest and apoptosis in human hepatocarcinoma cells; to attenuate thyroid stimulating hormone- and PDGF-dependent proliferation of thyroid cancer cell lines and smooth muscle cells, respectively, whereas it increases mitogenic signaling pathways in response to EGF in osteoblasts or upon activation of the Smoothed receptor in fibroblasts. Increased GRK2 levels also potentiate migration of epithelial cells toward fibronectin and sphingosine-1-phosphate.⁷⁵

Besides these canonical role, GRK2 can also initiate alternative signaling pathways and participate in cellular processes related to cell cycle progression, survival, or cell migration by phosphorylating and interacting with non-GPCR partners.^{76,77} Interestingly, the GRK2 “interactome” in different cell types includes several actors in vascular homeostasis and remodeling.^{78,79}

Besides regulating chemokine GPCRs, GRK2 phosphorylates PDGF receptors⁸⁰ and also modulates TGF- β signaling in epithelial cells⁸¹ or cardiac

fibroblasts.⁸² GRK2 inhibits PDGF-dependent chemotactic signaling in VSMCs⁸³ and modulates both vasoconstrictory and vasodilatory responses of VSMCs,⁸⁴ whereas increased GRK2 attenuates NO production by sinusoidal ECs in the context of liver injury.⁸⁵ However, the role of GRK2 in vessel formation and stability in other pathophysiological settings has not been addressed. Its dosage is important in determining how ECs (Endothelial Cells) integrate different relevant physiological stimuli and to balance TGF- β signaling to downstream pathways. Furthermore, ablation of GRK2 compromises postnatal angiogenesis and vascular remodeling in the retina and vasculogenesis during embryonic development as a result of defective vessel maturation, whereas GRK2 down regulation in ECs reduces pericyte coverage of tumoral vessels and potentiates tumor progression.

Rivas et al.,⁷⁸ identified that GRK2 is involved in counterbalancing the action of different angiogenic growth factors responsible for the activation of ECs (Endothelial cells).

GRK2 down regulation in ECs alters the endothelial barrier function and causes defective tube formation on Matrigel, a process that depends on profuse cellular polarization and morphogenetic rearrangements. Therefore, manipulation of tumor-associated angiogenesis represents a promising strategy to limit cancer progression and GRK2 down modulation could represent a novel marker for pathological vasculature. In particular GRK2 down regulation would be a relevant event in the angiogenic switch triggered by tumor cells by favoring a permissive microenvironment for tumor progression.

Notably, GRK2 levels are also altered in different malignant mammary cell lines⁸⁶ and enhanced GRK2 levels increase epithelial cell motility,^{87, 88} stressing that cell type-specific modulation of this kinase may participate in cancer development. As tumor progression is the result of the interplay between malignant cells themselves and their surrounding microenvironment, recent results suggest that opposite changes in GRK2 expression may occur in transformed epithelial cells and in the tumor endothelium to synergistically promote tumor cell invasiveness and intravasation.

Degradation of G-protein-coupled receptor kinase 2. Such functional complexity predicts that alterations in GRK2 levels and/or activity may have important effects on cell signaling. Interestingly, several pathological conditions such as congestive heart failure, hypertension⁸⁹ and rheumatoid arthritis (RA), among others, display altered GRK2 expression and

function.^{90,91} Salcedo et al.,⁸⁶ described that GRK2 is rapidly degraded by the proteasome pathway, and that β_2 -adrenergic receptor (β_2 AR) activation enhances GRK2 ubiquitination and turnover. It has been shown that agonist-dependent binding of β -arrestin to GPCRs supports GRK2 degradation by allowing the recruitment of c-Src and the phosphorylation of GRK2 on critical tyrosine residues.⁹² MAPK-mediated GRK2 phosphorylation also triggers GRK2 degradation in a process that is again dependent on β -arrestin function.⁹³

Proteasome degradation requires the orchestrated activities of the ubiquitin-activating enzyme (E1), ubiquitin conjugating enzymes (E2) and ubiquitin ligases (E3).⁹⁴ The specificity of target protein selection is determined by ubiquitin ligases, which interact with their substrates either directly or by means of adaptor molecules. Interestingly, β -arrestins are able to interact with Mdm2, a RING domain-containing E3-ubiquitin ligase involved in the control of tumor suppressor p53 activity.⁹⁵ β -Arrestin-mediated recruitment of Mdm2 to several GPCR complexes leads to different β -arrestin ubiquitination patterns,⁹⁶ which controls the characteristics of MAPK activation and receptor internalization.^{97,98} In this report, Alicia Salcedo et al.,⁸⁶ identify Mdm2 as an E3-ubiquitin ligase for GRK2 that is critically involved in kinase ubiquitination and degradation. Moreover, they put forward a new Mdm2-mediated pathway for the modulation of GRK2 cellular levels by IGF-1. The Mdm2 oncoprotein is an E3-ubiquitin ligase best known by its role in controlling p53 degradation and transcriptional activity.^{99,100} Growing evidence indicates that other proteins interact with Mdm2^{101, 102} and can be regulated by this ligase.^{103,104} It has been identified GRK2 as a new Mdm2 target.

Several lines of evidence support the notion that Mdm2 serves as an E3 ligase for GRK2 ubiquitination and is critical for modulating its degradation and cellular levels.

Modulation of Mdm2 by the PI3K/Akt pathway upon IGF1-R stimulation alters GRK2 degradation and augments kinase cellular levels, putting forward a new mechanism for controlling GRK2 expression. Mdm2 has been shown to control ubiquitination and stability of different molecules in response to membrane receptor occupancy.^{105, 106}

β_2 AR stimulation leads to the recruitment of Mdm2 to the receptor complex in a β -arrestin-dependent manner. Both β -arrestin1 and β -arrestin2 are able to interact with Mdm2 and therefore to bring this ligase to the vicinity

of activated receptors. It has been reported that β -arrestin1 also plays a role in GRK2 degradation by facilitating the β -agonist-triggered GRK2/Mdm2 association. β -arrestin might deliver Mdm2 to the receptor complex in an active form that is suitable to interact with and promote GRK2 ubiquitination, as has been reported for other targets. Mdm2 shuttles back and forth between the nucleus and the cytoplasm as a result of its interaction with different proteins. In this regard, it has been reported that β -arrestin2 promotes Mdm2 cytoplasmic relocation, whereas β -arrestin1 might cooperate with β -arrestin2 in the maintenance of an accessible cytosolic pool of Mdm2 for degradation of targets such as GRK2 in response to specific stimuli.

GRK2 and cancer. Interestingly, in addition to its reported alteration in cardiovascular and inflammatory pathologies emerging data indicate changes in GRK2 expression in certain tumors.¹⁰⁷ The fact that general but not cardiac-specific GRK2 knockout mice are embryonic lethal¹⁰⁸ further supports the notion that this protein could play a central, general role in key cellular processes as proliferation or migration. However, the potential involvement of this kinase in the cell cycle has not been addressed. Given that the control of the turnover of key kinases throughout the cell cycle represents a major regulatory mechanism in cell proliferation,¹⁰⁹ recently Penela et al. reported that phosphorylation of GRK2 by cyclin-dependent kinase 2 (CDK2) and subsequent interaction with the Pin1 prolyl-isomerase promotes its transient down-regulation in the G2 phase, and that this event is critical for adequate cell cycle progression and control.⁹²

In particular GRK2 protein levels progressively decay during G2 as a result of a degradation process triggered by the CDK2-dependent phosphorylation of GRK2 at residue S670. Inhibition of endogenous GRK2 phosphorylation by CDK2 or expression of a mutant unable to be phosphorylated at this residue (GRK2-S670A) completely prevents GRK2 down-regulation and delays cell cycle progression. Importantly, such “default” down-regulation is blocked upon activation of the G2 checkpoint, and the resultant accumulation of GRK2 protein levels inversely correlates with the extent of activation of the p53-dependent apoptotic responses.

In the last year, identification of GRK2 modulators/inhibitors is a very active fields of research.^{110,111}

Different small molecules inhibitors of GRK2 activity are currently available,^{112, 113} even if they are characterized by low sensitivity and specificity.^{114,115} Strategies to selectively inhibit the GRK2 activity have been attempted¹¹⁶ using shorter peptides^{117,118} or RNA aptamers.¹¹⁹ In particular, Anis et al. demonstrated that myristyl or lauryl glycine derivatives of short peptides derived from HJ loop of GRK2 are potent inhibitor of the kinase and possess hypoglycemic effect in animal models of Type 2 diabetes.

Starting from these peptides during my PhD I focused the attention on synthesis of new compounds with the aim to identify more potent and selective GRK2 antagonists.

¹ Hanahan, D.; Weinberg, RA. The hallmarks of cancer. *Cell* **2000**, 100, 57-70.

² Wong, R. SJ. Apoptosis in cancer: from pathogenesis to treatment. *Journal of Experimental & Clinical Cancer Research* **2011**, 30, 87.

³ Kerr, JFR.; Wyllie, AH.; Currie AR. Apoptosis: a basic biological phenomenon with wide-ranging implications in tissue kinetics. *Br J Cancer* **1972**, 26, 239-257.

⁴ Parrish, AB.; Freel, CD.; Kornbluth, S. Cellular Mechanisms Controlling Caspase Activation and Function. *Cold Spring Harb Perspect Biol* **2013**, 5.

⁵ Cerretti, DP.; Kozlosky, CJ.; Mosley, B.; Nelson, N.; Van Ness, K.; Greenstreet, TA.; March, CJ.; Kronheim, SR.; Druck, T.; Cannizzaro, LA. Molecular cloning of the interleukin-1 β converting enzyme. *Science* **1992**, 256, 97-100.

⁶ Thornberry, NA.; Lazebnik, Y. Caspases: Enemies within. *Science* **1998**, 281, 1312-1316.

⁷ Yuan, J.; Yankner, BA. Apoptosis in the nervous system. *Nature* **2000**, 407, 802-809.

⁸ Li, J.; Yuan, J. Caspases in apoptosis and beyond. *Oncogene* **2008**, 27, 6194-6206.

⁹ Boatright, KM.; Renatus, M.; Scott, FL.; Sperandio, S.; Shin, H.; Pedersen, IM.; Ricci, JE.; Edris, WA.; Sutherlin, DP.; Green, DR.; Salvesen, GS. A unified model for apical caspase activation. *Mol Cell* **2003**, 11, 529-541.

¹⁰ Baliga, BC.; Read, SH.; Kumar, S. The biochemical mechanism of caspase-2 activation. *Cell Death Differ* **2004**, 11, 1234-1241.

¹¹ Pop, C.; Timmer, J.; Sperandio, S.; Salvesen, GS. The apoptosome activates caspase-9 by dimerization. *Mol Cell* **2006**, 22, 269-275.

¹² Riedl, SJ.; Salvesen, GS. The apoptosome: Signaling platform of cell death. *Nat Rev Mol Cell Biol* **2007**, 8, 405-413.

- ¹³ Mahrus, S.; Trinidad, JC.; Barkan, DT.; Sali, A.; Burlingame, AL.; Wells, JA. Global sequencing of proteolytic cleavage sites in apoptosis by specific labeling of protein N termini. *Cell* **2008**, 134, 866-876.
- ¹⁴ Poreba, M.; Strozyk, A.; Salvesen, GS.; Drag, M. Caspase substrates and inhibitors. *Cold Spring Harb Perspect Biol* **2013**, 5, a008680.
- ¹⁵ Dix, MM.; Simon, GM.; Wang, C.; Okerberg, E.; Patricelli, MP.; Cravatt, BF. Functional interplay between caspase cleavage and phosphorylation sculpts the apoptotic proteome. *Cell* **2012**, 150, 426-440.
- ¹⁶ O' Brien, MA.; Kirby, R. Apoptosis: a review of pro-apoptotic and antiapoptotic pathways and dysregulation in disease. *J Vet Emerg Crit Care* **2008**, 18, 572-585.
- ¹⁷ Hengartner, MO. Apoptosis: corralling the corpses. *Cell* **2000**, 104, 325-328.
- ¹⁸ Schneider P.; Tschopp, J. Apoptosis induced by death receptors. *Pharm Acta Helv* **2000**, 74, 281-286.
- ¹⁹ Danial, NN.; Korsmeyer, SJ. Cell death: critical control points. *Cell* **2004**, 116, 205-219.
- ²⁰ Reed, JC. Bcl-2 family proteins: regulators of apoptosis and chemoresistance in haematologic malignancies. *Semin Haematol* **1997**, 34, 9-19.
- ²¹ Kroemer, G.; Galluzzi, L.; Brenner, C. Mitochondrial membrane permeabilisation in cell death. *Physiol Rev* **2007**, 87, 99-163.
- ²² LaCasse, EC.; Mahoney, DJ.; Cheung, HH.; Plenchette, S.; Baird, S.; Korneluk, RG. IAP-targeted therapies for cancer. *Oncogene* **2008**, 27, 6252-6275.
- ²³ Ghobrial, IM.; Witzig, TE.; Adjei, AA. Targeting apoptosis pathways in cancer therapy. *CA Cancer J Clin* **2005**, 55, 178-194.
- ²⁴ Szegezdi, E.; Fitzgerald, U.; Samali, A. Caspase-12 and ER stress mediated apoptosis: the story so far. *Ann NY Acad Sci* **2003**, 1010, 186-194.
- ²⁵ Kurokawa, M.; Kornbluth, S. Caspases and Kinases in a Death Grip. *Cell* **2009**, 138.
- ²⁶ Allan, LA.; Clarke, PR. Phosphorylation of caspase-9 by CDK1/cyclin B1 protects mitotic cells against apoptosis. *Mol Cell* **2007**, 26, 301-310.
- ²⁷ Heinrich, R.; Neel, BG.; Rapoport, TA. Mathematical models of protein kinase signal transduction. *Mol Cell* **2002**, 9, 957-970.
- ²⁸ Hornberg, JJ.; Bruggeman, FJ.; Binder, B.; Geest, CR.; de Vaate, AJ.; Lankelma, J.; Heinrich, R.; Westerhoff, HV. Principles behind the multifarious control of signal transduction. ERK phosphorylation and kinase/phosphatase control. *FEBS J* **2005**, 272, 244-258.
- ²⁹ Alonso, A.; Sasin, J.; Bottini, N.; Friedberg, I.; Osterman, A.; Godzik, A.; Hunter, T.; Dixon, J.; Mustelin, T. Protein tyrosine phosphatases in the human genome. *Cell* **2004**, 117, 699-711.

- ³⁰ Anderson, JM.; Van Itallie, CM.; Fanning, AS.; Setting up a selective barrier at the apical junction complex. *Curr Opin Cell Biol* **2004**, 16, 140-145.
- ³¹ Ostman, A.; Hellberg, C.; Bohmer, FD. Protein tyrosine phosphatases and cancer. *Nat Rev Cancer* **2006**, 6, 307-320.
- ³² Ostman, A.; Yang, Q.; Tonks, NK. Expression of DEP-1, a receptor-like protein-tyrosine-phosphatase, is enhanced with increasing cell density. *Proc Natl Acad Sci U.S.A.* **1994**, 91, 9680-9684.
- ³³ Trapasso, F.; Iuliano, R.; Boccia, A.; Stella, A.; Visconti, R.; Bruni, P.; Baldassarre, G.; Santoro, M.; Viglietto, G.; Fusco, A. Rat protein tyrosine phosphatase eta suppresses the neoplastic phenotype of retrovirally transformed thyroid cells through the stabilization of p27(Kip1). *Mol Cell Biol* **2000**, 20, 9236-9246.
- ³⁴ Paduano, F.; Dattilo, V.; Narciso, D.; Bilotta, A.; Gaudio, E.; Menniti, M.; Agosti, V.; Palmieri, C.; Perrotti, N.; Fusco, A.; Trapasso, F.; Iuliano, R. Protein tyrosine phosphatase PTPRJ is negatively regulated by microRNA-328. *FEBS J* **2013**, 280, 410-412.
- ³⁵ Trapasso, F.; Yendamuri, S.; Dumon, KR.; Iuliano, R.; Cesari, R.; Feig, B.; Seto, R.; Infante, L.; Ishii, H.; Vecchione, A.; Durning, MJ.; Croce, CM.; Fusco, A. Restoration of receptor-type protein tyrosine phosphatase eta function inhibits human pancreatic carcinoma cell growth in vitro and in vivo. *Carcinogenesis* **2004**, 25, 2107-2114.
- ³⁶ Ruivenkamp, C.; Hermsen, M.; Postma, C.; Klous, A.; Baak, J.; Meijer, G.; Demant, P. LOH of PTPRJ occurs early in colorectal cancer and is associated with chromosomal loss of 18q12-21. *Oncogene* **2003**, 22, 3472-3474.
- ³⁷ Iuliano, R.; Le Pera, I.; Cristofaro, C.; Baudi, F.; Arturi, F.; Pallante, P.; Martelli, M.L.; Trapasso, F.; Chiariotti, L.; Fusco, A. The tyrosine phosphatase PTPRJ/DEP-1 genotype affects thyroid carcinogenesis. *Oncogene* **2004**, 23, 8432-8438.
- ³⁸ Trapasso, F.; Drusco, A.; Costinean, S.; Alder, H.; Aqeilan, RI.; Iuliano, R.; Gaudio, E.; Raso, C.; Zanesi, N.; Croce, C. M.; Fusco, A. Genetic ablation of PtpRJ, a mouse cancer susceptibility gene, results in normal growth and development and does not predispose to spontaneous tumorigenesis. *DNA Cell Biol* **2006**, 25, 376-382.
- ³⁹ Zhu, JW.; Brdicka, T.; Katsumoto, TR.; Lin, J.; Weiss, A. Structurally distinct phosphatases CD45 and CD148 both regulate B cell and macrophage immunoreceptor signaling. *Immunity* **2008**, 28, 183-196.
- ⁴⁰ Kovalenko, M.; Denner, K.; Sandstrom, J.; Persson, C.; Gross, S.; Jandt, E.; Vilella, R.; Bohmer, F.; Ostman, A. Site-selective dephosphorylation of the platelet-derived growth factor beta-receptor by the receptor-like protein-tyrosine phosphatase DEP-1. *J Biol Chem* **2000**, 275, 16219-16226.

- ⁴¹ Palka, HL.; Park, M.; Tonks, NK. Hepatocyte growth factor receptor tyrosine kinase met is a substrate of the receptor protein-tyrosine phosphatase DEP-1. *J Biol Chem* **2003**, 278, 5728-5735.
- ⁴² Iervolino, A.; Iuliano, R.; Trapasso, F.; Viglietto, G.; Melillo, RM.; Carlomagno, F.; Santoro, M.; Fusco, A. The receptor type protein tyrosine phosphatase J antagonizes the biochemical and biological effects of RET-derived oncoproteins. *Cancer Res* **2006**, 66, 6280-6287.
- ⁴³ Berset, TA.; Hoier, EF.; Hajnal, A. The *C. elegans* homolog of the mammalian tumor suppressor Dep-1/Scc1 inhibits EGFR signaling to regulate binary cell fate decisions. *Genes Dev* **2005**, 19, 1328-1340.
- ⁴⁴ Hanahan, D.; Weinberg, RA. The hallmarks of cancer. *Cell* **2000**, 100, 57-70.
- ⁴⁵ Baker, JE.; Majeti, R.; Tangye, SG.; Weiss, A. Protein tyrosine phosphatase CD148-mediated inhibition of T-cell receptor signal transduction is associated with reduced LAT and phospholipase C gamma1 phosphorylation. *Mol Cell Biol* **2001**, 21, 2393-2403.
- ⁴⁶ Omerovic, J.; Clague, MJ.; Prior, IA. Phosphatome profiling reveals PTPN2, PTPRJ and PTEN as potent negative regulators of PKB/Akt activation in Ras-mutated cancer cells. *Biochem J* **2010**, 426, 65-72.
- ⁴⁷ Tsuboi, N.; Utsunomiya, T.; Roberts, RL.; Ito, H.; Takahashi, K.; Noda, M.; Takahashi, T. The tyrosine phosphatase CD148 interacts with the p85 regulatory subunit of phosphoinositide 3-kinase. *Biochem J* **2008**, 413, 193-200.
- ⁴⁸ Lampugnani, GM.; Zanetti, A.; Corada, M.; Takahashi, T.; Balconi, G.; Breviario, F.; Orsenigo, F.; Cattelino, A.; Kemler, R.; Daniel, TO.; Dejana, E. Contact inhibition of VEGF induced proliferation requires vascular endothelial cadherin, betacatenin, and the phosphatase DEP-1/CD148. *J Cell Biol* **2003**, 161, 793-804.
- ⁴⁹ Chabot, C.; Spring, K.; Gratton, JP.; Elchebly, M.; Royal, I. New role for the protein tyrosine phosphatase DEP-1 in Akt activation and endothelial cell survival. *Mol Cell Biol* **2009**, 29, 241-253.
- ⁵⁰ Whiteford, JR.; Xian, X.; Chaussade, C.; Vanhaesebroeck, B.; Nourshargh, S.; Couchman, JR. Syndecan-2 is a novel ligand for the protein tyrosine phosphatase receptor CD148. *Mol Biol Cell* **2011**, 22, 3609-3624.
- ⁵¹ Takahashi, K.; Mernaugh, RL.; Friedman, DB.; Weller, R.; Tsuboi, N.; Yamashita, H.; Quaranta, V.; Takahashi, T. Trombospondin-1 acts as a ligand for CD148 tyrosine phosphatase. *Proc Natl Acad Sci U.S.A.* **2012**, 109, 1985-90.
- ⁵² Paduano, F.; Ortuso, F.; Campiglia, P.; Raso, C.; Iaccino, E.; Gaspari, M.; Gaudio, E.; Mangone, G.; Carotenuto, A.; Bilotta, A.; Narciso, D.; Palmieri, C.; Agosti, V.; Artese, A.; Gomez-Monterrey, I.; Sala, M.; Cuda, G.; Iuliano,

R.; Perrotti, N.; Scala, G.; Viglietto, G.; Alcaro, S.; Croce, CM.; Novellino, E.; Fusco, A.; Trapasso, F. Isolation and functional characterization of peptide agonists of PTPRJ, a tyrosine phosphatase receptor endowed with tumor suppressor Activity. *ACS Chem Biol* **2012**, 7, 1666-1676.

⁵³ Ortuso, F.; Paduano, F.; Carotenuto A.; Gomez, IM.; Bilotta, A.; Gaudio, E.; Sala, M.; Artese, A.; Vernieri, E.; Dattilo, V.; Iuliano, R.; Brancaccio, D.; Bertamino, A.; Musella, S.; Alcaro, S.; Grieco, P.; Perrotti, N.; Croce, CM.; Novellino, E.; Fusco, A.; Campiglia, P.; Trapasso, F. Discovery of PTPRJ Agonist Peptides That Effectively Inhibit in Vitro Cancer Cell Proliferation and Tube Formation. *ACS Chem Biol* **2013**, 8, 1497-1506.

⁵⁴ Endicott, JA.; Noble, ME.; Johnson, LN. The structural basis for control of eukaryotic protein kinases. *Annu Rev Biochem* **2012**, 81, 587-613.

⁵⁵ Blume-Jensen, P.; Hunter, T. Oncogenic kinase signalling. *Nature* **2001**, 411, 355-365.

⁵⁶ Lin, J.; Gan, CM.; Zhang, X.; Jones, S.; Sjöblom, T.; Wood, LD.; Parsons, DW.; Papadopoulos, N.; Kinzler, KW.; Vogelstein, B.; Parmigiani, G.; Velculescu, VE. A multidimensional analysis of genes mutated in breast and colorectal cancers. *Genome Research* **2007**, 17, 1304-1318.

⁵⁷ Wood, LD.; Parsons, DW.; Jones, S.; Lin, J.; Sjöblom, T.; Leary, RJ.; Shen, D.; Boca, SM.; Barber, T.; Ptak, J.; Silliman, N.; Szabo, S.; Dezso, Z.; Ustyanksky, V.; Nikolskaya, T.; Nikolsky, Y.; Karchin, R.; Wilson, PA.; Kaminker, JS.; Zhang, Z.; Croshaw, R.; Willis, J.; Dawson, D.; Shipitsin, M.; Willson, JK.; Sukumar, S.; Polyak, K.; Park, BH.; Pethiyagoda, CL.; Pant, PV.; Ballinger, DG.; Sparks, AB.; Hartigan, J.; Smith, DR.; Suh, E.; Papadopoulos, N.; Buckhaults, P.; Markowitz, SD.; Parmigiani, G.; Kinzler, KW.; Velculescu, VE.; Vogelstein, B. The genomic landscapes of human breast and colorectal cancers. *Science* **2007**, 318, 1108-1113.

⁵⁸ Rusciano, MR.; Maione, AS.; Illario, M. Sisters Acts: Converging Signaling Between CaMKII and CaMKIV, Two Members of the Same Family. *Transl Med UniSa* **2012**, 4, 66-72.

⁵⁹ Ryutaro, K.; Fukushige, S.; Norifumi, S.; Tanabe, K.; Fukunaga, K.; Inui, S. CaMKII phosphorylates serine 10 of p27 and confers apoptosis resistance to HeLa cells. *Biochemical and Biophysical Research Communications* **2010**, 401, 350-355.

⁶⁰ Griffith, LC. Calcium/calmodulin-dependent protein kinase II: An unforgettable Kinase. *J Neurosci* **2004**, 24, 8391-8393.

⁶¹ Strack, S.; Barban, MA.; Wadzinski, BE.; Colbran, RJ. Differential inactivation of postsynaptic density-associated and soluble Ca²⁺/calmodulin-dependent protein kinase II by protein phosphatase 1 and 2A. *J Neurochem* **1997**, 68, 92119-92128.

- ⁶² Braun, AP.; Schulman, H. The multifunctional calcium/calmodulin-dependent protein kinase: from form to function. *Annu Rev Physiol* **1995**, 57, 417-445.
- ⁶³ Zhang, T.; Brown, JH. Role of Ca²⁺/calmodulin-dependent protein kinase II in cardiac hypertrophy and heart failure. *Cardiovasc Res* **2004**, 63, 476-486.
- ⁶⁴ Rokhlin, O.; Taghiyev, AF.; Bayer, KU.; Bumcrot, D.; Kotelianski, VE.; Glover, RA.; Cohen, MB. Calcium/calmodulin-dependent kinase II plays an important role in prostate cancer cell survival. *Cancer Biol Ther* **2007**, 6, 732-742.
- ⁶⁵ Mishra, S.; Mishra, JP.; Gee, K.; McManus, DC.; LaCasse, EC.; Kumar, A. Distinct role of calmodulin and calmodulin-dependent protein kinase-II in lipopolysaccharide and tumor necrosis factor- α -mediated suppression of apoptosis and antiapoptotic c-IAP2 gene. *J Biol Chem* **2005**, 280, 37536-37546.
- ⁶⁶ Guan, X.; Chen, L.; Wang, J.; Geng, H.; Chu, X.; Zhang, Q.; Du, L.; De, W. Mutations of phosphorylation sites Ser10 and Thr187 of p27Kip1 abolish cytoplasmic redistribution but do not abrogate G0/1 phase arrest in the HepG2 cell line. *Biochem Biophys Res Commun* **2006**, 347, 601-607.
- ⁶⁷ Fujita, N.; Sato, S.; Katayama, K.; Tsuru, T.; Akt-dependent phosphorylation of p27Kip promotes binding to 14-3-3 and cytoplasmic localization. *J Biol Chem* **2002**, 277, 28706-28713.
- ⁶⁸ Conqueret, O. New roles for p21 and p27 cell-cycle inhibitors: a function for each cell compartment?. *Trends Cell Biol* **2003**, 13, 65-70.
- ⁶⁹ Midorikawa, R.; Takei, Y.; Hirokawa, N. KIF4 motor regulates activity-dependent neuronal survival by suppressing PARP-1 enzymatic activity. *Cell* **2006**, 125, 371-383.
- ⁷⁰ Sherr, CJ. G1 phase progression: cycling on cue. *Cell* **1994**, 79, 551-555.
- ⁷¹ Gomez, IM.; Sala, M.; Rusciano, MR.; Monaco, S.; Maione, AS.; Iaccarino, G.; Tortorella, P.; D'Ursi, AM.; Scrima, M.; Carotenuto, A.; De Rosa, G.; Bertamino, A.; **Vernieri, E.**; Grieco, P.; Novellino, E.; Illario, M.; Campiglia, P. Characterization of a selective CaMKII peptide inhibitor. *European Journal of Medicinal Chemistry* **2013**, 62, 425-434.
- ⁷² Luttrell, LM. Composition and function of g protein-coupled receptor signalsomes controlling mitogen-activated protein kinase activity. *J Mol Neurosci* **2005**, 26, 253-264.
- ⁷³ DeWire, SM.; Ahn, S.; Lefkowitz, RJ.; Shenoy, SK. Beta-arrestins and cell signaling. *Annu Rev Physiol* **2007**, 69, 483-510.
- ⁷⁴ Ribas, C.; Penela, P.; Murga, C.; Salcedo, A.; García-Hoz, C.; Jurado-Pueyo, M.; Aymerich, I.; Mayor, Jr. F. The G protein-coupled receptor kinase (GRK) interactome: role of GRKs in GPCR regulation and signaling. *Biochim Biophys Acta* **2007**, 1768, 913-922.

⁷⁵ Penela, P.; Rivas, V.; Salcedo, A.; Mayor, Jr. F. G protein-coupled receptor kinase 2 (GRK2) modulation and cell cycle progression. *Proc Natl Acad Sci U S A* **2010**, 107, 1118-1123.

⁷⁶ Rivas, V.; Carmona, R.; Muñoz-Chápuli, R.; Mendiola, M.; Nogués, L.; Reglero, C.; Miguel-Martín, M.; García-Escudero, R.; Dorn II, GW.; Hardisson, D.; Mayor F Jr.; Penela, P. Developmental and tumoral vascularization is regulated by G protein-coupled receptor kinase 2. *J Clin Invest.* **2013**, 123, 4714-4730.

⁷⁷ Penela, P.; Murga, C.; Ribas, C.; Lafarga, V.; Mayor, Jr. F. The complex G protein-coupled receptor kinase 2 (GRK2) interactome unveils new physiopathological targets. *Br J Pharmacol* **2010**, 160, 821-832.

⁷⁸ Kiefer, F.; Siekmann, AF. The role of chemokines and their receptors in angiogenesis. *Cell Mol Life Sci* **2011**, 68, 2811-2830.

⁷⁹ Hellberg, C.; Ostman, A.; Heldin, CH. PDGF and vessel maturation. *Recent Results Cancer Res* **2010**, 180, 103-114.

⁸⁰ Wu, JH.; Goswami, R.; Kim, LK.; Miller, WE.; Peppel, K.; Freedman, NJ. The platelet-derived growth factor receptor-beta phosphorylates and activates G protein-coupled receptor kinase-2. A mechanism for feedback inhibition. *J Biol Chem* **2005**, 280, 31027-31035.

⁸¹ Ho, J.; Cocolakis, E.; Dumas, VM.; Posner, BI.; Laporte, SA.; Lebrun, JJ. The G protein-coupled receptor kinase-2 is a TGF β -inducible antagonist of TGF β signal transduction. *EMBO J* **2005**, 24, 3247-3258.

⁸² D'Souza, KM.; Malhotra, R.; Philip, JL.; Staron, ML.; Theccanat, T.; Jeevanandam, V.; Akhter, SA. G protein-coupled receptor kinase-2 is a novel regulator of collagen synthesis in adult human cardiac fibroblasts. *J Biol Chem* **2011**, 286, 15507-15516.

⁸³ Peppel, K.; Zhang, L.; Huynh, TT.; Huang, X.; Jacobson, A.; Brian, L.; Exum, ST.; Hagen, PO.; Freedman, NJ. Overexpression of G protein-coupled receptor kinase-2 in smooth muscle cells reduces neointimal hyperplasia. *J Mol Cell Cardiol* **2002**, 34, 1399-1409.

⁸⁴ Morris, GE.; Nelson, CP.; Standen, NB.; Challiss, RA.; Willets, JM. Endothelin signalling in arterial smooth muscle is tightly regulated by G protein-coupled receptor kinase 2. *Cardiovasc Res* **2010**, 85, 424-433.

⁸⁵ Liu, S.; Premont, RT.; Kontos, CD.; Zhu, S.; Rockey, DC. A crucial role for GRK2 in regulation of endothelial cell nitric oxide synthase function in portal hypertension. *Nat Med* **2005**, 11, 952-958.

⁸⁶ Salcedo, A.; Mayor, Jr. F.; Penela, P. Mdm2 is involved in the ubiquitination and degradation of G-protein-coupled receptor kinase 2. *EMBO J* **2006**, 25, 4752-4762.

⁸⁷ Penela, P.; Ribas, C.; Aymerich, I.; Eijkelkamp, N.; Barreiro, O.; Heijnen, CJ.; Kavelaars, A.; Sánchez-Madrid, F.; Mayor, Jr. F. G protein-coupled

receptor kinase 2 positively regulates epithelial cell migration. *EMBO J* **2008**, *27*, 1206-1218.

⁸⁸ Lafarga, V.; Aymerich, I.; Tapia, O.; Mayor, Jr. F.; Penela, P. A novel GRK2/HDAC6 interaction modulates cell spreading and motility. *EMBO J* **2012**, *31*, 856-869.

⁸⁹ Penela, P.; Murga, C.; Ribas, C.; Tutor, AS.; Peregrin, S.; Mayor, Jr. F. Mechanisms of regulation of G-protein-coupled receptor kinases (GRKs) and cardiovascular disease. *Cardiovasc Res* **2006**, *69*, 46-56.

⁹⁰ Penela, P.; Ribas, C.; Mayor, Jr. F. Mechanisms of regulation of the expression and function of G protein-coupled receptor kinases. *Cell Signal* **2003**, *15*, 973-981.

⁹¹ Metaye, T.; Gibelin, H.; Perdrisot, R.; Kraimps, JL. Pathophysiological roles of G-protein-coupled receptor kinases. *Cell Signal* **2005**, *17*, 917-928.

⁹² Penela, P.; Elorza, A.; Sarnago, S.; Mayor, Jr. F. Beta-arrestin- and c-Src-dependent degradation of G-protein-coupled receptor kinase 2. *EMBO J* **2001**, *20*, 5129-5138.

⁹³ Elorza, A.; Penela, P.; Sarnago, S.; Mayor, Jr. F. MAPK-dependent degradation of G protein-coupled receptor kinase 2. *J Biol Chem* **2003**, *278*, 29164-29173.

⁹⁴ Pickart, CM. Mechanisms underlying ubiquitination. *Annu Rev Biochem* **2001**, *70*, 503-533.

⁹⁵ Weissman, AM. Themes and variations on ubiquitylation. *Nat Rev Mol Cell Biol* **2001**, *2*, 169-178.

⁹⁶ Shenoy, SK.; McDonald, PH.; Kohout, TA.; Lefkowitz, RJ. Regulation of receptor fate by ubiquitination of activated beta 2-adrenergic receptor and beta-arrestin. *Science* **2001**, *294*, 1307-1313.

⁹⁷ Shenoy, SK.; Lefkowitz, RJ. Receptor-specific ubiquitination of beta-arrestin directs assembly and targeting of seven-transmembrane receptor signalosomes. *J Biol Chem* **2005**, *280*, 15315-15324.

⁹⁸ Wang, P.; Gao, H.; Ni, Y.; Wang, B.; Wu, Y.; Ji, L.; Qin, L.; Ma, L.; Pei, G. Beta-arrestin 2 functions as a G-protein-coupled receptor-activated regulator of oncoprotein Mdm2. *J Biol Chem* **2003**, *278*, 6363-6370.

⁹⁹ Yang, Y.; Li, CC.; Weissman, AM. Regulating the p53 system through ubiquitination. *Oncogene* **2004**, *23*, 2096-2106.

¹⁰⁰ Bond, GL.; Hu, W.; Levine, AJ. MDM2 is a central node in the p53 pathway: 12 years and counting. *Curr Cancer Drug Targets* **2005**, *5*, 3-8.

¹⁰¹ Lin, FT.; Chen, W.; Shenoy, S.; Cong, M.; Exum, ST.; Lefkowitz, RJ. Phosphorylation of beta-arrestin2 regulates its function in internalization of beta(2)-adrenergic receptors. *Biochemistry* **2002**, *41*, 10692-10699.

¹⁰² Girnita, L.; Girnita, A.; Larsson, O. Mdm2-dependent ubiquitination and degradation of the insulin-like growth factor 1 receptor. *Proc Natl Acad Sci USA* **2003**, 100, 8247-8252.

¹⁰³ Iwakuma, T.; Lozano, G. MDM2, an introduction. *Mol Cancer Res* **2003**, 1, 993-1000.

¹⁰⁴ Jin, Y.; Lee, H.; Zeng, SX.; Dai, MS.; Lu, H. MDM2 promotes p21waf1/cip1 proteasomal turnover independently of ubiquitylation. *EMBO J* **2003**, 22, 6365-6377.

¹⁰⁵ Pan, Y.; Chen, J. MDM2 promotes ubiquitination and degradation of MDMX. *Mol Cell Biol* **2003**, 23, 5113-5121.

¹⁰⁶ Uchida, C.; Miwa, S.; Kitagawa, K.; Hattori, T.; Isobe, T.; Otani, S.; Oda, T.; Sugimura, H.; Kamijo, T.; Ookawa, K.; Yasuda, H.; Kitagawa, M. Enhanced Mdm2 activity inhibits pRB function via ubiquitin dependent degradation. *EMBO J* **2005**, 24, 160-169.

¹⁰⁷ Métayé, T.; Gibelin, H.; Perdrisot, R.; Kraimps, JL. Pathophysiological roles of G-protein-coupled receptor kinases. *Cell Signal* **2005**, 17, 917-928.

¹⁰⁸ Matkovich, SJ.; Diwan, A.; Klanke, JL.; Hammer, DJ.; Marreez, Y.; Odley, AM.; Brunskill, EW.; Koch, WJ.; Schwartz, RJ.; Dorn, GW 2nd. Cardiac-specific ablation of G-protein receptor kinase 2 redefines its roles in heart development and beta-adrenergic signaling. *Circ Res* **2006**, 99, 996-1003.

¹⁰⁹ Nigg, EA. Mitotic kinases as regulators of cell division and its checkpoints. *Nat Rev Mol Cell Biol* **2001**, 2, 21-32.

¹¹⁰ Gomez-Monterrey, I.; Carotenuto, A.; Cipolletta, E.; Sala, M.; **Vernieri, E.**; Limatola, A.; Bertamino, A.; Musella, S.; Grieco, P.; Trimarco, B.; Novellino, E.; Iaccarino, G.; Campiglia, P. SAR study and conformational analysis of a series of novel peptide G protein-coupled receptor kinase 2 (GRK2) inhibitors. *Byopolimers* **2014**, 101, 121-128.

¹¹¹ Carotenuto, A.; Cipolletta, E.; Gomez-Monterrey, I.; Sala, M.; **Vernieri, E.**; Limatola, A.; Bertamino, A.; Musella, S.; Sorriento, D.; Grieco, P.; Trimarco, B.; Novellino, E.; Iaccarino, G.; Campiglia, P. Design, synthesis and efficacy of novel G protein-coupled receptor kinase 2 inhibitors. *Eur J Med Chem* **2013**, 69, 384-92.

¹¹² Setyawan, J.; Koide, K.; Diller, TC.; Bunnage, ME.; Taylor, S.; Nicolai, K. C.; Brunton, LL. *Mol Pharmacol* **1999**, 56, 370-376.

¹¹³ Iino, M.; Furugori, T.; Mori, T.; Moriyama, S.; Fukuzawa, A.; Shibano, T. *J Med Chem* **2002**, 45, 2150-2159.

¹¹⁴ Benovic, JL.; Stone, WC.; Caron, MG.; Lefkowitz, RJ. *J Biol Chem* **1989**, 264, 6707-6710.

¹¹⁵ Takeda Pharmaceuticals Company Limited, Ikeda, S., kaneko, M., Fujiwara, S. World patent WO2007034846.

¹¹⁶ Winstel, R.; Ihlenfeldt, HG.; Jung, G.; Krasel, C.; Lohse, M. *J Biochem Pharmacol* **2005**, 70, 1001-1008.

¹¹⁷ Niv, MY.; Rubin, H.; Cohen, J.; Tsirolnikov, L.; Licht, T.; Peretzman-Shemer, A.; Cnàan, E.; Tartakovsky, A.; Stein, I.; Albeck, S.; Weinstein, I.; Goldenberg-Furmanov, M.; Tobi, D.; Cohen, E.; Laster, M.; Ben-Sasson, S. A.; Reuveni, H. *J Biol Chem* **2004**, 279, 1242-1255.

¹¹⁸ Anis, Y.; Leshem, O.; Reuveni, H.; Wexler, I.; Ben Sasson, R.; Yahalom, B.; Laster, M.; Raz I.; Ben Sasson, S.; Shafrir, E.; Ziv, E. *Diabetologia*, **2004**, 47, 1232-1244.

¹¹⁹ Mayer, G.; Wulffen, B.; Huber, C.; Brockmann, J.; Flicke, B.; Neumann, L.; Hafenbradl, D.; Kleb, BM.; Lohse, MJ.; Krasel, C.; Blind, M. *RNA* **2008**, 14, 524-534.

CHAPTER 2

**Synthesis, characterization and biological evaluation of PTPRJ
(protein tyrosine phosphatase receptor like-j) agonists**

Abstract PTPRJ is a receptor protein tyrosine phosphatase involved in both physiological and oncogenic pathways. Our work group previously reported that its expression is strongly reduced in the majority of explored cancer cell lines and tumor samples; moreover, its restoration blocks in vitro cancer cell proliferation and in vivo tumor formation. By means of a phage display library screening, we recently identified two peptides able to bind and activate PTPRJ, resulting in cell growth inhibition and apoptosis of both cancer and endothelial cells. Here, on a previously discovered PTPRJ agonist peptide, [CHHNLTHAC], we synthesized and assayed a panel of nonapeptide analogues with the aim to identify specific amino acid residues responsible for peptide activity. These second-generation nonapeptides were tested on both cancer and primary endothelial cells (HeLa and HUVEC, respectively). Interestingly, one of them ([CHHALTHAC]) was able to both dramatically reduce cell proliferation and effectively trigger apoptosis of both HeLa and HUVECs compared to its first-generation counterpart. Moreover this peptide significantly inhibited in vitro tube formation on Matrigel. Our compound inhibited ERK1/2 phosphorylation and cell proliferation in breast cancer cells (MCF-7 and SKBr3), while no effects were observed on primary normal human mammary endothelial cells (HMEC). Molecular modeling and NMR studies on these peptides reporting the possibility of self-aggregation states and highlighting new hints of structure-activity relationship. Thus, our results indicate that this nonapeptide might represent a great potential lead for the development of novel targeted anticancer drugs.

Furthermore and in order to enhance the potency of this peptide, we performed different modification on this hit, including changes to disulfide bridge with lactam bridge, changes in specific position and changes to Cysteine with its analog (Penicillamine).

Keywords PTPRJ, Ala scan peptide, disulfide bridge, lactam bridge, microwave, HeLa cells, HUVEC cells, Molecular Modeling.

Abbreviations Abbreviations used for amino acids and designation of peptides follow the rules of the IUPACIUB Commission of Biochemical Nomenclature in *J Biol Chem* **1972**, 247, 977-983. Amino acid symbols denote L-configuration unless indicated otherwise.

The following additional abbreviations are used:

DCM, dichloromethane; DIPEA, N,N-diisopropylethyl-amine; DMF, N,N-dimethylformamide; iPr_3SiH , or TIS triisopropylsilane; TFA, trifluoroacetic acid; Fmoc, 9-fluorenyl-methoxycarbonyl; HOBt, Nhydroxy- benzotriazole; HBTU, 2-(1H-benzotriazole-1-yl)-1,1,3,3-tetramethyluronium hexafluoro - phosphate; Trt, trityl; Pbf, 2,2,4,6,7-pentamethyldihydro benzofuran-5-sulfonyl; RP HPLC, reversed-phase high performance liquid chromatography; ESI, electrospray ionization; LCQ, liquid chromatography quadrupole mass spectrometry; HUVEC, Human umbilical vein endothelial cells.

1. Introduction

Reversible tyrosine phosphorylation, which is governed by the balanced action of protein tyrosine kinases (PTKs) and protein-tyrosine phosphatases (PTPs), regulates important signaling pathways that are involved in the control of cell proliferation, adhesion and migration.

The distinct but complementary function of these enzymes is emphasized by recent studies, in which kinases have been implicated in controlling the amplitude of signaling responses, whereas phosphatases are thought to have an important role in controlling the rate and duration of the response.^{1,2}

The first PTP was purified in 1988, approximately 10 years after the discovery of tyrosine kinases.³ It is now known that PTPs constitute a large, structurally diverse family of tightly regulated,⁴ highly specific enzymes with important regulatory roles.^{5,6}

It is also clear that PTPs have both inhibitory and stimulatory effects on cancer associated signaling processes, and that deregulation of PTP function is associated with tumorigenesis in different types of human cancer.

The PTP-superfamily includes 109 genes, compared to 90 human PTK genes, suggesting similar levels of complexity between the two families.

1.1 Protein Tyrosine Phosphatases

PTPs are broadly divided into receptor-like forms and non-receptor forms.⁷ The receptor-like PTPs have a single transmembrane domain and variable extracellular domains.

The intracellular parts of most of the receptor-like PTPs contain two tandem PTP domains (D1 and D2) with most, if not all, of the catalytic activity residing in D1. In many cases, the extracellular domains include immunoglobulin like domains and fibronectin type III domains, similar to the extracellular domains of cellular adhesion molecules. Non-receptor PTPs have striking structural diversity and often contain sequences that target them to specific subcellular locations or enable their binding to specific proteins (Figure 1). The catalytic PTP domain spans approximately 280 amino acids and contains a highly conserved active site with a Cysteine residue that is required for catalytic activity. Dephosphorylation of substrates occurs through a two-step mechanism consisting of the formation of a covalent PTP-phosphate intermediate that is subsequently hydrolysed.

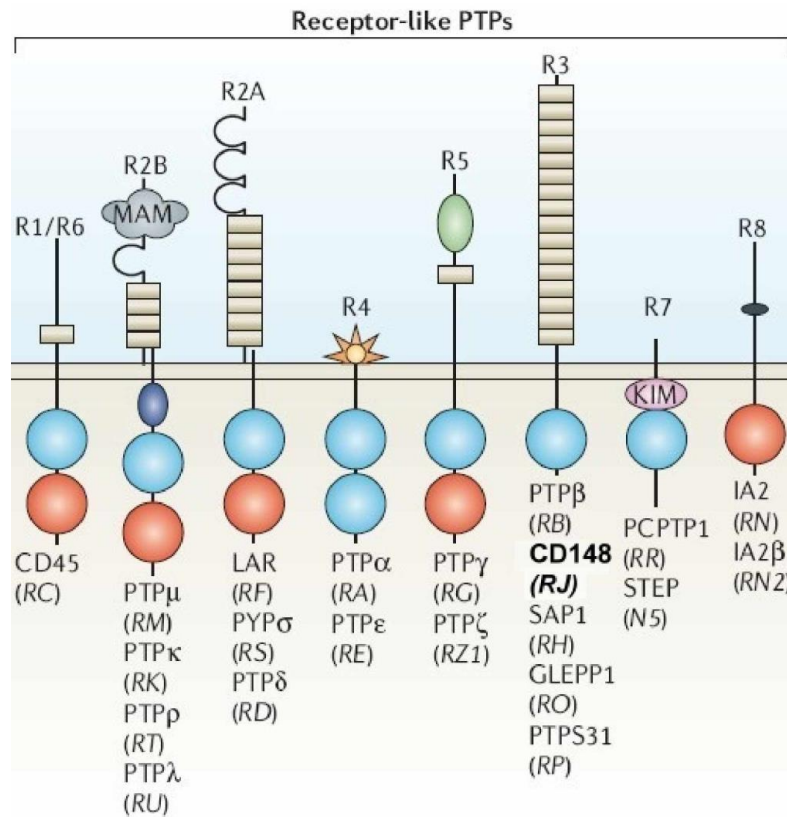


Figure 1. Schematic view of the domain composition of all RPTP family members. The intracellular part consists of one catalytically active PTP domain (blue) and, in some subfamilies, a PTP domain with little or no catalytic activity (red), which is likely to have a regulatory function.

CD148 or PTPRJ is a type-III RPTP with a broad pattern of tissue expression. It is expressed on fibroblasts and endothelium, as well as epithelial and hematopoietic cells.^{8,9} The CD148 gene, also known as *Ptprj*, is located on chromosome 11p11.12 in humans, and consists of 25 exons distributed over 150 Kb of genomic DNA. The protein contains a bulky extracellular domain of 970 amino acids organized in eight fibronectin type III repeats, a 25-amino acid long transmembrane domain and a 342 amino acid cytoplasmic portion with a single catalytic domain. Its mass varies from 200 to 250 KDa depending on different N- or O-glycosylations in the extracellular domain.

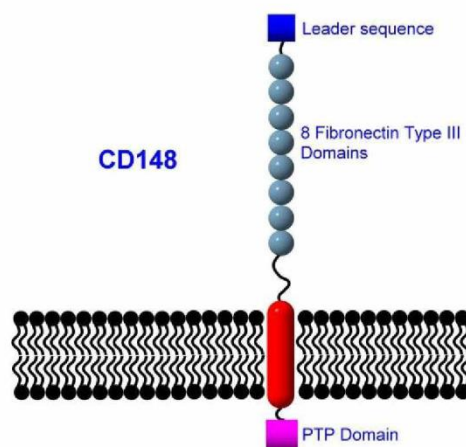


Figure 2. Schematic view of the CD148 molecule.

1.2 Biochemical Activity of CD148

As mentioned above, the activity of many PTPs may be regulated by phosphorylation, and this seems to occur in the case of CD148. Jallal et al.¹⁰ reported that CD148 is tyrosine-phosphorylated after stimulation with epithelial growth factor (EGF), although no change in phosphatase activity was documented. Even if it does not affect CD148 phosphatase activity, this phosphorylation event might have an important role in promoting interactions with SH2-containing proteins involved in the metabolic networks in which CD148 signal transduction pathways participate. Although protein dimerization is a key mechanism that simulates PTK activity, PTPs are generally not regulated in this way. Some lines of evidence, however, suggest that CD148 could indeed dimerize. In fact, the transmembrane domain contains the same dimerization consensus sequence¹¹ found in RPTP α , whose dimerization inhibits its phosphatase activity.¹² It is not clear if dimerization inhibits or induces CD148 phosphatase activity, since experimental data lead to conflicting results. For example, in lymphocytes CD148 dimerization (induced by cross-linking) was shown to induce proliferation; on the contrary, in endothelial cells dimerization induced by a bivalent antibody seems to act in an opposite way, promoting CD148 activation.¹³

1.3 CD148 acts as a Tumor Suppressor

Like many phosphatases, PTPRJ plays a role in cancer, its down-regulation being documented in different kinds of tumors. Additionally, in cultured breast cancer cells CD148 re-expression led to a five- to ten-fold reduction in cell growth.¹⁴ Similar findings were later reported in pancreatic, thyroid,¹⁵ and colon cancer cells.^{16,17}

CD148 re-expression was also described to induce differentiation in breast and thyroid undifferentiated tumor cells.¹⁸ To understand the role of CD148 in cancer, many studies were carried out to analyze *Ptprj* gene status in human tumors. The most thorough analysis identified *Ptprj* as the functional gene at the mouse colon-cancer susceptibility locus, *Sccl*.¹⁶ This locus was originally defined based on its segregation with colon cancer susceptibility after crossing cancer-resistant and cancer-susceptible mouse strains. Sequence differences in *Ptprj* between the cancer-susceptible and cancer-resistant strains were also identified, supporting the theory that tumor susceptibility is conferred by certain *Ptprj* variants.

PTPRJ status has also been analyzed in human tumors.¹⁹ Loss of heterozygosity, occurring in the absence of acquired mutation in the remaining allele, has been found in breast, colon, lung and thyroid cancers, implicating *Ptprj* haploid insufficiency as a transforming mechanism in humans.

In association with these studies, different allelic variants of human *Ptprj* were identified; these variations result in CD148 proteins that have differences in their extracellular-domain residues.²⁰

1.3.1 CD148 Regulates Cell Growth and Cell Cycle

The tumor-suppressive role of CD148 was clearly displayed in experiments where highly malignant thyroid cells, after transduction by a retrovirus carrying CD148, appeared to acquire a normal phenotype and showed increased adhesion, restoration of differentiation, reduced proliferation and decreased tumorigenicity.¹⁵ The same report established that CD148 induced a

G1 growth arrest by suppressing the degradation of the cyclin-dependent kinase inhibitor p27kip1 protein.

Therefore, it could be assumed that CD148 is a cell regulator that maintains cells in a controlled proliferation state. When CD148 is overexpressed, cells show a reduction in cell proliferation,²¹ while when there is a deficiency in CD148 cells proliferate uncontrollably.

For this reason we designed and synthesized a library of peptides agonist of this phosphatase in order to stimulate PTPRJ overexpression.

2. Aim of work

Trapasso et al.²² identified PTPRJ-binding peptides from a combinatorial phage display library in a cell free assay. Two peptide, whose specificity were tested in vitro, were also responsible of both biochemical and biological PTPRJ mediated effects, as we observed both dephosphorylation of PTPRJ targets and cell growth inhibition of HeLa and HUVEC cells. In particular, it has been described the isolation and characterization of synthetic peptides that interact with PTPRJ ectodomain and are able to trigger its signaling.

In this context and as part of a wide research program aimed to the identification of new PTPRJ-targeted anticancer agents, I focused the attention on PTPRJ 19 (named peptide **1** in the Table 1) and PTPRJ 24 that in vitro, were shown to be responsible for both biochemical and biological PTPRJ-mediated effects. In fact, the administration of both PTPRJ 19 ([Cys-His-His-Asn-Leu-Thr-His-Ala-Cys]-OH) and PTPRJ 24 ([Cys-Leu-His-His-Tyr-His-Gly-Ser-Cys]-OH) peptides to human cervical HeLa cancer cell line and human umbilical vein endothelial cells (HUVECs) dramatically reduced the extent of both MAPK phosphorylation, a critical mediator of mitogenic signals, and total phospho-tyrosine levels and, conversely, induced a significant increase of the cell cycle inhibitor p27Kip1. Moreover, these PTPRJ agonist peptides both reduce proliferation and trigger apoptosis of treated cells.²³

Therefore, during my PhD, I considered PTPRJ 19 (peptide **1**) as a valuable starting point for the development of a novel class of potential chemotherapeutic agents.

Several general approaches to development different libraries of peptides have been used: (a) L- Ala scanning analysis to check the contribution of the various amino acid residues to the agonist activity of peptide **1**; (b) implementation of various global and local conformational constraints *via* peptide cyclizations and employment of constrained amino acids; and (c) manipulation of steric factors that influence protein-ligand interactions.

2.1 Alanine scanning approach (peptides **1-10**)

In a first classical approach, a series of *L*-Ala substituted analogues of peptide **1** were synthesized in order to evaluate the amino acid side chains involved in the interaction with the target molecule (peptides **1-10**, Table 1).

Table 1. Structure, inhibition activities, and analytical data of peptides **1-10**.

PTPRJ peptides	Sequence	HPLC k ^a	ESI MS		% of cell growth inhibition ^b		
			Found	Calc.	24h	48h	72h
1	[CHHNLTHAC]	3.34	1931.2	1033.5	-	4.5±1.4	19±2.82
2	CHHNLTHAC	3.28	1035.1	1035.7	-	-	4±1.4
3	AHHNLTHAC	3.22	1003.1	1003.7	-	-	-
4	[CAHNLTHAC]	3.56	967.1	967.6	16.5±2.12	30±2.82	32.0±4.2
5	[CHANLTHAC]	3.56	967.1	967.4	28±5.5	46±4.2	51±1.4
6	[CHHALTHAC]	3.44	990.1	990.4	48.0±2.82	62.5±4.9	66.5±2.12
7	[CHHNATHAC]	3.26	991.0	991.4	-	2±1.5	19±4.2
8	[CHHNLAHAC]	3.45	1003.1	1003.2	-	-	19±4.2
9	[CHHNLTAAAC]	3.56	967.1	967.6	-	4.5±2.13	20±1.4
10	CHHNLTHAA	3.22	1003.1	1003.5	-	-	-

^ak^a=[(peptide retention time-solvent retention time)/solvent retention time]. ^bThe relative cell growth was expressed as a percentage of the growth observed in untreated cells at 24, 48, and 72h. ^bThe results are presented as mean values ± SD of at least three independent experiments.

Here, it has been demonstrated that peptide **6**, a derivative of peptide **1**, generated through an Ala Scan analysis, was able to (a) reduce the

phosphorylation of ERK1/2; (b) inhibit HeLa cancer cell proliferation, and (c) trigger apoptosis in a much more efficient way than its lead compound.²³

HUVEC cell proliferation was also inhibited by peptide **6**, although to a lower extent compared to HeLa cells. Moreover, it effectively blocked in vitro HUVEC tube formation (see Results and Discussion session). These results strongly encourage the pursuit of this path for the development of a novel class of targeted anticancer drugs.

At the same time, we decided to consider peptide **1** a valuable starting point for the development of a novel class of potential chemotherapeutic agents replacing disulfide ¹Cys-⁹Cys ring with lactam bridges to provide varying size of the ring by substituting with different bridging residues.

2.2 Lactam cyclic peptides (peptides 11-17)

Taking in mind that any attempt to design a peptide for therapeutic use would then be aided by a clear understanding of the structural elements that are responsible for its interaction with biological target, we have begun a study to address the roles of the disulfide bridge in the activity of peptide lead, compound **1**.

Herein, we present the synthesis and the biological activities of new analogues containing a more stable lactam bridge with the aim to implement the global conformational constraint and the ring size. These strategies, previously reported in several biologically relevant peptides such as urotensine,²⁴ interleukin-8,²⁵ somatostatin,²⁶ HIV gp41 antigenic loop,²⁷ will allow to evaluate the structural importance of both ring size and bridge chemical nature on the biological activity for the new analogues.

In particular, the Cysteines at positions 1 and 9 were replaced by amino acids bearing an amino ((2,3)-diaminopropionic acid (Dap), ornithine (Orn) or lysine (Lys)) and carboxylic (Asp or Glu) functions on the side chain, respectively; these two side chains were subsequently linked to form the lactam bridge (peptides **11-17**, Table 2).

Table 2. Structure, inhibition activities, and analytical data of peptides **11-17**.

PTPRJ peptides	Sequence	HPLC k ^{ra}	ESI MS		% of cell growth inhibition ^b		
			Found	Calc.	24h	48h	72h
11	[KHHNLTHAD]	3.26	1054.7	1054.1	5±4.3	10±4.3	10±5.5
12	[OmHHNLTHAD]	3.19	1041.7	1041.2	1.18±5.5	1.88±2.2	13±3.2
13	[KHHNLTHAE]	3.25	1068.6	1068.1	-	2±3.30	4.0±3.3
14	[OmHHNLTHAE]	3.29	1054.6	1054.2	-	10±1.10	10±1.3
15	[DapHHNLTHAE]	3.31	1026.7	1026.6	-	9	9
16	[DHHNLTHAK]	3.23	1054.4	1054.2	1±4.5	2±4.5	3±1.1
17	[EHHNLTHAK]	3.26	1068.5	1068.3	4.3±6.6	20±5.6	19.7±3.4

^ak^r=[(peptide retention time-solvent retention time)/solvent retention time].^bThe relative cell growth was expressed as a percentage of the growth observed in untreated cells at 24, 48, and 72h. ^bThe results are presented as mean values ± SD of at least three independent experiments.

2.3 Alanine scanning approach (peptides 18-24)

Once that the biological investigations of the first series of compounds were completed (paragrafe 2.1), we realized that it was necessary to evaluate if there are other amino acid side chains involved in the interaction with the target molecule. Therefore, being interested in the development of analogues with higher inhibitory potency, we decided to apply for the second time an Alanine scanning approach to the most active peptide, peptide 6 ([CHHALTHAC]) (peptides **18-24**, Table 3).

Table 3. Structure, inhibition activities, and analytical data of peptides **18-24**.

PTPRJ peptides	Sequence	HPLC k ^{ra}	ESI MS		% of cell growth inhibition ^b		
			Found	Calc.	24h	48h	72h
18	AHHALTHAC	3.54	960.4	958.1	3.7±2.2	10.0±3.2	10.0±4.4
19	[CAHALTHAC]	3.33	922.2	921.1	-	10.0±3.4	9.5±3.2
20	[CHAALTHAC]	3.75	922.4	921.1	-	25.0±3.5	25.0±2.2
21	[CHHAATHAC]	3.25	945.4	945.1	2.7±2.6	18.5±2.3	19.0±1.1
22	[CHHALAHAC]	3.76	958.1	957.1	9.76±3.5	7.9±2.4	28.0±3.2
23	[CHHALTAAC]	3.56	922.2	921.1	9.76±2.5	20.1±2.2	42.1±2.9
24	CHHALTHAA	3.26	960.1	958.1	4.3±2.1	20.0±2.3	19.7±3.7

^ak^r=[(peptide retention time-solvent retention time)/solvent retention time].^bThe relative cell growth was expressed as a percentage of the growth observed in untreated cells at 24, 48, and 72h. ^bThe results are presented as mean values ± SD of at least three independent experiments.

Here, it has been demonstrated that no one compound generated through the second Ala scan analysis, was able to inhibit HeLa cancer cell proliferation in a greater extent of peptide 6.

2.4 Changes to disulfide bridge (peptides 25-29)

Interestingly, peptide 6 was responsible for a 66.5% reduction of cell proliferation versus 20% of the lead peptide, compound 1. Therefore, it was considered as a valuable starting point to design new analogues containing both a modified disulfide bridge (series 1, Table 4) and changes in position four, from Alanine to the most simple and no chiral amino acid (Glycine) and a restricted amino acid (Proline) to assess if it is important both the chirality and steric size (series 2, Table 4).

Table 4. Structure, inhibition activities, and analytical data of peptides 25-29.

PTPRJ peptides	Sequence	HPLC k ^a	ESI MS		% of cell growth inhibition ^b		
			Found	Calc.	24h	48h	72h
25	[PenHHALTHAPen]	3.24	1043.3	1043.2	5.0±2.1	20.0±5.4	30.0±3.8
26	[PenHHALTHACys]	3.55	1016.3	1015.2	5.0±3.4	10.0±4.6	30.0±1.4
27	[CysHHALTHAPen]	3.75	1016.6	1015.2	-	4.4±6.2	30.0±5.2
28	[CHHGLTHAC]	3.21	976.5	975.1	50.3±5.6	72.3±1.4	75.1±2.82
29	[CHHPLTHAC]	3.36	1016.3	1016.1	38.5±2.12	40.2±2.82	70.0±3.2

^ak'=[(peptide retention time-solvent retention time)/solvent retention time].^bThe relative cell growth was expressed as a percentage of the growth observed in untreated cells at 24, 48, and 72h. ^bThe results are presented as mean values ± SD of at least three independent experiments.

Although peptide cyclization generally induces structural constraints, the size of cyclization can affect the binding affinity of cyclic peptides. In this case, the substitution of Cysteine with Penicillamine (a superior analogue) brings a loss of activity compared with peptide 6.

Interestingly, we found a peptide with a significant increase in inhibitory activity. Peptide **28** was responsible for a 75.1% reduction of cell proliferation versus 66.5% of peptide 6. Instead peptide **29** had an inhibitory activity similar to peptide 6. The substitution of Alanine with Glycine leads to the loss of

chirality in side chain. It suggests it is not necessary the chirality in four residue.

The cyclic structure of Proline forces the ϕ angle to $-65^\circ \pm 15^\circ$, thus preventing the formation of a α -helix, and promoting the formation of a β -turn. Besides, while the barrier to secondary amide cis/trans isomerization is about 10 kcal/mol, the presence of Proline reduces the barrier to just 2 kcal/mol, hence influencing the biological behaviour of peptides.²⁸

In this case, the substitution of Alanine with Proline does not lead an increase in the inhibitory activity, moreover it is maintained.

2.5 Changes to increase stability of peptides (peptides 30-33)

The introduction of D-amino acids²⁹ in a sequence can give the peptide an increased stability, since only a few enzymes that effectively hydrolyse peptide bonds involving D-amino acids have been discovered and characterized in multicellular organisms.

Moreover, D-residues often enforce a different conformation of the peptide,³⁰ and strongly influence receptor affinity and selectivity.

Focused on peptide 6 we decided to change L-Alanine in four with its D-analogue and with D-Proline, to assess the importance of conformation and chirality (peptides 31-32, Table 5).

Moreover, the most promising peptide, compound 6, was also investigated by solution NMR in water solution. NMR parameters of the peptide indicated high conformation flexibility illustrated, for example, by the absence of medium range diagnostic NOEs apart from a weak signal between H β s of ⁴Ala and HN of ⁶Thr. This signal indicates that a β -turn structure centered on residues ⁴Ala⁵Leu is present in a population of conformers. Upfield shift of HN signals of residues ⁵Leu and ⁶Thr, confirms this hypothesis being indicative of the presence of H-bonds involving these amide protons. For this reason we decided to synthesize peptide 33 with ⁵Gly instead ⁵Leu to test the importance of H-bonds.

The reduction of the cycle often increases the stability of peptides, which can prolong their biological activity. For this reason we wanted to check if the

reduction of ring size could improve the inhibitory activity of peptide. Therefore, we decided to eliminate ⁸Ala to reduce the ring size and also to check if it is an essential residue (peptide **30**).

Table 5. Structure, inhibition activities, and analytical data of peptides **28-31**.

PTPRJ Peptides	Sequence	HPLC	ESI MS	
		k' ^a	Found	Calc.
30	[CHHGLTHC]	3.33	905.2	905.0
31	[CHHaLTHAC]	3.24	990.3	990.1
32	[CHHpLTHAC]	3.28	1016.3	1016.2
33	[CHHNGTHAC]	3.26	977.3	977.1

^ak'=[(peptide retention time-solvent retention time)/solvent retention time].

At the same time, we decided to design a new library of peptides, starting from biological results mentioned above with the aim to increase the affinity and stability of peptide, manipulating steric factors that influence protein-ligand interactions.

2.6 Changes in specific position (peptides 34-42)

To extend structure-activity relationships for these series of inhibitors, analyzing the inhibitory activity of peptides 1-10 (Table 1), we decided to bring forward two different approaches: a) changes ⁴Ala with aliphatic, positive and negative charged and aromatic amino acid; b) changes ³His with aliphatic, positive and negative charged and aromatic amino acid.

In particular, we focused on peptides 5 and 6 that showed an inhibitory activity higher than 50%.

Table 6. Structure, inhibition activities, and analytical data of peptides **34-42**.

PTPRJ Peptides	Sequence	HPLC k ^{2a}	ESI MS	
			Found	Calc.
34	[CHHLLTHAC]	3.44	1033.1	1032.7
35	[CHHVLTHAC]	3.42	1019.1	1018.2
36	[CHHDLTHAC]	3.41	1034.4	1034.2
37	[CHHFLTHAC]	3.46	1067.4	1066.3
38	[CHLALTHAC]	3.32	967.3	966.2
39	[CHVALTHAC]	3.33	953.4	952.1
40	[CHDALTHAC]	3.37	969.5	968.3
41	[CHFALTHAC]	3.39	1001.6	1000.3
42	[CHOrnALTHAC]	3.26	968.1	967.5

^ak²=[(peptide retention time-solvent retention time)/solvent retention time].

PTPRJ peptides 34-37 represent an alteration of peptide 6, with the replacement of ⁴Ala with ⁴Leu, ⁴Val, ⁴Asp and ⁴Phe. The same approach was applied in residue 3, added the same amino acids and then ³Orn instead ³His (peptide **42**). The biological activity assays are in progress.

2.7 Changes in lactam bridge (peptides 43-45)

Valuating the biological results obtained with peptides 11-17, the only one that seems to have an inhibitory activity similar than peptide lead, compound 1, is the peptide **17** (19.7% versus 19%) containing a lactam bridge between Glutamic acid and Lysine. Considering the importance of amino acid in four position we wanted to check if the activity of this compound increased with the substitution of ⁴Asn with ⁴Ala, ⁴Gly or ⁴Pro (peptides **43-45**, Table 7).

Table 7. Structure and analytical data of peptides **43-45**.

PTPRJ peptides	Sequence	HPLC	ESI MS	
		k ^{'a}	Found	Calc.
43	[EHHAL ^A THAK]	3.25	1026.1	1025.4
44	[EHHGL ^A THAK]	3.20	1012.3	1011.4
45	[EHHPL ^A THAK]	3.34	1070.3	1069.4

$$^a k' = [(peptide\ retention\ time - solvent\ retention\ time) / solvent\ retention\ time].$$

The biological activity assays are in progress.

2.8 An improvement in the synthesis of PTPRJ analogue, peptide 6

A first attempt to prepare peptide 6 by a standard Fmoc procedure using Wang resin as starting material clearly showed that optimization would be required. For this reason we prepared this compound on acid-labile 2Cl-Trt resin by solid-phase synthesis of linear peptide sequences.

We obtained significant difference in PTPRJ analogue synthesis (see Chemistry section, paragraph 3.4 and Appendix B).

In view of this, common problems during peptide synthesis, purification, and handling can be minimized. Several tips should be taken into consideration whenever possible in the design of a peptide. Chemically synthesized peptides carry free amino and carboxy termini, being electrically charged in general. In order to remove this electric charge, peptide ends are often modified by N-terminal acetylation and/or C-terminal amidation.

Table 8. Structure and analytical data of peptides **46**.

PTPRJ Pepides	Sequence	HPLC	ESI MS	
		k ^{'a}	Found	Calc.
46	Ac[CHH ^A ALTHAC]NH ₂	3.35	1031.4	1031.2

$$^a k' = [(peptide\ retention\ time - solvent\ retention\ time) / solvent\ retention\ time].$$

For internal sequences derived from native proteins, it may be necessary to cap either or both the N- and C-termini to avoid introducing a charge where

there is none in the native sequence. The C-terminus and N-terminus can be capped as an amide (peptide amide-CONH₂ instead of peptide acid-COOH) and acetyl group respectively. Sometimes synthesizing a peptide modified by N-terminal acetylation and/or C-terminal amidation increases its stability and quality.

In fact there are some advantages:

- peptide ends are uncharged, compared to standard synthetic peptides, so modified peptide more closely mimic the native protein. This increases their ability to permeate cells. Therefore, these modifications are required for intracellular, *in-vivo* assays and *in-vitro* functional studies;

- stability toward digestions by aminopeptidases is enhanced therefore these peptides can be used as substrate in enzyme assays;

- peptide ends are blocked against synthetase activities;

- acetylated peptides serve as optimized enzyme substrates amidation of peptides enhances activity of peptide hormones and it also prolongs their shelf life.

Having some problems about synthesis and purification of disulfide peptides: the overall quality of the material was rather low due to a sticky peptide therefore a difficult characterization with the first oxidative method (see paragraph 3.2.1), we check if N-terminal acetylation and/or C-terminal amidation lead to an improvement in the yield (Table 8).

These improvements can be combined to produce a linear precursor clean enough to be oxidized as a crude product, thus increasing the efficiency of the synthetic approach.

In conclusion, these changes resulted in a product with an HPLC profile significantly cleaner than earlier attempt (see Chemistry section).

3. Chemistry

3.1 General procedure for synthesis

The synthesis of peptides (**1-46**) was performed according to the solid phase approach using standard Fmoc methodology in a manual reaction

vessel.³¹ The first amino acid, N^αFmoc-Xaa-OH, was linked onto the Wang resin and was attached to the resin using HOBt/HBTU as an activating agent and a catalytic amount of DMAP.

Fmoc-Cys(Trt)-Wang resin was used to avoid the use of DMAP and collateral reactions due to its.

The following protected amino acids were then added stepwise. Each coupling reaction was accomplished using a HBTU and HOBt as coupling reagents in the presence of DIEA. The N^α-Fmoc protecting groups were removed by treating the protected peptide resin with a 25% solution of piperidine in DMF (1 × 5min and 1 × 25min).

For peptide 46, the last N^α-Fmoc was removed and the amino group was acetylated with acetic anhydride and DIPEA in DCM/DMF for 1h and 30 min.

In addition, after each step of deprotection and after each coupling step, Kaiser test was performed to confirm the complete removal of the Fmoc protecting group, respectively, and to verify that complete coupling has occurred on all the free amines on the resin. Then Kaiser test was performed to confirm the acetylation reaction.

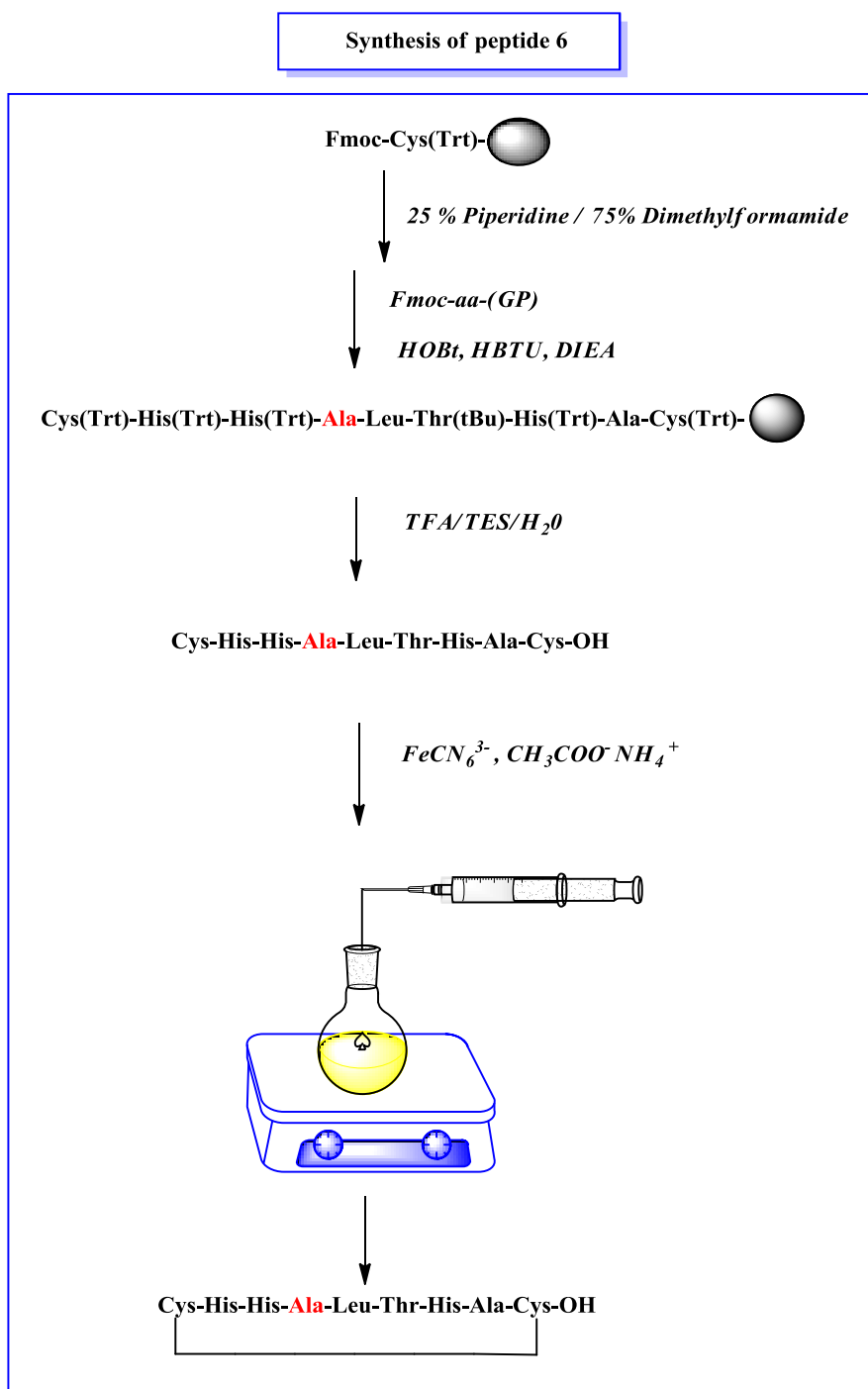
The N-terminal Fmoc group was removed as described above, and the peptide was released from the resin with TFA/iPr₃SiH/H₂O (90:5:5) for 3 h. The resin was removed by filtration, and the crude peptide was recovered by precipitation with cold anhydrous ethyl ether to give a white powder and then lyophilized.

3.2 General method of disulfide bridge formation

3.2.1 Oxidative method with Potassium Ferrocyanide

Oxidation of cysteinyl peptides to form cyclic disulfide-bonded peptides is generally carried out using dilute solutions of peptide in aqueous or aqueous/organic media at weakly basic pH. The classical oxidizing agent K₃Fe(CN)₆ was used in our procedure with the principle that a low concentration of the linear (reduced) peptide is necessary for oxidation.³² Thus, oxidation was performed by slow dropping of a solution of the peptide

into a reaction vessel containing an excess (1.2 eq.) of the oxidizing agent in aqueous solution. The concentration of the reduced peptide was regulated by controlling the speed of addition of the peptide with the help of an automated syringe pump (Scheme 1).



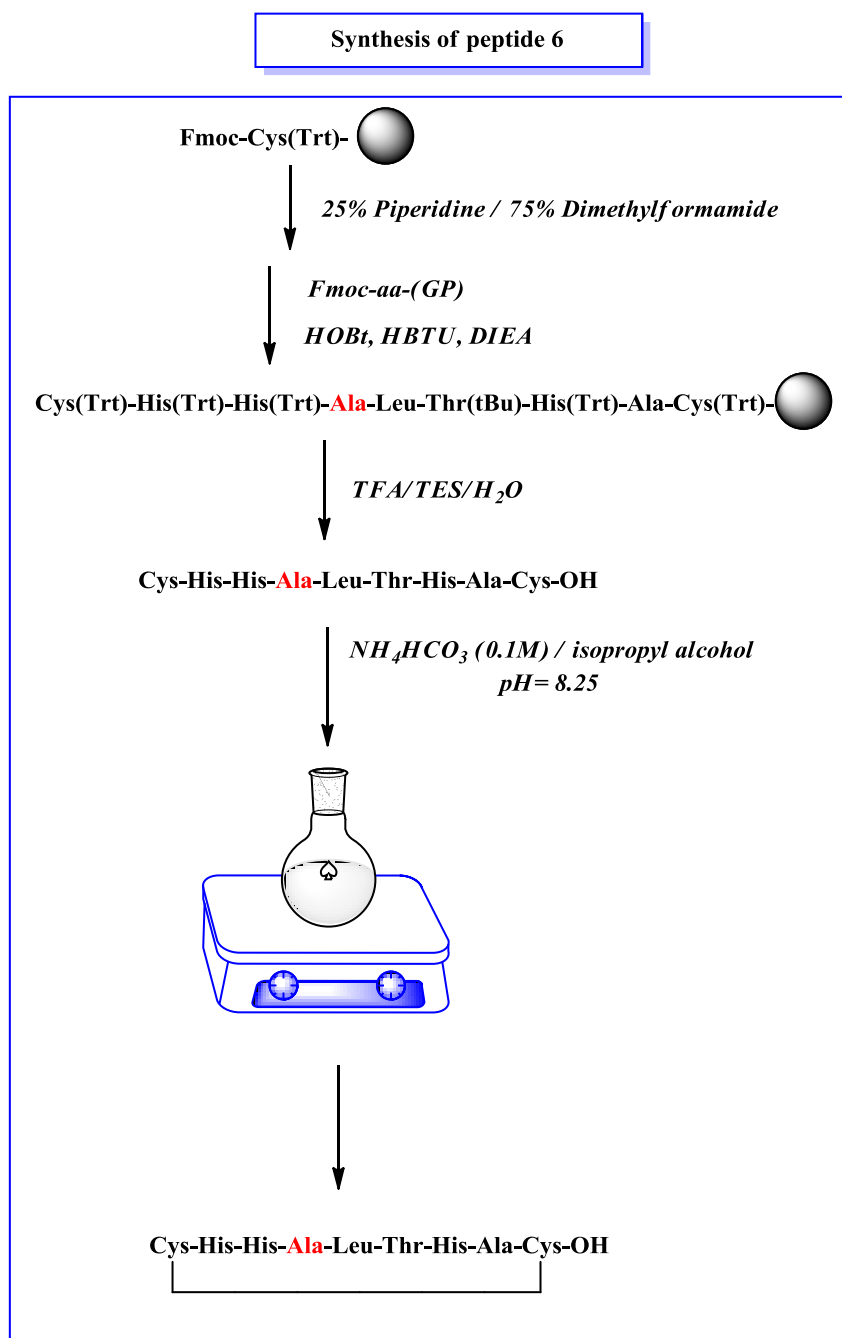
Scheme 1. Synthesis and oxidative folding of peptide 6 (1).

Progress of the folding reaction was monitored by analytical HPLC and, once completed, the target products were purified to homogeneity by preparative RP-HPLC, and subsequently lyophilized. Analytical purity and molecular weight were determined by analytical RP-HPLC and ESI mass spectrometry.

This first attempt to prepare peptide 6 clearly showed that optimization would be required. The overall quality of the material was rather low due to a sticky peptide therefore a difficult characterization. A different oxidative approach was used with the aim to improve the overall quality.

3.2.2 Oxidative method with NH_4HCO_3 / isopropyl alcohol

Air oxidation was carried out by dissolving the lyophilized crude peptide in NH_4HCO_3 /isopropyl alcohol (pH 8.25) with vigorous stirring at RT for 1 h. Prior to purification, the solution was acidified to pH 3 with TFA and analyzed by analytical HPLC. The solution was concentrated and then lyophilized (Scheme 2).³³



Scheme 2. Synthesis and oxidative folding of peptide 6 (2).

In contrast, replacement of the first oxidative method with this one resulted in a product with an HPLC profile significantly cleaner than the previous attempt and with better resolution (Figure 3).

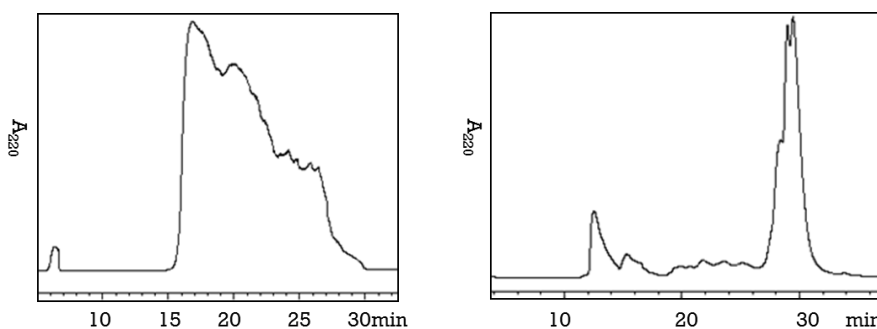


Figure 3. HPLC preparative crude profile of peptide 6 with different oxidative methods.

3.3 Synthesis of lactam analogues (peptides 11-17, 43-45)

The preparation of cyclic peptides, 11-17 and 43-45 through a side-chain-to-side-chain cyclization, was carried out after removal of the Allyl/Alloc protection according to strategy reported by Grieco et al.³⁴ Peptide analytical data are reported in Table 2 and 7.

3.4 Synthesis of disulfide cyclic peptides with 2Cl-Trt resin (peptides 6, 28-29)

A first approach to prepare PTPRJ analogues by a standard Fmoc procedure using Wang resin or Fmoc-Cys(Trt)-Wang resin, as starting material clearly showed that optimization would be required. Accordingly, while LC-MS analysis of the crude product showed the expected peptide without Alanine-Cysteine in C-terminal (m/z 818) as the main peak (Figure 4), the overall quality of the material was rather low.

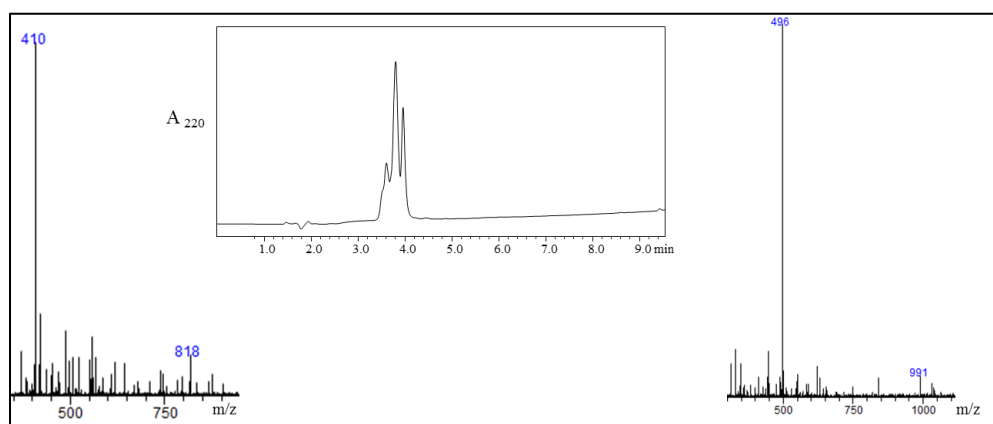


Figure 4. HPLC crude profile of peptide 6 and ESI-MS spectrum of peptide 6: $[M+2H]^{2+}$ (m/z 496), and ESI-MS spectrum of peptide 6 without $^8\text{Ala}^9\text{Cys}$ (m/z 818).

The synthesis of compounds 6, 28 and 29 were prepared on acid-labile 2Cl-Trt resin by solid-phase synthesis of linear peptide sequences, using the Fmoc protection strategy, followed by cyclization with NH_4HCO_3 /isopropyl alcohol as previously described.

At this point it was clear that the replacement of Wang resin with 2Cl-Trt resin had meant a significant difference in PTPRJ analogue synthesis.

2-Chlorotrityl chloride resin is an acid labile resin for peptide synthesis using Fmoc-amino acids. The steric bulk and mild acid conditions for cleavage make 2-chlorotrityl resins useful in many applications. Additionally, Fmoc-amino acids can be attached to 2-chlorotrityl chloride resin with essentially no racemization. Amino acid 2-chlorotrityl resins can be alternatives to Fmoc-amino acid Wang resins where racemization of the first Fmoc-amino acid is common as with Cys and His. The steric size of 2Cl-Trt group not allow the formation of diketopiperazine. Therefore, the formation of diketopiperazine for intramolecular bond of ammine group of the second amino acid to the ester bond is not favorite.

The first N^α -Fmoc amino acid and DIPEA were dissolved in dry dichloromethane (DCM) containing, if necessary, a small amount of dry DMF (enough to facilitate dissolution of the acid). This was added to the resin and

stirred for 30-120 min. Other N^α -Fmoc amino acids were sequentially coupled as previously described.³⁵

General procedure for cyclization: A solution of the linear protected peptide was added at room temperature to a reaction flask containing a solution of HOBt, HBTU and DIPEA in DMF. The mixture was stirred for 24 h at room temperature and monitored by TLC.

3.5 Purification and characterization

All crude peptides were purified by RP-HPLC on a preparative C18-bonded silica column using a Shimadzu SPD 10A UV/VIS detector, with detection at 215 and 254 nm.

All peptides were characterized with analytical RP-HPLC and peptides molecular weights were determined by ESI mass spectrometry and LC-MS in a LC-MS 2010 instrument fitted with a C18 column. All analogues showed >97% purity when monitored at 215 nm. Homogeneous fractions, as established using analytical HPLC, were pooled and lyophilized.

3.5.1 Chromatographic optimization

During my PhD, an improvement for purification and characterization of peptides were done.

The choice of the chromatographic column is a crucial step for an efficient chromatographic separations with better resolution, higher sensitivity and improved peak capacities.

For this reason, we used the core shell technology to increase resolution, reducing time processing.

Core-shell particle technology provides striking increases in peak capacity and resolution at lower backpressure, giving chromatographers the ability to achieve ultra-high performance on any system, HPLC or UHPLC.

A uniform porous silica layer is grown around a solid, spherical silica core, providing effective retention and selectivity with improved resolution, speed, and recovery. Next, optimizing the pore size and shell thickness for intact

proteins or smaller peptide fragments provides well-defined depth penetration of biomolecules leading to maximum separation power.

Concerning chromatographic columns for preparative HPLC, the Jupiter HPLC column portfolio, including Jupiter 300 and Jupiter Proteo, offers optimized reversed phase solutions for protein characterization and purification. With these columns, one can identify, purify, and analyze almost any protein. In particular, 300 Å column designed for intact protein purification and analysis allowed a separation of proteins $\geq 10,000$ MW producing excellent peak shape and resolution of protein samples. Instead 90 Å column engineered for peptide mapping and peptide separations allowed a separation of proteins and peptides $\leq 10,000$ MW, increasing peak capacity and resolution. Specifically, we used a preparative Jupiter Proteo column for all PTPRJ analogues and GRK2 inhibitors instead Jupiter 300 column for other compounds we will see in the third chapter.

For all these reasons, an alternative oxidative method together with an improvement in HPLC purification and characterization allowed us to achieve the amount of solid pure product ca. 5 times higher than with the standard procedure.

4. Results and discussion

4.1 PTPRJ Ala scan peptide derivatives inhibit HeLa cancer cell proliferation

Through a phage display library screening, Trapasso et al., recently identified two nonapeptides (named PTPRJ 19 and 24, peptide **1** and **2**) with the ability to bind and trigger PTPRJ activity; these peptides could induce MAPK dephosphorylation and inhibit cell growth of HeLa and HUVEC cells, although to a low extent.²³ Here, in order to generate PTPRJ peptide agonists with improved biological activity, we (a) investigated the role of the peptide circularization, synthesizing a peptide 1 derivative deprived of the disulfide bridge between the first and the last Cysteine residues, and then (b) pursued an Ala scan procedure consisting in the systematic substitution of each peptide 1 residue with a L-Alanine (Table 1).

This latter approach resulted in the generation of a panel of nine peptides, named peptide 1 to 10. All new derivatives were tested in HeLa cancer cells for the assessment of their ability to inhibit cell proliferation; cells were treated with 160 μ M concentration of each compound, and cell count was performed 24, 48, and 72 h after treatment. Interestingly, peptide **6** was responsible for a reduction of cell proliferation up to 66.5% versus 20% of peptide lead (Figure 5). Values of cell growth inhibition for all tested peptides in this experiment are reported in Table 1.

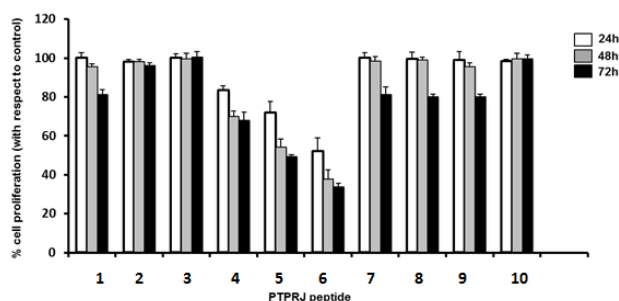


Figure 5. Cell growth inhibition induced by PTPRJ peptides in HeLa cells. Relative cell growth (as a percentage of the growth observed in untreated cells) at different intervals of treatments (from 24 to 72 h) is reported. HeLa cells were treated once with PTPRJ peptides for 24 h (white columns) or treated every 24 h for 48 h (gray columns) and for 72 h (black columns). Results represent the mean \pm SD of three independent experiments. *P < 0.05, **P < 0.01, ***P < 0.001 compared to untreated cells by unpaired two-tailed Student's t test.

The above-reported data suggested important structure-activity relationships for this small library of derivatives. First, the disulfide bridge appears to have effect upon cell growth inhibition as demonstrated by our previous work.²³ In fact, all three linear compounds used, namely, peptide 2 (that only differs from PTPRJ 19 for the absence of the disulfide bridge) and peptide 3 and peptide 10 (which incorporate an Ala residue at position 1 and 9, respectively), lost their ability to activate PTPRJ (Table 1).

Second, the most interesting result was obtained with peptides modified at the peptide 1 N-terminus. In fact, the substitution of ³His or ⁴Asn into the cyclic peptide 1 by Ala produced a dramatic increase in the biological activity of the corresponding analogues (peptide **5** or peptide **6**), resulting in a cell

growth inhibition ranging from two to three times higher compared to their lead compound. In particular, the observed effect was time dependent, generating a 48%, 62.5%, and 66.5% reduction of HeLa cell number at 24, 48, and 72 h, respectively for peptide **6**. These data suggest that either a lack of polar side chains in these positions or the introduction of low hindrance, lipophilic features is well accepted.

Finally, the substitution of ⁵Leu or ⁶Thr or ⁷His residues by Ala (peptide 7, 8 and 9) did not modify the weak cell growth inhibition levels exhibited by peptide lead.

4.1.1 Ala scan PTPRJ 19 (peptide 1) derivatives negatively modulate ERK1/2 phosphorylation and induce apoptosis of HeLa cancer cells

According to recent published results,²³ treatment of HeLa cells with 160 μ M peptide 1 resulted in a dramatic reduction of the ERK1/2 phosphorylation; the dephosphorylation effect reported in previous investigation was rapid and transient and reached its peak within 15 min after treatment. In order to test the effects of the newly Ala scan generated derivatives on ERK1/2 phosphorylation, we used the same approach as previously reported.²³ HeLa cells were treated with 160 μ M concentration of the most potent antiproliferative compounds described in the previous section (peptides 4-6). As shown in Figure 6A, peptides 4 and 5 reduced the ERK1/2 phosphorylation extent in a short term; these results are comparable to those observed with their precursor. Interestingly, the treatment with peptide **6** induced a time-dependent reduction of ERK1/2 phosphorylation that reached its maximum at 60 min. ERK1/2 phosphorylation was also assessed 12, 24, and 48 h after peptide 6 treatment of HeLa cells; as shown in Figure 6B, we observed a slight reduction of ERK1/2 phosphorylation extent in all cases. To further expand the concept of functional specificity of the peptide 6/PTPRJ interaction, we knocked-down endogenous PTPRJ protein with specific siRNAs in HeLa cells. Forty-eight hours after transfection, cells were treated with either peptide 6 and scramble peptide (typically used as a negative controls to show that a specific sequence is critical to the protein function or activity), and 1 h later

we evaluated the ERK1/2 phosphorylation extent. Interestingly, ERK1/2 phosphorylation of PTPRJ knocked-down cells treated with peptide 6 was higher compared to control treated with peptide 6 alone, suggesting that ERK1/2 dephosphorylation is mediated by the PTPRJ protein levels (Figure 6C).

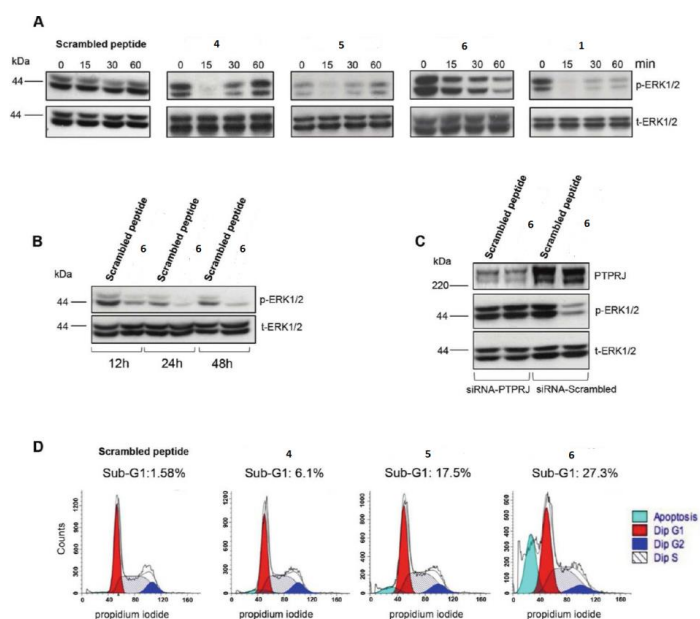


Figure 6. Peptides 4-6 synthetic peptides suppress phosphorylation of ERK1/2 and induce cell death of HeLa cancer cells. (A) HeLa cells were seeded in 6-well plates and, 24 h later, treated with 160 μ M peptides 4-6, lead compound, or scrambled peptide at 0, 15, 30, and 60 min. Cell lysates were subjected to immunoblotting using a phospho-specific ERK1/2 (p-ERK) antibody. Blots were stripped and reprobed for total ERK1/2 as a loading control. (B) HeLa cells were treated either with 160 μ M peptide 6 or scrambled peptide, and cells were collected at the indicated intervals (12, 24, and 48 h). Cell lysates were subjected to immunoblots using phospho-specific ERK1/2 (p-ERK). Blots were stripped and reprobed for total ERK1/2 antibody as a loading control. (C) HeLa cells were transfected with either 100 nM PTPRJ or scrambled siRNAs and 48 h later were treated with either 160 μ M peptide 6 or scrambled peptide for 1 h. Cell lysates were subjected to immunoblotting using an anti-PTPRJ antibody and a phospho-specific ERK1/2 (p-ERK) antibody. Blots were stripped and reprobed for total ERK1/2 as a loading control. (D) Representative experiment of cell cycle analysis of HeLa cells treated with 4-6 synthetic peptides. The percentage of sub-G1 population is reported on the top of each histogram. Data analysis was performed with ModFit LTTM cell cycle analysis software.

We also evaluated cell cycle perturbations induced by peptides 4-6 on HeLa cells. Twenty four hours after treatment, cells were collected and investigated by flow cytometric analysis; in Figure 6D is indicated the percentage of a sub-G1 population, suggestive of apoptotic cell death.

Interestingly, while the administration of peptide 4 was able to trigger cell death only in 6.1% of cell population, HeLa cells treated with peptide 5 and 6 showed a 17.5% and 27.3% of dead cells, respectively.

4.1.2 Peptide 6 partly inhibits cell proliferation of HUVECs and blocks in vitro tube formation

In order to investigate the biological effects of peptide 6 on normal endothelial cells, HUVECs were treated with 160 μ M peptide. Similarly to what observed with HeLa cells, peptide 6 significantly reduced the ERK1/2 phosphorylation extent in HUVEC cells in a time-dependent manner (Figure 7A). No differences in ERK1/2 phosphorylation were observed in HUVEC cells after a scramble peptide administration (data not shown). Instead, cell growth assessment performed 24, 48, and 72 h after treatment showed a different behavior in HUVEC compared to HeLa cells. In fact, no significant differences were noticed 24 h after treatment compared to the control, while a 48% inhibition was reported with HeLa cells. Moreover, we only observed a 28% and 32% of cell growth inhibition 48 and 72 h after treatment, respectively (Figure 7B) versus 62.5% and 66.5% described 48 and 72 h after treatment of HeLa cells, respectively (see Table 1). To investigate the role of VEGFR2 on peptide 6-mediated ERK1/2 dephosphorylation and cell growth inhibition on HUVECs, we assayed the phosphorylation state of VEGFR2 in VEGF stimulated HUVECs treated with or without peptide 6. As reported in Figure 7C, we observed a significant reduction of phospho-VEGFR2, thus suggesting an impaired signaling by this receptor in cells treated with peptides 6. The production of tubular structures is an important step in angiogenesis; therefore, as PTPRJ activity antagonizes VEGFR2 function,³⁶ we investigated the role of peptide 6 on HUVEC tube formation. As shown in Figure 7D, control HUVEC cells, plated on Matrigel and incubated either with control

medium or a scramble peptide, formed lumen-like structures, while HUVEC cells treated with peptide **6** formed fewer tubes as well as fewer and weaker anastomoses.

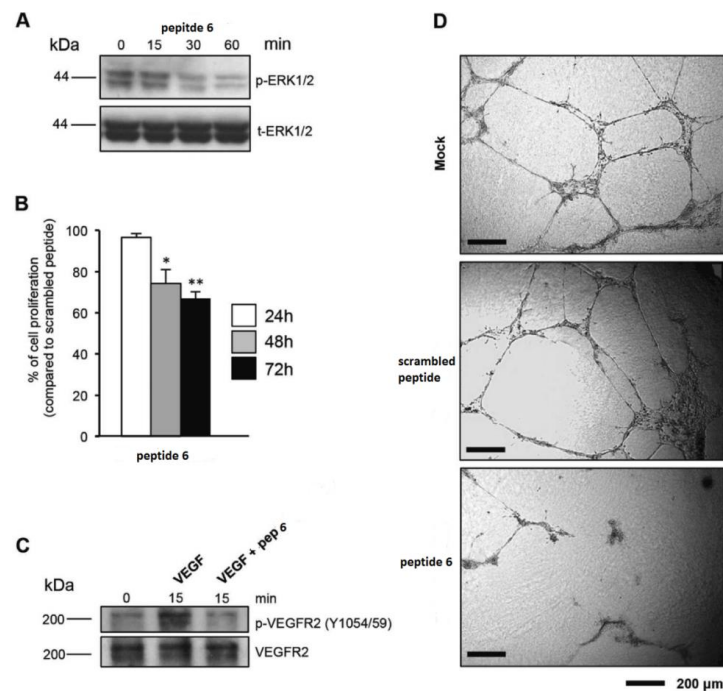


Figure 7. Peptide 6 negatively modulates ERK1/2 phosphorylation and inhibits both cell proliferation and tube formation of HUVEC endothelial cells. (A) Peptide 6 suppresses phosphorylation of ERK1/2 in HUVECs; cells were treated with 160 μ M peptide 6 and collected at the indicated intervals (15–60 min). Cell lysates were subjected to immunoblots using phospho-specific ERK1/2 (p-ERK). Blots were stripped and reprobed for total ERK1/2 antibody as a loading control. (B) Cell growth inhibition induced by peptide 6 in HUVECs at 24 h (white columns), treated every 24 h for 48 h (gray columns) and every 24 h for 72 h (black column). Results represent the mean \pm SD of three independent experiments. * $P < 0.05$, ** $P < 0.01$ compared to scrambled peptide by unpaired two-tailed Student's *t* test. (C) HUVECs were serum starved, stimulated with 20 ng/mL of VEGF, treated 15 min with or without peptide 6, and then lysed. VEGFR2 phosphorylation levels were detected by immunoblotting with a phospho-specific VEGFR2 (Y1054/1059) antibody. Membranes were stripped and immunoblotted with a VEGFR2 antibody. (D) Peptide 6 inhibits tube formation of primary endothelial cells on Matrigel. Representative photograph of antitube formation activity of peptide 6. HUVECs (2.5×10^4 /well) were untreated or preincubated either with peptide 6 or scrambled peptide (100 μ M) for 30 min before being seeded onto the solidified Matrigel for 18 h. (scale bar: 200 μ M).

4.1.3 Peptide 6 negatively modulates ERK1/2 phosphorylation and reduces cell proliferation of mammary

Cancer Cells. To evaluate if the effects of peptide **6** on HeLa cells could be considered a general event in cancer cells, we also included in our investigation two mammary cancer cell lines, MCF-7 and SKBr3, which both express endogenous PTPRJ (data not shown). Both cell lines were treated with 160 μ M peptide 6, as previously described, and both ERK1/2 phosphorylation and growth rate were assessed. This compound negatively modulated ERK1/2 phosphorylation extent in the short term (Figure 8A); moreover, we observed a significant cell growth inhibition resulting in a reduction of about 40% compared to controls in both cell lines (Figure 8C) at 72 h.

To check if peptide **6** administration was toxic to normal cells, the above-described experiments were also carried out on primary human mammary epithelial cells (HMECs). Intriguingly, no effects on both ERK1/2 phosphorylation and proliferation were observed in normal cells (Figure 8B, C).

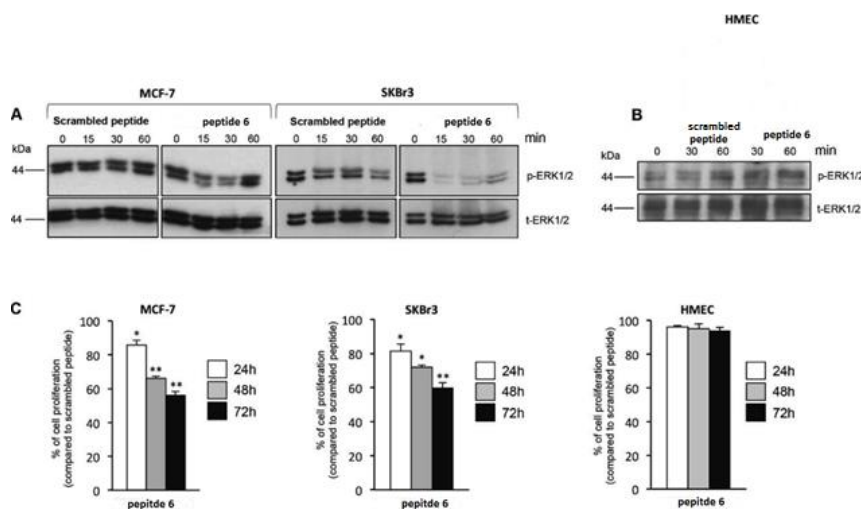


Figure 8. Peptide 6 negatively modulates ERK1/2 phosphorylation and reduces cell proliferation of human mammary cancer cells. (A) MCF-7 and SKBr3 cells were seeded in 6-well plates and, 24 h later, treated with either 160 μ M peptide 6 or scrambled peptide, and lysed at 0, 15, 30, 60 min. Cell lysates were subjected to immunoblotting using a phospho-specific ERK1/2 (p-ERK) antibody. Blots were stripped and reprobed for total ERK1/2 as a loading control. (B) HMECs were treated with 160 μ M peptide 6 or scrambled peptide, and cells were collected at the indicated intervals. Cell lysates were subjected to immunoblots using phospho-specific ERK1/2 (p-ERK). Blots were stripped and reprobed for total ERK1/2 antibody as a loading control. (C) Cell growth rate of MCF7, SKBr3, and HMECs by peptide 6 peptide. Relative cell growth (as a percentage of the growth observed in cells treated with scrambled peptide) at different intervals of treatments (from 24 to 72 h) is reported. Cells were treated once with peptide 6 and scrambled peptides for 24 h (white columns) or treated every 24 h for 48 h (gray columns) and for 72 h (black columns).

Results represent the mean \pm SD of three independent experiments. *P < 0.05, **P < 0.01 compared to scrambled peptide by unpaired two-tailed Student's t test.

4.1.4 Molecular Modeling of Ala scan PTPRJ-binding derivatives suggests supramolecular aggregation states

Monte Carlo (MC) conformational search, docking experiments, thermodynamics, and statistical analyses were performed with the aim to rationalize at molecular level the biological properties of our PTPRJ agonist peptides comparing their structural features to those of the lead compound, peptide 1 (see Experimental section for further details).

As in the case of other PTPRJ peptide binders, the MC search of peptide 1 to -10 revealed a large number of local minimum energy conformers (data not shown). Following the same computational approach reported in recent communication,²³ the self-aggregation trend of the new peptides was investigated by means of docking simulation coupled to thermodynamics and statistical analyses (see Experimental section). Results clearly indicate that all peptides formed multiple conformation self aggregates with 1:1 stoichiometry (data not shown).

Peptides 3-5 and 7-10 reported an overall complexes stabilization (ΔG) notably weaker than that of peptide 1. Only peptide 6 maintained a thermodynamic profile comparable to the lead compound. Statistic data, obtained by coupling Boltzmann population and clustering analyses, revealed for all new derivatives, excluding peptide 5, a number of possible geometry clusters larger than peptide lead and, with the exception of derivative 3, increased population of the global minimum energy structures.

Graphic inspection of the most stable complexes and their α carbons alignment onto peptide lead strongly indicated that only the derivative 6 could be related to the lead compound (Figure 9), while all other derivatives were different in terms of both shape and chemical features exposition.

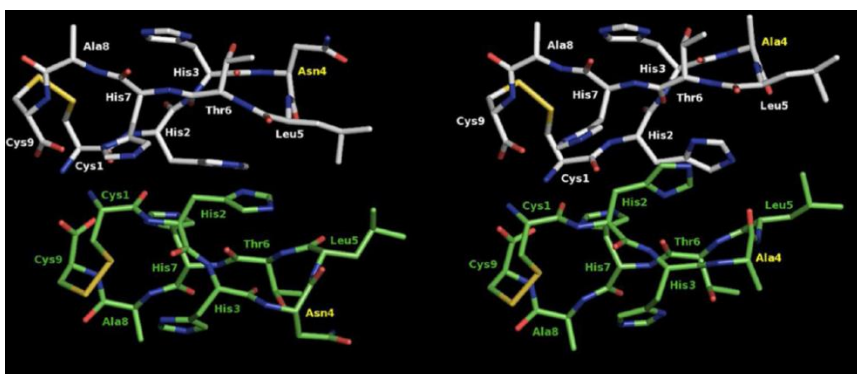


Figure 9. Graphic comparison of peptide lead (on the left) and peptide 6 (on the right) most stable self-aggregates. Peptides are depicted in polytube, and complex subunits are colored in CPK and green carbons, respectively.

4.1.5 NMR analysis indicates that peptide 6 folds as a β -Turn and shows propensity to dimerization

The most promising peptide, derivative **6**, was also investigated by solution NMR in water solution. Similarly to its precursor, peptide lead, the spectra showed splitting of the signals. Complete ^1H NMR chemical shift assignments were achieved for the most intense signal pattern according to the Wüthrich procedure³⁷ (data not shown). NMR parameters of the peptide indicated high conformation flexibility illustrated, for example, by the absence of medium range diagnostic NOEs apart from a weak signal between H β s of ^4Ala and HN of ^6Thr . This signal indicates that a β -turn structure centered on residues $^4\text{Ala}^5\text{Leu}$ is present in a population of conformers. Upfield shift of HN signals of residues ^5Leu and ^6Thr , compared to the corresponding in peptide 1 and relatively low temperature coefficient of HN-6 ($-\Delta\delta/\Delta T = 4.3$ ppb/K), confirms this hypothesis being indicative of the presence of H-bonds involving these amide protons. Unfortunately, diagnostic H α -HN $i,i+2$ NOE signal between residues 4 and 6 could not be observed due to overlapping. This turn structure is in accordance with the molecular modeling results (Figure 9). Furthermore, to check the aggregation state of peptide 6 under the NMR conditions, STD-NMR experiments were recorded (data not shown).³⁸ As for peptide lead, on-resonance irradiation induces detectable STD signals with relative STD effect of about 1% (0.7% was found for peptide 1), suggesting that aggregation properties of the two peptides are similar with high propensity to dimerization.

4.2 Lactam cyclic peptide derivatives action on HeLa cancer cell proliferation (peptides 11-17)

Peptide cyclization is a well established approach to improve peptide biological activity³⁹ which stems from reduced conformational freedom of the parent peptide and thus a better defined secondary structure required for efficient receptor-ligand interaction, *i.e.*, “bioactive conformation”.⁴⁰ It has been previously noted that the success of a peptide cyclization depends

strongly on the probability of juxtaposition of the reactive groups of the linear peptide precursor, and is usually encumbered by side reactions, most notably, oligomerizations and cyclo oligomerizations.

Depending on its functional groups, a peptide can be cyclized in four different ways: head-to-tail (C-terminus to N-terminus), head-to-side chain, side chain-to-tail or side-chain-to-side-chain. Of the various methods of synthesizing cyclic peptides, most often the final ring-closing reaction is a lactamization, a lactonization or the formation of a disulfide bridge. For example, an effective side-chain-to-side-chain macrocyclization involves a condensation reaction between side chains of aspartic or glutamic acid and lysine residues.⁴¹ Therefore, the replacement of the disulfide bridge by a chemically more stable moiety appeared as an attractive alternative.

In this case, in order to generate PTPRJ peptide agonists with improved biological activity, we investigated the role of the peptide circularization, synthesizing a peptide 1 derivatives. These compounds derived of the lactam bridge with the aim to implement the global conformational constraint and the ring size (Table 2).

This latter approach resulted in the generation of a panel of seven peptides, named peptide 11 to 17. All new derivatives were tested in HeLa cancer cells for the assessment of their ability to inhibit cell proliferation; cells were treated with 160 μ M concentration of each compound, and cell count was performed 24, 48, and 72 h after treatment. Interestingly, no one peptides were responsible for a reduction of cell proliferation greater of peptide 6 (Figure 10). Values of cell growth inhibition for all tested peptides in this experiment are reported in Table 2.

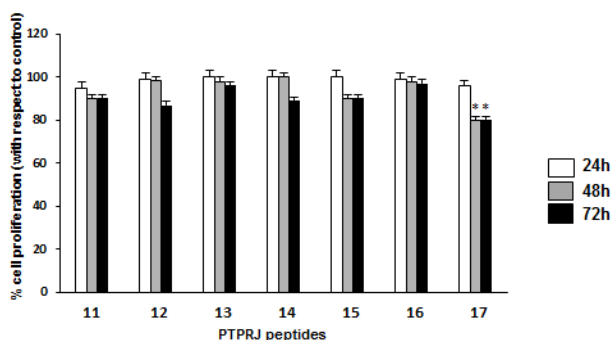


Figure 10. Cell growth inhibition induced by PTPRJ peptides in HeLa cells. Relative cell growth (as a percentage of the growth observed in untreated cells) at different intervals of treatments (from 24 to 72 h) is reported. HeLa cells were treated once with PTPRJ peptides for 24 h (white columns) or treated every 24 h for 48 h (gray columns) and for 72 h (black columns). Results represent the mean \pm SD of three independent experiments. * $P < 0.05$, ** $P < 0.01$, *** $P < 0.001$ compared to untreated cells by unpaired two-tailed Student's *t* test.

The above-reported data suggested important structure-activity relationships for this small library of derivatives. First, disulfide bridge appears to have more effect upon cell growth inhibition respect to lactam bridge. In fact, six compounds lost their ability to activate PTPRJ except peptide **17**. This compound presents a lactam bridge with a negative charged in side chain in N-terminal residue and a positive charged in side chain in C-terminal residue. These substitutions produce an increase in the biological activity of the corresponding analogues (peptides 11-16), resulting in a cell growth inhibition ranging from one to two times higher compared to other lactam cyclic peptides. In particular, the observed effect was time dependent, generating a reduction of HeLa cell number only at 48 and 72 h (20 and 19.7 % respectively) resulting in an improvement at 48h in term of reduction of HeLa cell number. Instead at 72h the activity we get more or less similar with respect to the peptide lead, peptide 1. This data suggest that either an acid side chain in N-terminal residue and a basic side chain in C-terminal residue is well accepted.

4.3 PTPRJ Ala scan peptide 6 derivatives action on HeLa cancer cell proliferation

Through Alanine scanning procedure, we wanted to evaluate if there are amino acid side chains involved in the interaction with the target molecule. Therefore, being interested in the development of analogues with higher inhibitory potency, we decided to apply for the second time an Alanine scanning approach to the most active peptide, compound 6.

This latter approach resulted in the generation of a panel of seven peptides, named 18-24. All new derivatives were tested in HeLa cancer cells for the assessment of their ability to inhibit cell proliferation; cells were treated with 160 μ M concentration of each compound, and cell count was performed 24, 48, and 72 h after treatment (Figure 11).

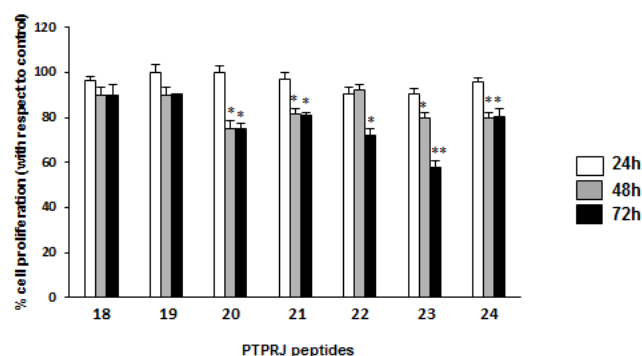


Figure 11. Cell growth inhibition induced by PTPRJ peptides in HeLa cells. Relative cell growth (as a percentage of the growth observed in untreated cells) at different intervals of treatments (from 24 to 72 h) is reported. HeLa cells were treated once with PTPRJ peptides for 24 h (white columns) or treated every 24 h for 48 h (gray columns) and for 72 h (black columns). Results represent the mean \pm SD of three independent experiments. * $P < 0.05$, ** $P < 0.01$, *** $P < 0.001$ compared to untreated cells by unpaired two-tailed Student's t test.

Interestingly, compound **23** was responsible for a reduction of cell proliferation up to 40% versus 20% of peptide 1.

In particular, the observed effect was time dependent, generating a 20.1% and 42.1% reduction of HeLa cell number at 48 h and 72 h respectively. These data suggest that either a lack of polar and positive charged in side chains

(⁷His) in this position or the introduction of low hindrance, lipophilic features is well accepted.

4.4 Peptides 25-29 action on HeLa cancer cell proliferation

Although peptide cyclization generally induces structural constraints, the size of cyclization within the sequence can affect the binding affinity of cyclic peptides. In this case, the substitution of Cysteine with Penicillamine (a superior analogue) brings a loss of activity compared to peptide 6 (30.0% versus 66.5%).

Interestingly, we find a peptide with a significant increase in inhibitory activity. Peptide **28** was responsible for a 75.1% reduction of cell proliferation versus 66.5% of the peptide 6. Instead compound **29** has an inhibitory activity similar to peptide 6 (70.0% versus 66.5%) (Figure 12).

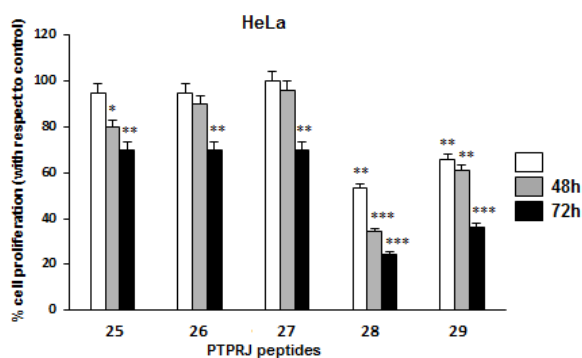


Figure 12. Cell growth inhibition induced by PTPRJ peptides in HeLa cells. Relative cell growth (as a percentage of the growth observed in untreated cells) at different intervals of treatments (from 24 to 72 h) is reported. HeLa cells were treated once with PTPRJ peptides for 24 h (white columns) or treated every 24 h for 48 h (gray columns) and for 72 h (black columns). Results represent the mean \pm SD of three independent experiments. *P < 0.05, **P < 0.01, ***P < 0.001 compared to untreated cells by unpaired two-tailed Student's t test.

All new derivatives were tested in HeLa cancer cells for the assessment of their ability to inhibit cell proliferation; cells were treated with 160 μ M concentration of each compound, and cell count was performed 24, 48, and 72 h after treatment.

In particular, the observed effect was time dependent, like previous results, like generating a 75.1% and 70.0% reduction of HeLa cell number only at 72 h, for peptide **28** and **29** respectively. These data suggest that either a lack of chirality in side chain (⁴Gly) or the introduction of steric hindrance increase the activation of the target.

For peptides **30-46** the biological assays are in progress.

5. Conclusion

As recently reviewed,⁴² protein phosphatases represent a very interesting target for the development of novel therapeutics. The ability of PTPRJ to counteract the signaling from several protein kinases either transmembrane or soluble involved in the aberrant mitogenic signals^{43,44} makes this protein tyrosine phosphatase receptor a particularly intriguing target for the generation of a novel class of protein kinase inhibitors as anticancer drugs^{45,46} in addition to monoclonal antibodies and small molecules already available for current cancer therapies.^{47,48}

Being interested in the development of small-molecule agonists of PTPRJ, we focused our attention on PTPRJ 19 (peptide **1**) that in vitro, was shown to be responsible for both biochemical and biological PTPRJ-mediated effects. Several general approaches to development different libraries of peptides have been used and in particular from L-Ala scanning analysis it was identified peptide **6** as a potent agonist of PTPRJ. It showed ability in blocking the organization of HUVECs into tubular structures in Matrigel; this finding further supports the idea that peptide **6** could be a useful tool in the design and discovery of additional agents that can inhibit pathologic neovascularization. We were interested to modify the structure of the most active peptide with the aim to generate peptidomimetics to be used in cancer treatment. Therefore, recent results on analogues of peptide **6** demonstrate that compound **28** inhibits cell proliferation of 75.1% instead 66.5% of peptide lead. In conclusion, our study represents a significant advancement in the structure-activity relationship knowledge related to the presented class of PTPRJ agonist peptides; moreover, our findings strongly encourage the applications of further

chemical modifications to PTPRJ peptides with the aim to create a novel class of small molecules with improved biological activity with the final goal to translate them into clinical practice.

6. Experimental section

6.1 Synthesis of Ala scan PTPRJ derivatives

The synthesis of PTPRJ analogues was performed according to the solid phase approach using standard Fmoc methodology in a manual reaction vessel.³¹ N^α-Fmoc-protected amino acids, Wang-resin, Fmoc-Cys(Trt)-Wang resin, 2Cl-Trt resin, HOBt, HBTU, DIEA, DMAP, Piperidine, and trifluoroacetic acid were purchased from Iris Biotech (Germany). Peptide synthesis solvents, reagents, and CH₃CN for HPLC were reagent grade and were acquired from commercial sources and used without further purification unless otherwise noted. The first amino acid (for disulfide bridge peptides) N^α-Fmoc-Cys(Trt)-OH or N^α-Fmoc-Pen(Trt)-OH was coupled to Wang resin (0.2 g, 0.7 mmol of NH₂/g). The following protected amino acids were then added stepwise: N^α-Fmoc-Ala-OH, N^α-Fmoc-Gly-OH, N^α-Fmoc-Pro-OH, N^α-Fmoc-Val-OH, N^α-Fmoc-Asp(tBu)-OH, N^α-Fmoc-Phe-OH, N^α-Fmoc-Orn(Boc)-OH, N^α-Fmoc-DAla-OH, N^α-Fmoc-DPro-OH, N^α-Fmoc-His(N_(im)-trityl (trt))-OH, N^α-Fmoc-Thr(O-tert-butyl (tBu))-OH, N^α-Fmoc-Leu-OH, N^α-Fmoc-Asn (N_γ-trityl, trt)-OH, N^α-Fmoc-Cys(trt)-OH.

Each coupling reaction was accomplished using a 3-fold excess of amino acid with HBTU and HOBt in the presence of DIEA (6 equiv). The N^α-Fmoc protecting groups was removed by treating the protected peptide resin with a 25% solution of Piperidine in DMF (1 × 5 min and 1 × 25 min).

The peptide resin was washed three times with DMF, and the next coupling step was initiated in a stepwise manner. The peptide resin was washed with DCM (3×), DMF (3×), and DCM (3×), and the deprotection protocol was repeated after each coupling step.

The N-terminal Fmoc group was removed as described above, and the peptide was released from the resin with TFA/*i*Pr₃SiH/H₂O (90:5:5) for 3 h.

The resin was removed by filtration, and the crude peptide was recovered by precipitation with cold anhydrous ethyl ether to give a white powder and then lyophilized.

6.2 General method of disulfide bridge formation

6.2.1 Method of disulfide bridge formation with Potassium Ferrocyanide

A solution of $K_3Fe(CN)_6$ was prepared as follows: 1 mmol (330 mg) of $K_3Fe(CN)_6$ was dissolved in a mixture of water (100 mL) and CH_3CN (20 mL), a saturated solution of ammonium acetate (20 mL) was added to it and the pH was adjusted to 8.5 with concentrated ammonium hydroxide.¹⁴

A solution of the linear peptide (0.25 mmol) in 20% aqueous CH_3CN was added to the above solution dropwise overnight with the help of a push±pull syringe. After the overnight reaction, glacial acetic acid was added to the reaction mixture to obtain pH 4.0, followed by 20 mL of Amberlite IRA-68 anion-exchange resin (pre-equilibrated with 2.0 M HCl) and the suspension was stirred for 30 min until the solution turned colorless and the resin turned yellow. The resin was suction-filtered and the filtrate rotoevaporated using 1-butanol to form a water/1-butanol azeotrope. The residual oil was lyophilized overnight to yield a pale yellow solid.

6.2.2 Method of disulfide bridge formation with NH_4HCO_3 /isopropyl alcohol

Air oxidation was carried out by dissolving 50 mg of the lyophilized crude peptide in 90 mL of 1:1 0.1 M NH_4HCO_3 /isopropyl alcohol (pH 8.25) with vigorous stirring at RT for 1 h. Prior to purification, the solution was acidified to pH 3 with TFA and analyzed by analytical HPLC. The solution was concentrated using a rotary evaporator at 30°C and then lyophilized.³³

6.3 Synthesis of lactam analogues (peptides 11-17, 43-45)

The corresponding linear peptides were synthesized as described above and the amino acids N^α -Fmoc-Asp(Allyl)-OH, N^α -Fmoc-Glu(Allyl)-OH and N^α -Fmoc-Lys(Alloc)-OH, N^α -Fmoc-Orn(Alloc)-OH and N^α -Fmoc-Dap(Alloc)-OH were used as lactam precursors. After linear assembly, the N^γ -Alloc and the Allyl groups were removed according to the following procedure: 200 mg of peptide resin was washed with dichloromethane (DCM) under Ar and a solution of PhSiH_3 (24 equiv) in 2 mL of DCM was added. Subsequently a solution of $\text{Pd}(\text{PPh}_3)_4$ (0.25 equiv) in 6 mL of DCM was added and the reaction was allowed to proceed under Ar for 30min. The peptide resin was washed with DCM (3x), DMF (3x) and DCM (4x), and the deprotection protocol was repeated (3x). The macrocyclic lactam ring formation was mediated by addition of HBTU (6 equiv), HOBT (6 equiv) and DIPEA (12 equiv) for 2 h.²⁴ The process was repeated if necessary (Kaiser test used to monitor completion). The N-terminal Fmoc group was removed and the peptide was released from the resin as described above.

6.4 Synthesis of disulfide cyclic peptides with 2-Cl Trt resin (peptides 6, 28-29)

The title peptides were synthesized using a 2-chlorotrityl chloride resin. The first N^α -Fmoc amino acid (0.6–1.2 equiv relative to the resin for 2-chlorotrityl resin) and DIPEA (4 equiv relative to amino acid) were dissolved in dry dichloromethane (DCM) (approx. 10 mL per gram of resin) containing, if necessary, a small amount of dry DMF (enough to facilitate dissolution of the acid). This was added to the resin and stirred for 30-120 min. After stirring, the resin was washed with 3×DCM/MeOH/DIPEA (17:2:1), 3×DCM, 2×DMF and 2×DCM. Other N^α -Fmoc amino acids (4 equiv.) were sequentially coupled as previously described. The final cleavage with AcOH/MeOH/DCM (1:1:8) resulted in protected peptides.³⁵

6.5 Purification and characterization of PTPRJ derivatives

All crude cyclic peptides were purified by RP-HPLC on a preparative C18-bonded silica column (Phenomenex, Jupiter Proteo 90Å, 100 mm × 21.2 mm, 10µm) using a Shimadzu SPD 10A UV-Vis detector, with detection at 210 nm and 254 nm. The column was perfused at a flow rate of 15 mL/min with solvent A (10%, v/v, water in 0.1% aqueous TFA), and a linear gradient from 10% to 90% of solvent B (80%, v/v, acetonitrile in 0.1% aqueous TFA) over 15 min was adopted for peptide elution. Analytical purity and retention time (tR) of each peptide were determined using HPLC conditions in the above solvent system (solvents A and B) programmed at a flow rate of 1 mL/min using a linear gradient from 10% to 90% B over 15 min, fitted with Phenomenex, Aeris XB-C18 column (150 mm × 4.60 mm, 3.6 µm). All analogues showed >97% purity when monitored at 215 nm. Homogeneous fractions, as established using analytical HPLC, were pooled and lyophilized.

At the same time, LC-MS was performed in a LC-MS 2010 instrument (Shimadzu) fitted with a C-18 column (Phenomenex, Aeris XB-C18 column (150 mm × 4.60 mm, 3.6 µm) eluted with a 10-90% linear gradient of B into A for all compounds.

To check and to have a confirmation of peptides molecular weights were used ESI mass spectrometry. ESI-MS analysis in positive ion mode, were made using a Finnigan LCQ Deca ion trap instrument, manufactured by Thermo Finnigan (San Jose, CA, USA), equipped with the Excalibur software for processing the data acquired. The sample was dissolved in a mixture of water and methanol (50/50) and injected directly into the electrospray source, using a syringe pump, which maintains constant flow at 5 µL/ min. The temperature of the capillary was set at 220°C.

6.6 Biological section

6.6.1 Cell lines and transfections

HeLa cervical cancer cells and MCF-7 and SKBr3 mammary cancer cells were purchased from the American Type Culture Collection (ATCC). Cells were cultured in RPMI medium 1640 supplemented with 10% heat-inactivated FBS (Invitrogen).

Human umbilical vein endothelial cells (HUVEC) (Clonetics) were cultured in M199 medium (Sigma-Aldrich) supplemented with 10% FBS, heparin (100 µg/mL; Sigma-Aldrich), and 10 ng/mL endothelial cell growth factor. Human mammary epithelial cells (HMECs) were purchased from Invitrogen and cultured as recommended by the manufacturer. Transfections were made with Lipofectamine 2000 (Invitrogen) by following the manufacturer's instructions; 4×10^5 cells were seeded in 6-well plates and transfected with 100 nM of either PTPRJ-specific and scrambled siRNAs, as previously described.⁴⁹

Human recombinant VEGF165 was purchased from ORF Genetics.

6.6.2 Cell survival assay

To assess peptides-mediated inhibition of cell proliferation, HeLa and HUVECs were treated once with peptides for 24 h or treated every 24 h for 48 h and every 24 h for 72 h at the concentration of 160 µM. At the end of treatments, cells were trypsinized and counted, and cell viability was determined by the trypan blue dye exclusion test. The results were expressed as percent variation in the number of viable cells treated with PTPRJ-peptides compared with control peptide treated cells.

6.6.3 Antibodies and Western Blot analysis

ERK1/2, VEGFR2, and phospho-ERK1/2 antibodies were purchased from Santa Cruz Biotechnology (Santa Cruz, CA). Phospho-VEGFR2 Y1054/59

was purchased by Invitrogen. Horseradish peroxidase (HRP)-conjugated anti-goat and anti-rabbit immunoglobulins were also from Santa Cruz Biotechnology. Cells were scraped in ice-cold phosphatase-buffered saline (PBS) and lysed in NP-40 lysis buffer containing 50 mM Tris- HCl, pH 7.5, 150 mM NaCl, 1% NP-40, one protease inhibitor mixture tablet per 10 mL of buffer (Compleat, Roche Diagnostics), 1 mM Na_3VO_4 , and 50 mM NaF. Lysates were passed several times through a 21-gauge needle and incubated for 30 min on ice. Cellular debris was pelleted by centrifugation at 10,000g for 15 min at 4°C. Protein concentrations were determined using the Bradford protein assay dye (Bio-Rad Laboratories, Hercules, CA). Total cell lysates were separated by SDS-PAGE and transferred to PVDF membranes. Membranes were blocked in 5% nonfat dry milk (Bio-Rad) and then probed for about 2 h with primary antibodies. After incubation with specific (HRP)-conjugated secondary antibodies, protein bands were revealed by the ECL detection system (Santa Cruz Biotechnology).

6.6.4 Cell cycle distribution analysis

The cells were plated at 0.5×10^6 cells/60 mmdish and sequential treated every 24 h for 72 h with 160 μM peptides (Invitrogen, Carlsbad, CA). Cells were harvested and fixed with cold 70% ethanol. Before analysis, cells were washed with PBS and stained with a solution containing 50 $\mu\text{g}/\text{mL}$ propidium iodide, 250 $\mu\text{g}/\text{mL}$ RNAase, and 0.04% Nonidet P40 (NP40) for 30 min at RT in the dark.

The fluorescence of stained cells was analyzed by flow cytometry using a FACSCanto (Becton Dickinson). A flow cytometric sub-G1 peak was detected on DNA plots using ModFit LT cell cycle analysis software (Verity software House).

6.6.5 Endothelial cell tube formation assay

Unpolymerized Matrigel (Becton Dickinson, Mountain View, CA) was placed (50 μL per well) in a 96-well microtiter plate (0.32 cm^2 per well) and polymerized for 1 h at 37°C. HUVECs (2.5×10^4 well) were preincubated

with peptide 6 or scrambled peptide (100 μM) for 30 min before being seeded onto the solidified Matrigel. After incubating in media for 18 h, cells were fixed, and tube formation was analyzed by light microscopy (Leica, Germany). Two random fields were chosen in each well.

6.7 NMR spectroscopy

Samples for NMR spectroscopy were prepared by dissolving the appropriate amount of peptide in 0.55 mL of $^1\text{H}_2\text{O}$ and 0.05 mL of $^2\text{H}_2\text{O}$ or 0.60 mL of $^2\text{H}_2\text{O}$ containing phosphate-buffered saline (50 mM) at pH 4.0 and 5°C . NMR spectra were recorded on a Varian INOVA 700 MHz spectrometer equipped with a z-gradient 5 mm triple-resonance probe head. Spectra were calibrated relative to TSP (0.00 ppm) as internal standard. One-dimensional (1D) NMR spectra were recorded in the Fourier mode with quadrature detection.

Water suppression was achieved by using the double-pulsed field gradient spin-echo (DPFGSE) scheme.⁵⁰ 2D TOCSY⁵¹ and NOESY⁵² spectra were recorded in the phase-sensitive mode using the method from States et al.⁵³ Data block sizes were 2048 addresses in t_2 and 512 equidistant t_1 values. Before Fourier transformation, the time domain data matrices were multiplied by shifted \sin^2 functions in both dimensions. A mixing time of 70 ms was used for the TOCSY experiments. NOESY experiments were run with mixing time of 200-600 ms. The quantitative analysis of NOESY spectra was obtained using the interactive program package XEASY.⁵⁴ The temperature coefficients of the amide proton chemical shifts were calculated from TOCSY experiments performed at different temperatures in the range $5\text{-}15^\circ\text{C}$ by means of linear regression. STD-NMR (25) experiments were performed in $2\text{H}_2\text{O}$ solution with on-resonance and off-resonance saturation at $\delta = -2$ and -16 ppm, respectively. Typically, 512 scans were recorded for each STD spectrum (saturation time = 2 s). The relative STD effect (STD%) was calculated as the ratio between the intensity (expressed as S/N ratio) of the signals in the STD spectrum and that of the signals in the ^1H NMR spectrum.

6.7.1 Molecular Modeling

3D theoretical models of all peptides were built by means of L series residues using ver. 9.1 of the Maestro GUI.⁵⁵

Using the Monte Carlo (MC) search, implemented in MacroModel ver. 9.843,⁵⁶ for each compound, by randomly rotate all possible dihedral angles, one million of conformations were generated. Each MC structure was optimized using 10000 steps of the Polak Ribiere Conjugate Gradient algorithm and energy evaluated with the all atoms notation of AMBER* force field.⁵⁷ Water solvent effects were mimicked according to the GB/SA implicit model.⁵⁸ Conformers with similar internal energies, within 4.184 kJ/mol, were geometrically compared one each other by computing the root-mean-square deviation (RMSd) onto their not hydrogen atoms and were considered duplicate if the RMSd value was lower than 0.05 Å. Boltzman population analysis was performed, at 300° K, onto all MC sampled structures reporting internal energy within 50 kJ/mol from the global minimum. MC ensembles were submitted to cluster analysis using an RMSd cutoff distance equal to 0.5 Å, computed onto the non-hydrogen atoms.⁵⁹ Boltzman population data were considered for weighting the cluster analysis results. Aggregation processes were investigated using our in house docking software MolInE^{60,61} that automatically generated bimolecular complexes. Each MC conformer with a Boltzman population larger than 0.1% was considered as both host and guest. According to MolInE methodology, the autorecognition of our peptides was systematically explored by rigid body roto-translation of the guest, with respect to the host. Docking configurations were energy evaluated using the all atoms notation of the AMBER* force field. Water environment was mimicked by defining the dielectric constant equal to 80. The MolInE grid resolution (GR) and van der Waals compression factor (x) were fixed to 6 and 0.6, respectively. The same force field, environment, and deduplication criterion, previously described for the MC search, were adopted for taking into account induced fit phenomena and to discard equivalent structures. The thermodynamics module of MolInE was used to evaluate the stability of the complexes calculating the corresponding binding energies.

6.7.2 Statistical methods and data analysis

All experiments were performed in triplicate from at least three independent experiments, and data shown are the means \pm standard deviation (SD). When only two groups were compared, statistical differences were assessed with unpaired two-tailed Student's t test. Statistical analyses were performed using GraphPad Prism 5 software. For all analyses, differences were considered significant if $P < 0.05$.

¹ Heinrich, R.; Neel, BG.; Rapoport, TA. Mathematical models of protein kinase signal transduction. *Mol Cell* **2002**, 9, 957-970.

² Hornberg, JJ.; Bruggeman, FJ.; Binder, B.; Geest, CR.; de Vaate, AJ.; Lankelma, J.; Heinrich, R.; Westerhoff HV. Principles behind the multifarious control of signal transduction. ERK phosphorylation and kinase/phosphatase control. *FEBS J* **2005**, 272, 244-258.

³ Tonks, NK.; Diltz, CD.; Fischer, EH. Purification of the major proteintyrosine- phosphatases of human placenta. *J Biol Chem* **1988**, 263, 6722-6730.

⁴ Alonso, A.; Sasin, J.; Bottini, N.; Friedberg, I.; Osterman, A.; Godzik, A.; Hunter, T.; Dixon, J.; Mustelin, T. Protein tyrosine phosphatases in the human genome. *Cell* **2004**, 117, 699- 711.

⁵ Andersen, JN.; Mortensen, OH.; Peters, GH.; Drake, PG.; Iversen, LF.; Olsen, OH.; Jansen, PG.; Andersen, HS.; Tonks, NK.; Møller, NP. Structural and evolutionary relationships among protein tyrosine phosphatase domains. *Mol Cell Biol* **2001**, 21, 7117-7136.

⁶ Ostman, A.; Bohmer, FD. Regulation of receptor tyrosine kinase signaling by protein tyrosine phosphatases. *Trends Cell Biol* **2001**, 11, 258-266.

⁷ Ostman, A.; Hellberg, C.; Bohmer, FD. Protein-tyrosine phosphatases and cancer. *Nat Rev Cancer* **2006**, 6, 307-320.

⁸ Borges, LG.; Seifert, RA.; Grant, FJ.; Hart, CE.; Disteché, CM.; Edelhoff, S.; Solca, FF.; Lieberman, MA.; Lindner, V.; Fischer, EH.; Lok, S.; Bowen-Pope, DF. Cloning and characterization of rat density-enhanced phosphatase-1, a protein tyrosine phosphatase expressed by vascular cells. *Circ Res* **1996**, 79, 570-580.

⁹ Honda, H.; Inazawa, J.; Nishida, J.; Yazaki, Y.; Hirai, H. Molecular cloning, characterization, and chromosomal localization of a novel protein-tyrosine phosphatase, HPTP eta. *Blood* **1994**, 84, 4186-4194.

¹⁰ Jallal, B.; Mossie, K.; Vasiloudis, G.; Knyazev, P.; Zachwieja, J.; Clairvoyant, F.; Schilling, J.; Ullrich, A. The receptor-like protein-tyrosine phosphatase DEP-1 is constitutively associated with a 64-kDa protein serine/threonine kinase. *J Biol Chem* **1997**, 272, 12158-12163.

¹¹ Chin, CN.; Sachs, JN.; Engelman, DM. Transmembrane homodimerization of receptor-like protein tyrosine phosphatases. *FEBS Lett* **2005**, 579, 3855-3858.

¹² Jiang, G.; den Hertog, J.; Su, J.; Noel, J.; Sap, J.; Hunter, T. Dimerization inhibits the activity of receptor-like protein-tyrosine phosphatase- α . *Nature* **1999**, 401, 606-610.

¹³ Takahashi, T.; Takahashi, K.; Mernaugh, RL.; Tsuboi, N.; Liu, H.; Daniel, TO. A monoclonal antibody against CD148, a receptor-like tyrosine phosphatase, inhibits endothelial-cell growth and angiogenesis. *Blood* **2006**, 108, 1234-1242.

¹⁴ Keane, MM.; Lowrey, GA.; Ettenberg, SA.; Dayton, MA.; Lipkowitz, S. The protein tyrosine phosphatase DEP-1 is induced during differentiation and inhibits growth of breast cancer cells. *Cancer Res* **1996**, 56, 4236-4243.

¹⁵ Trapasso, F.; Iuliano, R.; Boccia, A.; Stella, A.; Visconti, R.; Bruni, P.; Baldassarre, G.; Santoro, M.; Viglietto, G.; Fusco, A. Rat protein tyrosine phosphatase eta suppresses the neoplastic phenotype of retrovirally transformed thyroid cells through the stabilization of p27(Kip1). *Mol Cell Bio* **2000**, 20, 9236-9246.

¹⁶ Ruivenkamp, CA.; van Wezel, T.; Zanon, C.; Stassen, AP.; Vlcek, C.; Csikos, T.; Klous, AM.; Tripodis, N.; Perrakis, A.; Boerrigter, L.; Groot, PC.; Lindeman, J.; Mooi, WJ.; Meijjer, GA.; Scholten, G.; Dauwerse, H.; Paces, V.; van Zandwijk, N.; van Ommen, GJ.; Demant, P. PtpRJ is a candidate for the mouse colon-cancer susceptibility locus Scc1 and is frequently deleted in human cancers. *Nat Genet* **2002**, 31, 295-300.

¹⁷ Trapasso, F.; Yendamuri, S.; Dumon, KR.; Iuliano, R.; Cesari, R.; Feig, B.; Seto, R.; Infante, L.; Ishii, H.; Vecchione, A.; During, MJ.; Croce, CM.; Fusco, A. Restoration of receptor-type protein tyrosine phosphatase eta function inhibits human pancreatic carcinoma cell growth in vitro and in vivo. *Carcinogenesis* **2004**, 25, 2107-2114.

¹⁸ Iuliano, R.; Trapasso, F.; Le Pera, I.; Schepis, F.; Sama, I.; Clodomi, A.; Dumon, KR.; Santoro, M.; Chiariotti, L.; Viglietto, G.; Fusco, A. An adenovirus carrying the rat protein tyrosine phosphatase eta suppresses the growth of human thyroid carcinoma cell lines in vitro and in vivo. *Cancer Res* **2003**, 63, 882-886.

¹⁹ Iuliano, R.; Le Pera, I.; Cristofaro, C.; Baudi, F.; Arturi, F.; Pallante, P.; Martelli, ML.; Trapasso, F.; Chiariotti, L.; Fusco, A. The tyrosine phosphatase PTPRJ/DEP-1 genotype affects thyroid carcinogenesis. *Oncogene* **2004**, 23, 8432-8438.

²⁰ Ruivenkamp, C.; Hermsen, M.; Postma, C.; Klous, A.; Baak, J.; Meijer, G.; Demant, P. LOH of PTPRJ occurs early in colorectal cancer and is associated with chromosomal loss of 18q12-21. *Oncogene* **2003**, 22, 3472-3474.

- ²¹ Kellie, S.; Craggs, G.; Bird, IN.; Jones, GE. The tyrosine phosphatase DEP-1 induces cytoskeletal rearrangements, aberrant cell-substratum interactions and a reduction in cell proliferation. *J Cell Sci* **2004**, 117, 609-618.
- ²² Paduano, F.; Ortuso, F.; Campiglia, P.; Raso, C.; Iaccino, E.; Gaspari, M.; Gaudio, E.; Mangone, G.; Carotenuto, A.; Bilotta, A.; Narciso, D.; Palmieri, C.; Agosti, V.; Artese, A.; Gomez-Monterrey, I.; Sala, M.; Cuda, G.; Iuliano, R.; Perrotti, N.; Scala, G.; Viglietto, G.; Alcaro, S.; Croce, C.M.; Novellino, E.; Fusco, A.; Trapasso, F. Isolation and functional characterization of peptide agonists of PTPRJ, a tyrosine phosphatase receptor endowed with tumor suppressor activity. *ACS Chem Biol* **2012**, 7, 1666-1676.
- ²³ Ortuso, F.; Paduano, F.; Carotenuto, A.; Gomez, IM.; Bilotta, A.; Gaudio, E.; Sala, M.; Artese, A.; Vernieri, E.; Dattilo, V.; Iuliano, R.; Brancaccio, D.; Bertamino, A.; Musella, S.; Alcaro, S.; Grieco, P.; Perrotti, N.; Croce, CM.; Novellino, E.; Fusco, A.; Campiglia, P.; Trapasso, F. Discovery of PTPRJ Agonist Peptides That Effectively Inhibit in Vitro Cancer Cell Proliferation and Tube Formation. *ACS Chem Biol* **2013**, 8, 1497-1506.
- ²⁴ (a) Grieco, P.; Carotenuto, A.; Campiglia, P.; Zampelli, E.; Patacchini, R.; Maggi, CA.; Novellino, E.; Rovero, P. A new, potent urotensin II receptor peptide agonist containing a Pen residue at the disulfide bridge. *J Med Chem* **2002**, 45, 4391-4394. (b) Grieco, P.; Carotenuto, A.; Patacchini, R.; Maggi, CA.; Novellino, E.; Rovero, P. Design, Synthesis, Conformational Analysis, and Biological Studies of Urotensin-II Lactam Analogues. *Bioorg Med Chem* **2002**, 10, 3731-3739.
- ²⁵ Rajarathnam, K.; Sykes, BD.; Dewald, B.; Baggiolini, M.; Clark-Lewis, I. Disulfide Bridges in Interleukin-8 Probed Using Non-Natural Disulfide Analogues: Dissociation of Roles in Structure from Function. *Biochemistry* **1999**, 38, 7653-7658.
- ²⁶ Thuriéau, C.; Janiak, P.; Krantic, S.; Guyard, C.; Pillon, A.; Kucharczyk, N.; Vilaine, JP.; Fauchere, JL. *Eur J Med Chem* **1995**, 30, 115.
- ²⁷ Limal, D.; Briand, JP.; Dalbon, P.; Jolivet, M. *J Peptide Res* **1988**, 52, 121.
- ²⁸ MacArthur, MW.; Thornton, JM. Influence of proline residues on protein conformation. *J Mol Biol* **1991**, 218, 397-412.
- ²⁹ Luthman, K.; Hacksell, U.; In Krogsgaard-Larsen, P.; Liljefors, T; Madsen, U; Eds. Textbook of drug design and discovery. 3rd Ed. London: Taylor & Francis **2002**, 459-85.
- ³⁰ Durani, S. Protein design with L- and D-alpha-amino acid structures as the alphabet. *Acc Chem Res* **2008**, 41, 1301-1308.
- ³¹ Atherton, E.; Sheppard, RC. Solid-Phase Peptide Synthesis: A Practical Approach. IRL Press, Oxford, U.K. **1989**.

- ³² Balse, PM.; Kim, HJ.; Han, G.; Hruby, VJ. Evaluation of new base-labile 2-(4-nitrophenylsulfonyl) ethoxycarbonyl (Nsc)-amino acids for solid-phase peptide synthesis. *J Peptide Res* **2000**, 56, 70-79.
- ³³ Miranda, LP.; Alewood, PF. Accelerated chemical synthesis of peptides and small proteins. *Proc Natl Acad Sci U.S.A.* **1999**, 96, 1181-1186.
- ³⁴ Grieco, P.; Gitsu, PM.; Hruby, VJ. Preparation of 'side-chain-to-side-chain' cyclic peptides by Allyl and Alloc strategy: potential for library synthesis. *J Pept Res* **2001**, 57, 250-256.
- ³⁵ Chen, X.; Park, R.; Shahinian, AH.; Bading, JR.; Conti, PS. Pharmacokinetics and tumor retention of 125I-labeled RGD peptide are improved by PEGylation. *Nucl Med Biol* **2004**, 31, 11-19.
- ³⁶ Lampugnani, MG.; Zanetti, A.; Corada, M.; Takahashi, T.; Balconi, G.; Breviario, F.; Orsenigo, F.; Cattelino, A.; Kemler, R.; Daniel, TO.; Dejana, E. Contact inhibition of VEGF-induced proliferation requires vascular endothelial cadherin, beta-catenin, and the phosphatase DEP-1/CD148. *J Cell Biol* **2003**, 161, 793-804.
- ³⁷ Wüthrich, K. NMR of Proteins and Nucleic Acids. *John Wiley & Sons, Inc., New York* **1986**.
- ³⁸ Mayer, M.; Meyer, B. Characterization of ligand binding by saturation transfer difference NMR spectroscopy. *Angew Chem Int Ed* **1999**, 38, 1784-1788.
- ³⁹ Mayorov, AV.; Cai, M.; Palmer, ES.; Liu, Z.; Cain, JP.; Vagner, J.; Trivedi, D.; Hruby, VJ. Solid-Phase Peptide Head-to-Side Chain Cyclodimerization: Discovery of C2-Symmetric Cyclic Lactam Hybrid α -Melanocyte-Stimulating Hormone (MSH)/Agouti-Signaling Protein (ASIP) Analogues with Potent Activities at the Human Melanocortin Receptors. *Peptides* **2010**, 31, 1894-1905.
- ⁴⁰ Kessler, H.; Gratias, R.; Hessler, G.; Gurrath, M.; Müller, G. Conformation of cyclic peptides. Principle concepts and the design of selectivity and superactivity in bioactive sequences by 'spatial screening'. *Pure & Appl Chem* **1996**, 68, 1201-1205.
- ⁴¹ White, CJ.; Yudin, AK. Contemporary strategies for peptide macrocyclization. *Nature Chemistry* **2011**, 3.
- ⁴² De Munter, S.; Köhn, M.; Bollen, M. Challenges and opportunities in the development of protein phosphatase-directed therapeutics. *ACS Chem Biol* **2013**, 8, 36-45.
- ⁴³ Kovalenko, M.; Denner, K.; Sandström, J.; Persson, C.; Gross, S.; Jandt, E.; Vilella, R.; Böhmer, F.; Ostman, A. Site-selective dephosphorylation of the platelet-derived growth factor beta-receptor by the receptor-like protein-tyrosine phosphatase DEP-1. *J Biol Chem* **2000**, 275, 16219-16226.

⁴⁴ Palka, HL.; Park, M.; Tonks, NK. Hepatocyte growth factor receptor tyrosine kinase met is a substrate of the receptor protein-tyrosine phosphatase DEP-1. *J Biol Chem* **2003**, 278, 5728-5735.

⁴⁵ Iervolino, A.; Iuliano, R.; Trapasso, F.; Viglietto, G.; Melillo, RM.; Carlomagno, F.; Santoro, M.; Fusco, A. The receptor-type protein tyrosine phosphatase J antagonizes the biochemical and biological effects of RET-derived oncoproteins. *Cancer Res* **2006**, 66, 6280-6287.

⁴⁶ Berset, TA.; Hoier, EF.; Hajnal, A. The *C. elegans* homolog of the mammalian tumor suppressor Dep-1/Sccl inhibits EGFR signaling to regulate binary cell fate decisions. *Genes Dev* **2005**, 19, 1328-1340.

⁴⁷ Lampugnani, MG.; Zanetti, A.; Corada, M.; Takahashi, T.; Balconi, G.; Breviario, F.; Orsenigo, F.; Cattelino, A.; Kemler, R.; Daniel, TO.; Dejana, E. Contact inhibition of VEGF-induced proliferation requires vascular endothelial cadherin, beta-catenin, and the phosphatase DEP-1/CD148. *J Cell Biol* **2003**, 161, 793-804.

⁴⁸ Sacco, F.; Tinti, M.; Palma, A.; Ferrari, E.; Nardoza, AP.; Hooft van Huijsduijnen, R.; Takahashi, T.; Castagnoli, L.; Cesareni, G. Tumor suppressor density-enhanced phosphatase-1 (DEP-1) inhibits the RAS pathway by direct dephosphorylation of ERK1/2 kinases. *J Biol Chem* **2009**, 284, 22048-22058.

⁴⁹ Paduano, F.; Dattilo, V.; Narciso, D.; Bilotta, A.; Gaudio, E.; Menniti, M.; Agosti, V.; Palmieri, C.; Perrotti, N.; Fusco, A.; Trapasso, F.; Iuliano, R. Protein tyrosine phosphatase PTPRJ is negatively regulated by microRNA-328. *FEBS J* **2013**, 280, 401-412.

⁵⁰ Hwang, TL.; Shaka, AJ. Water suppression that works. Excitation sculpting using arbitrary wave-forms and pulsed-field gradients. *J Magn Reson* **1995**, 112, 275-279.

⁵¹ Braunschweiler, L.; Ernst, RR. Coherence transfer by isotropic mixing: application to proton correlation spectroscopy. *J Magn Reson* **1983**, 53, 521-528.

⁵² Jenner, J.; Meyer, BH.; Bachman, P.; Ernst, RR. Investigation of exchange processes by two-dimensional NMR spectroscopy. *J Chem Phys* **1979**, 71, 4546-4553.

⁵³ States, DJ.; Haberkorn, RA.; Ruben, DJ. A two dimensional nuclear Overhauser experiment with pure absorption phase four quadrants. *J Magn Reson* **1982**, 48, 286-292.

⁵⁴ Bartels, C.; Xia, TH.; Billeter, M.; Guntert, P.; Wuthrich, K. The program XEASY for computer-supported NMR spectral analysis of biological macromolecules. *J Biomol NMR* **1995**, 6, 1-10.

⁵⁵ Schrödinger LLC, New York, NY., **2010**, <http://www.schrodinger.com>.

⁵⁶ Mohamadi, F.; Richard, NGJ.; Guida, WC.; Liskamp, R.; Lipton, M.; Caufield, C.; Chang, G.; Hendrickson, T.; Still, WC. MacroModel-an integrated software system for modeling organic and bioorganic molecules using molecular mechanics. *J Comput Chem* **1990**, 11, 440-467.

⁵⁷ McDonald, DQ.; Still, WC. AMBER* Torsional Parameters for the Peptide Backbone. *Tetrahedron Lett* **1992**, 33, 7743-7746.

⁵⁸ Still, WC.; Tempczyk, A.; Hawley, RC.; Hendrickson, T. Semianalytical treatment of solvation for molecular mechanics and dynamics. *J Am Chem Soc* **1990**, 112, 6127-6129.

⁵⁹ Daura, X.; Gademann, K.; Jaun, B.; Seebach, D.; Van Gunsteren, WF.; Mark, AE. Peptide folding: When simulation meets experiment. *Angew Chem Int* **1999**, 38, 236-240.

⁶⁰ Alcaro, S.; Gasparrini, F.; Incani, O.; Mecucci, S.; Misiti, D.; Pierini, M. A "quasi-flexible" automatic docking processing for studying stereoselective recognition mechanisms. Part I. Protocol validation. *J Comput Chem* **2000**, 21, 515-530.

⁶¹ Alcaro, S.; Gasparrini, F.; Incani, O.; Caglioti, L.; Pierini, M.; Villani, C. "Quasi flexible" automatic docking processing for studying stereoselective recognition mechanisms, part 2: Prediction of $\Delta\Delta G$ of complexation and ¹H-NMR NOE correlation. *J Comput Chem* **2007**, 28, 1119-1128.

CHAPTER 3

**SAR studies and conformational analysis of a series of novel
peptides
G protein-coupled receptor kinase 2 (GRK2) inhibitors**

Abstract G protein-coupled receptor kinase 2 (GRK2) is a relevant signaling node of the cellular transduction network, playing major roles in the physiology of various organs/tissues including the heart and blood vessels. Emerging evidence suggests that GRK2 is up regulated in pathological situations such as heart failure, hypertrophy, hypertension and is involved in the progression of cellular cycle. Therefore its inhibition offers a potential therapeutic solution to these diseases like hypertension, heart failure and cancer. We performed a SAR study and a NMR conformational analysis of peptides derived from HJ loop of GRK2 and able to selectively inhibit GRK2. Moreover, we explored the GRK2 inhibitory activity of a library of cyclic peptides derived from the HJ loop of G protein-coupled receptor kinases 2 (GRK2). The design of these cyclic compounds was based on the conformation of the HJ loop within the X-ray structure of GRK2. One of these compounds, potently and selectively inhibited the GRK2 activity, being more active than its linear precursor.

In a cellular system, this peptide confirms the beneficial signaling properties of a potent GRK2 inhibitor. Preferred conformations of the most potent analogue were investigated by NMR spectroscopy.

Keywords GRK2 inhibitors, cardiovascular system, peptide Ala scan, cyclic peptides, peptidomimetics, NMR conformational analysis.

Abbreviations Abbreviations used for amino acids and designation of peptides follow the rules of the IUPACIUB Commission of Biochemical Nomenclature in *J Biol Chem* **1972**, 247, 977-983. Amino acid symbols denote L-configuration unless indicated otherwise.

The following additional abbreviations are used:

DPC, dodecylphosphocholine; SAR, structure-activity relationship; DCM, dichloromethane; DIPEA, N,N-diisopropylethyl-amine; DMF, N,N-dimethylformamide; $i\text{Pr}_3\text{SiH}$, or TIS triisopropylsilane; TFA, trifluoroacetic acid; Fmoc, 9-fluorenyl-methoxycarbonyl; HOBt, Nhydroxy-benzotriazole; HBTU, 2-(1H-benzotriazole-1-yl)-1,1,3,3-tetramethyluronium hexafluoro -phosphate; Trt, trityl; Pbf, 2,2,4,6,7-pentamethyldihydro benzofuran-5-sulfonyl; RP HPLC, reversed-phase high performance liquid chromatography; ESI, electrospray ionization; LCQ, liquid chromatography

quadrupole mass spectrometry; ATP, adenosine triphosphate; EDTA, Ethylenediaminetetraacetic acid; EGTA, ethylene glycol tetraacetic acid; cAMP cyclic adenosine monophosphate.

1. Introduction

The G protein-coupled receptor kinase family (GRKs) constitutes a group of seven protein kinases that specifically recognize and phosphorylate agonist-activated G protein-coupled receptors (GPCRs).¹ GRKs-mediated receptor phosphorylation triggers the binding of arrestin proteins² that uncouple receptors from G proteins leading to rapid desensitization.^{3,4} As a result of β -arrestin binding, phosphorylated receptors are also targeted for clathrin-mediated endocytosis, a process that classically serves to re-sensitize and recycle receptors back to the plasma membrane.⁵

In addition, both arrestins and GRKs participate in signal propagation, cooperating in the assembly of macromolecular complexes in the receptor environment and interacting with different components of signal transduction. The seven mammalian GRKs family can be divided into three subfamilies based on sequence and functional similarity: visual GRK subfamily (GRK1 and GRK7), the β -adrenergic receptor kinase (GRK2/GRK3), and the GRK4 subfamily (GRK4, GRK5 and GRK6).⁶ All GRKs share a common structural architecture that includes a N-terminal regulator of G protein signaling homology domain (RH), a central kinase catalytic domain, and a C-terminal region containing a pleckstrin homology domain (PH).⁷ The best-characterized member of this family is the ubiquitously expressed GRK2, also known as β -adrenergic receptor kinase 1 (β -ARK1).⁸

In the past 20 years, GRK2 emerges as a key node in signal transduction pathway playing a major role in the agonist-specific desensitization of several metabolism-related GPCRs, including the β -adrenergic, melanocortin, endothelin, and glucose-dependent insulinotropic polypeptide receptors.^{9,10} GRK2 can also phosphorylate other membrane receptors,¹¹ as well as non-receptor substrates, acting as effector in the regulation of diverse cellular phenomena from cardiovascular and immune cell functionality¹² to migration

and cell cycle progression.^{13,14} Furthermore, GRK2 may also contribute to modulate cellular responses in a phosphorylation-independent manner thanks to its ability to interact with a plethora of proteins involved in signaling and trafficking.¹⁵ All these functional interactions predict that alterations in GRK2 levels and/or activity may have important effects in human diseases,¹⁶ as those reported in several relevant cardiovascular,¹⁷ inflammatory,¹⁸ or cancer pathologies.^{19,20}

In this regard, many attentions are focused on the role for GRK2 as both an extrinsic and intrinsic cell-cycle regulator (Figure 1). GRK2 expression has been reported to have distinct impacts on cell proliferation and mitogenic signaling depending on both the cell type and the mitogenic stimuli analysed. GRK2 inhibits TGF-mediated cell growth arrest and apoptosis in human hepatocarcinoma cells.²¹ On the other hand, GRK2 attenuates serum- or PDGF-induced proliferation of thyroid cancer cell lines²² and smooth muscle cells,²³ respectively, whereas its expression increases MAPK signaling in response to EGF in HEK-293 cells²⁴ and GRK2 kinase activity is required for IGF-1-triggered proliferation and mitogenic signaling in osteoblasts.²⁵

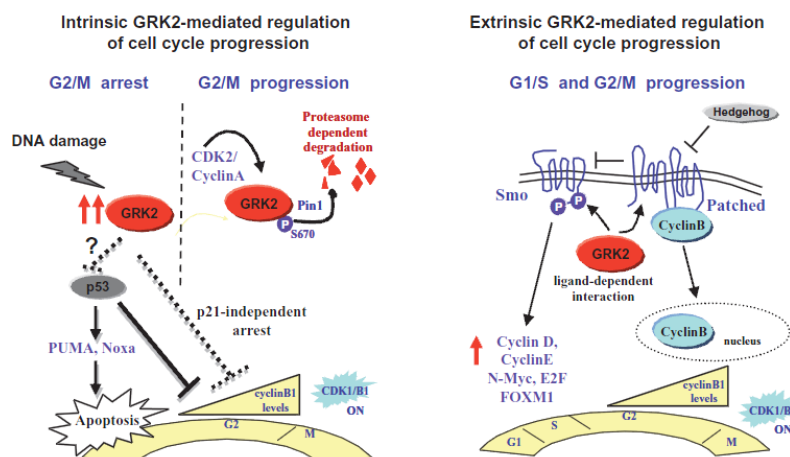


Figure 1. GRK2 interactome involved in the modulation of cell cycle progression. GRK2 is linked to diverse regulatory networks acting at specific stages of the cell cycle. In response to both extrinsic and intrinsic cues, GRK2 protein plays a critical role in driving cell progression through G1/S and G2/M transitions in a kinase-dependent and independent manner. GRK2 is part of an intrinsic pathway that ensures timely progression of cell cycle at G2/M by means of its functional interaction with CDK2/cyclinA and Pin1.¹³ Such pathway is disrupted upon DNA damage, when GRK2 appears to turn into a pro-arresting factor that promotes increased cell survival and to dampen p53-dependent responses by mechanisms that remain to be established (dotted lines/question mark). On the other hand, GRK2 contributes to the Hedgehog/Smoothened-triggered control of cell proliferation by promoting Smo activity and relieving the Patched-dependent inhibition of cyclin B. CDK, cyclin-dependent kinase; GRK, G protein-coupled receptor kinase.

In addition, GRK2 has been recently shown to establish a complex network of novel functional interactions during cell cycle progression that are critical for timely G2/M transition. It has found that GRK2 levels are controlled intrinsically by the cell-cycle machinery under normal conditions and in response to DNA damage, and differentially contribute either to cell cycle progression or cell arrest in a receptor-independent manner. GRK2 protein levels are transiently down-regulated during the G2/M transition by a mechanism involving CDK2-mediated phosphorylation of GRK2 at S670, what drives binding to the prolyl-isomerase Pin1 and subsequent degradation. Preventing GRK2 phosphorylation at this residue impedes normal GRK2 down regulation and markedly delays cell cycle progression.¹³ Interestingly, the ‘default’ GRK2 protein decay in G2 is prevented in the presence of DNA damaging agents that trigger cell cycle arrest such as doxorubicin. Moreover,

in cells with higher steady-state levels of the kinase, increased stabilized GRK2 levels in such conditions inversely correlate with the p53 response and the induction of apoptosis, strongly suggesting that GRK2 contributes to orchestrate G2/M checkpoint mechanisms, helping to restrict the apoptotic fate of arrested cells. As it has been reported that GRK2 is up-regulated in the context of oncogenic signaling,^{26,27} it is tempting to suggest that inhibition of GRK2 expression might sensitize cells to drug-induced DNA damage.

The increasingly complex GRK2 'interactome' puts forward this kinase is a relevant signaling node of the cellular transduction network. The intricacy of this network of functional interactions and the participation of this protein in basic cellular processes as migration and cell cycle progression or cardiovascular cell functionality predicts that alterations in GRK2 levels and/or activity, as those reported in several relevant cardiovascular, inflammatory or cancer pathologies, may have important effects in human disease. This makes of this kinase a potentially interesting diagnostic marker and therapeutic target.

In the last year, identification of GRK2 modulators/inhibitors is a very active fields of research.

Different small molecules inhibitors of GRK2 activity are currently available, even if they are characterized by low sensitivity and specificity.^{28,29} Strategies to selectively inhibit the GRK2 activity have been attempted using shorter peptides^{30,31} or RNA aptamers.^{32,33} In particular, Anis et al.³¹ demonstrated that myristyl or lauryl glycine derivatives of short peptides derived from HJ loop of GRK2, such as KRX-683₁₀₇ and KRX-683₁₂₄ (Table 1), are potent inhibitor of the kinase and possess hypoglycemic effect in animal models of Type 2 diabetes. The peptide fragments of these compounds closely resemble the catalytic fragment 383-390 KLLRGHSP of GRK2. This fragment is composed by the last part of the α -helix F (residues 383-386) and the first part of a strand (residues 387-390) within the HJ loop. Several crystallographic and mutational studies, have pointed to HJ- α G residues as being involved in substrate binding and in binding to upstream activators. Based on these findings, this fragment and, more concretely, compounds **1** and

2 appeared to be valuable starting points for the development of novel specific and more potent GRK2 inhibitors.

Table 1. Different peptide fragments considered in this study.

Peptide	Sequence
383-390HJ loop GRK2	K L L R G H S P
KRX-683 ₁₀₇	Myristyl G L L R r H S
KRX-683 ₁₂₄	Lauryl G L L R r H S I
1	G L L R r H S
2	G L L R r H S I

2. Aim of work

Previous results obtained by Anis et al.,³¹ point to the selected peptides, **1** and **2**, as interesting lead compounds for the development of a novel class of effective chemotherapeutic agents.

2.1 Alanine scanning approach and changes in ⁵D-Arg (peptides 3-18)

First of all, we decided to apply to peptide leads L-Alanine scanning approach, a classical chemical approach to check the relevance of each residue for the biological activity of the peptide (peptides **3-15**, Table 2). To verify the effect of chirality, the D-Arg at position 5 was also replaced by D-Ala (peptides **16** and **17**).

Table 2. Structure and inhibition activities of linear peptides **1-18**.

Peptide	Sequence	HPLC ^d	ESI-MS (M+H)		GRK2 Inhib.	
		k ^o	Calcd	Found	ROS ^b	MBP ^c
1	GLLRrHS	1.70	836.97	837.66	47.6±5.5	54.2±6.1
3	GALRrHS	1.68	793.89	795.52	<5	<5
4	GLARrHS	1.68	793.89	795.52	<5	<5
5	GLLArHS	1.74	751.86	752.61	42.2±9.7	38.2±4.5
6	GLLRAHS	1.74	751.86	752.52	<5	<5
7	GLLRrAS	1.76	770.91	771.60	13.5±6.4	25.6±5.7
8	GLLRrHA	1.68	821.91	821.60	22.3±5.4	28.8±9.2
2	GLLRrHSI	1.72	950.13	950.70	49.6±6.3	60.2±5.0
9	GALRrHSI	1.72	908.05	908.55	45.7±12.3	54.5±9.1
10	GLARrHSI	1.72	908.05	908.68	46.6±12.3	47.7±7.2
11	GLLArHSI	1.78	865.02	865.50	45.7±6.2	42.1±7.8
12	GLLRAHSI	1.78	865.62	865.53	<5	<5
13	GLLRrASI	1.80	884.07	884.65	<5	<5
14	GLLRrHAI	1.78	934.13	934.82	<5	<5
15	GLLRrHSA	1.72	908.05	908.48	<5	<5
16	GLLRaHS	1.74	751.86	752.48	55.5±4.7	54.2±3.2
17	GLLRaHSI	1.78	865.62	865.50	63.2±9.7	55.5±6.0
18	GLLRRHS	1.74	836.86	837.79	20.5±5.7	28.4±3.5

^aData represent mean values (±SD) of three independent determinations. ^bGRK2 purified protein activity (50 ng) was tested on rod outer segments (ROS) in presence or absence of 1µM inhibitors. ^cGRK2 purified protein activity (50 ng) was tested on Myelin Basic Protein (MBP) in presence or absence of inhibitors. ^dk^o=[(peptide retention time-solvent retention time)/ solvent retention time].

The effectiveness of these peptides to inhibit GRK2 kinase activity was assessed by in vitro assay using GRK2 purified protein and the G protein-coupled receptor rod outer segments (ROS) as a substrate (Table 2) in presence of [γ -³²P]- adenosine triphosphate (ATP).

With a quick scan we found that peptide 1 causes a $47.6\pm 5.5\%$ inhibition of GRK2 activity on ROS. We found that indeed, substitution with a neutral D-amino acid such as Alanine maintained the inhibitory properties of the resulting peptide **16** ($55.5\pm 4.7\%$).

A similar approach was assessed for peptide 2. First of all, 2 causes a $49.6\pm 6.3\%$ decrease in GRK2 activity. Similarly to peptide 1, the reinstallation of D-chirality in residue 5 restores the inhibitory properties of resulting peptide **17** on GRK2 ($63.2\pm 9.7\%$) which showed the highest GRK2 inhibition potency of the series.³⁴

To test the specificity of the peptides for GRK2 rather than for the substrate, we also repeated the same experiment using as substrate Myelin Basic Protein (MBP). MBP is an ideal model substrate, since this basic protein can be phosphorylated at multiple sites (Ser-11, Ser-55, Ser-8, Ser-132, Ser-55, Ser-161, and Ser-46) from several kinase types.³⁵ Therefore, in this study we have used the myelin basic protein as conventional substrate for in vitro kinase assay. With this substrate, we observed a similar inhibition pattern as for ROS (Table 2).

Furthermore, to better understand the importance of chirality in residue 5 we synthesized an analogue of peptide 1 with ⁵L-Arg (peptide **18**). This compound causes a $20.5\pm 5.7\%$ inhibition of GRK2 activity instead of $47.6\pm 5.5\%$ for peptide lead suggested an important role of chirality. Furthermore, conformational analysis of these peptides clearly indicated that their structures are very similar to the X-ray structure of the fragment encompassing the HJ loop of the GRK2, indicating that the isolated peptide could keep the 3D structure of the protein segment. Based on these results, we designed, synthesized, and evaluated the GRK2 inhibitor activities of a small libraries of cyclic peptides.

2.2 Design of cyclic peptides (peptides 19-24)

The attention was focused on peptides lead, 1 and 2, that selectively inhibit GRK2 *in vitro*. Their NMR solution conformations are very similar to the crystal structure of the fragment encompassing the HJ loop of the GRK2 (pdb

entry 3CIK, Figure 2). Hence, it can be hypothesized that the active conformation of the peptides resemble the HJ loop crystal structure.

Accordingly, the stabilization of the peptide 3D structure by, for example, the cyclization of these linear compounds can be considered as a valid approach to the identification of more potent, (stable and selective) compounds. As evident from Figure 2, N- and C-terminal sides of the loop fragment are relatively close (~ 5 Å), hence we first carried out a head-to-tail cyclization of peptides 1 and 2 leading to peptides 19 and 20, respectively (Table 3).

The design of a second group of cyclic peptides is based on the consideration that, in the GRK2 crystal structure, the amino group of Lys383 side chain points towards the Ser389 side chain (Figure 2).

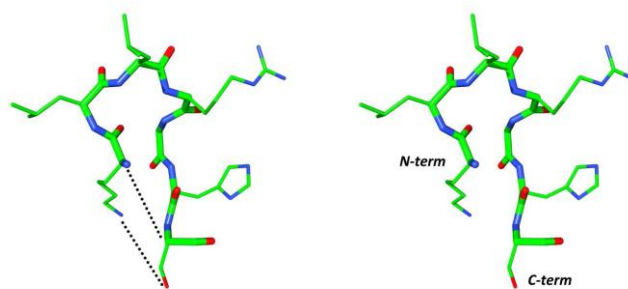


Figure 2. Stereoview of the crystal structure of the fragment 383-390 of GRK2 (1, pdb entry 3CIK). Heavy atoms are shown with different colours (carbon, green; nitrogen, blue; oxygen, red). Hydrogen atoms are not shown for clarity. Cyclization strategies are shown as dotted lines.

Hence, the stabilization of the peptide structure was also sought through a side chain-to-side chain cyclization approach. The cyclic peptides 21 and 22 (Table 3) were synthesized from linear peptides which contain the original residue Lys383 of GRK2 instead of ¹Gly and an Asp residue in place of ⁷Ser residue. These two residues are linked by a side chain amide bond. For comparative purpose the analogues 23 and 24, containing the original Gly387 residue at the position 5, were also synthesized and tested for their activity to inhibit GRK2.³⁶

The effectiveness of these peptides to inhibit GRK2 kinase activity was assessed by in vitro assay using GRK2 (GRK5) purified protein and the G protein-coupled receptor rod outer segments (ROS) as a substrate (Table 3) in presence of [γ - 32 P]- adenosine triphosphate (ATP).

Table 3. Structure, inhibition activities, and analytical data of peptides **19-24**.

Peptide	Sequence	HPLC ^c k'	ESI-MS (M+H)		Inhib	
			Calcd	Found	GRK2 ^b	GRK5 ^b
1^d	GLLRrHS	1.70	836.97	837.66	47.6±5.5	<5
2^d	GLLRrHSI	1.72	950.13	950.70	49.6±6.3	<5
19	[GLLRrHS]	1.70	819.96	820.53	47.8±6.0	<5
20	[GLLRrHSI]	1.85	933.12	933.80	37.2±10.7	<5
21	[KLLRrHD]	1.72	919.09	920.13	36.3±4.4	<5
22	[KLLRrHD]I	1.75	1032.25	1033.11	55.3±4.6	<5
23	[KLLRGHD]	1.76	819.47	820.51	47.2±4.5	<5
24	[KLLRGHD]I	1.78	933.12	933.68	33.7±7.8	<5

^aData represent mean values (\pm SD) of three independent determinations. ^bGRK2 and GRK5 purified proteins activity (50 ng) were tested on rod outer segments (ROS) in presence or absence of 1 mM inhibitors. ^ck'=[(peptide retention time-solvent retention time)/ solvent retention time]. ^dAlready reported in reference 11.

2.2.1 NMR Analysis of cyclic peptide **22**

NMR analysis of peptide **22** was performed in water and DPC micelle solutions. No standard α -helix or β -sheet structure from H _{α} CSI (chemical shift index) values,³⁷ and no unambiguous medium- or long-range backbone NOE connectivities were found in the NOESY spectrum of the peptides. In contrast, several NMR parameters indicate that peptides are better structured in DPC solution and that they share very similar conformations.

Superposition of the 10 lowest energy conformers of **22** is shown in Figure 3.

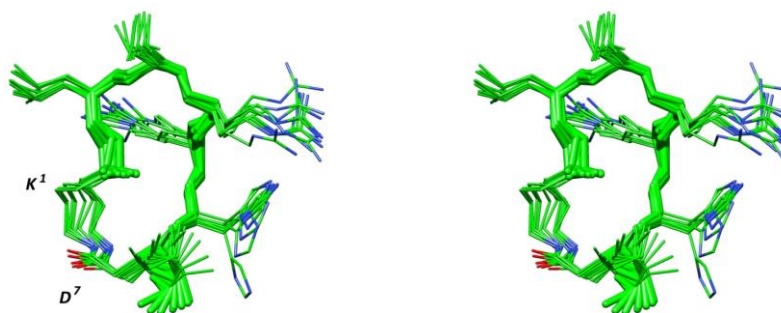


Figure 3. Stereoview of the 10 lowest energy conformers of 22. Structures were superimposed using the backbone heavy atoms. Heavy atoms are shown with different colors (carbon, green; nitrogen, blue; oxygen, red). Hydrogen atoms are not shown for clarity.

The first β -turn structure is stabilized by a hydrogen bond between the carbonyl oxygen of ¹Lys and the amide hydrogen of ⁴Arg. Residues 6 and 7 are in extended conformations, residue 8 is more flexible. The side chain are also well defined, the RMSD for all heavy atoms is 0.74 Å. The side chains of ⁴Arg and ⁶His are close and form a positively charged hydrophilic surface while ²Leu and ³Leu side chains establish a hydrophobic surface pointing in the opposite direction.

At the same time, we decided to consider peptide 1 and 2 as a valuable starting point for the development of a novel class of potential chemotherapeutic agents carrying out N- and C- terminal deletions with the aim to identify more potent and selective peptide derivatives.

2.3 Design of a small truncation library and di-Ala approach (peptides 25-30)

Truncation library can be used to identify the shortest amino acid sequence needed for the peptide activity. The truncation process is carried out via a systemic reduction of residues from each flank of the original peptide. With the knowledge of the positions of key residues elucidated through Alanine Scanning library, the construction of the truncation library could also be centered around these key amino acid residues.

Ala scan results (Table 2) indicated that, while C-terminal residues are important for the activity of both peptides, N-terminal residues ²Leu and ³Leu are important only for the shorter peptide 1. ⁴Arg side chain is of little importance for the activity of both the peptides, in contrast the substitution with a neutral *D*-amino acid such as Alanine does not change the inhibitory properties of peptides 1 and 2, thus suggesting an important role for the chirality of amino acid 5 rather than for the side chain.

For this reason, we synthesized peptides 25-26 obtained from N- and C-terminal deletions of peptide 1. Considering that only C-terminal residues are important for the activity of peptides 2 we synthesized compound 28 containing only C-terminal residues.

To investigate the importance of C-terminal residues, in term of charges and steric hindrance, we used a di-Alanine scanning approach (peptides **29-30**). It is an important tool for peptide sequence optimization. It identifies amino acids of interest at a given position and substitutes the amino acid(s) near this position with the smallest chiral amino acid, Alanine, to explore side-chain contributions of near amino acid to the interaction.

Table 4. Structure, inhibition activities, and analytical data of peptides **25-30**.

Peptide	Sequence	HPLC ^c	ESI-MS (M+H)		Inhib (%±SD) ^a	
		k'	Calcd	Found	GRK2 ^b	GRK5 ^b
1^d	GLLRrHS	1.70	836.97	837.66	47.6±5.5	<5
2^d	GLLRrHSI	1.72	950.13	950.70	49.6±6.3	<5
25	LRrH	1.54	579.69	580.12	38.2±6.0	<5
26	LLRr	1.65	555.71	556.23	50.5±9.7	<5
27	rHS	1.43	397.42	398.41	10.3±4.4	<5
28	rHSI	1.67	510.58	511.41	35.4±4.6	<5
29	GLLArAS	1.74	685.21	686.13	35.7±6.4	<5
30	GLLRrAA	1.76	754.92	755.35	22.6±4.7	<5

^aData represent mean values (±SD) of three independent determinations. ^bGRK2 and GRK5 purified proteins activity (50 ng) were tested on rod outer segments (ROS) in presence or absence of 1 mM inhibitors. ^ck'=[(peptide retention time-solvent retention time)/ solvent retention time]. ^dAlready reported in reference 11.

The effectiveness of these peptides to inhibit GRK2 kinase activity was assessed by in vitro assay using GRK2 (GRK5) purified protein and the G protein-coupled receptor rod outer segments (ROS) as a substrate (Table 4) in presence of [γ - 32 P]- adenosine triphosphate (ATP).

From previous preliminary results we observed an improvement on inhibitory activity of tetrapeptide, compound **26** than peptide lead, 1.

2.4 Design of cyclic peptides starting from tetrapeptide (peptides 26-40)

Compound 22, a lactam cyclic peptide, remains the most active peptide and above it leads to an increase in β_2 AR density, in HEK-293 cells, consistent with an effective inhibition of GRK2.

Being interested to identify the most active and at the same time the most stable peptide, we decided to apply two different approaches:

i) Stabilization of tetrapeptide, compound 26, through a head-to tail cyclization approach;

ii) Enhancement of ring size synthesizing lactam bridge analogues, starting from peptide 26.

Head-to-tail cyclic peptides, important targets in peptide synthesis over decades, have attracted considerable interest in recent years. The reason for this interest stems from the observation that constraining of the highly flexible linear peptides by cyclization induces or stabilizes the bioactive conformation of peptides. Furthermore, cyclic peptides are more resistant to proteolysis than their linear counterparts due to the lack of exopeptidase cleavage sites.³⁸

i) The synthesis of peptide 31 allows us to have a more rigid structure of side chain-to-side chain cyclization. Furthermore, head-to tail cyclization allows us to have a peptide with minor possible conformers.

ii) We decided to stabilize the peptide with the introduction of lactam bridge. Therefore, we designed a library of lactam cyclic derivatives from tetrapeptide, peptide 26.

In particular, in N-terminal and C-terminal domain at positions 1 and 6 amino acids bearing an amino ((2,3)-diaminopropionic acid (Dap), ornithine (Orn) or lysine (Lys)) and carboxylic (Asp or Glu) functions on the side chain,

respectively, were added; these two side chains were subsequently linked to form the lactam bridge (peptides **32**, **34-40** Table 5).

Focused on inhibitory activity of compound 21 and 22 we found that peptide 22, containing a ⁸Ile inhibits GRK2 activity of 55.3% instead of 36.3% for peptide 21. It suggests an important role of ⁸Ile. For this reason we decided to synthesize peptide 33, [KLLRrD]I.

Table 5. Structure and analytical data of peptides **31-40**.

Peptide	Sequence	HPLC ^a k'	ESI-MS (M+H)	
			Calcd	Found
1^b	GLLRrHS	1.70	836.97	837.66
2^b	GLLRrHSI	1.72	950.13	950.70
22	[KLLRrHD]I	1.75	1032.25	1033.11
26	LLRr	1.65	555.71	556.23
31	[LLRr]	1.71	538.75	539.60
32	[KLLRrD]	1.77	780.91	781.64
33	[KLLRrD]I	1.86	894.13	894.72
34	[KLLRrE]	1.75	794.98	795.23
35	[OrnLLRrD]	1.79	767.02	768.13
36	[DabLLRrD]	1.84	752.76	753.25
37	[DapLLRrD]	1.81	738.54	739.86
38	[OrnLLRrE]	1.78	780.93	781.25
39	[DabLLRrE]	1.72	766.76	767.23
40	[DapLLRrE]	1.74	752.43	753.79

^ak'=[(peptide retention time solvent retention time)/ solvent retention time].

^bAlready reported in reference 32.

Recently, peptides 31-33 were tested to verify if they inhibit GRK2 kinase activity. Peptide 31 and 33 appear to inhibit GRK2 activity in a similar manner to peptide 2. Peptide 32 causes a 25.3±1.2% inhibition of GRK2 activity

instead of $49.6 \pm 6.3\%$ for peptide 2 suggested an important role of ^8Ile (data not shown).

2.5 Design of peptidomimetic

Use of peptidomimetics is one of the most recent methods of drug design and development in medicinal chemistry. Peptidomimetics typically are small protein-like molecules designed to mimic natural peptides or proteins.³⁹

They typically arise either from modification of an existing peptide, or by designing similar systems that mimic peptides, such as peptoids and β -peptides. These mimetics, whose structures were mainly derived from natural peptides, should have the ability to bind to their natural targets in the same way of the natural sequences and hence should produce the same biological effects.

It is possible to design these molecules in such a way that they show the same biological effects as their peptide role models, but with enhanced properties like a higher proteolytic stability, higher bioavailability and also often with improve selectivity or potency.⁴⁰

Moreover it is known that the isosteric replacement of a peptide bond represents an important and general tool in design of peptidomimetics together with the incorporation of conformationally restricted units, such as rings, into a peptide sequence to force it to adopt a known, biologically active conformation.⁴¹

In peptidomimetics, alterations to the side chain groups or the peptide backbone are used to improve the peptide's stability and/or biological activity. Since most linear peptides can easily be degraded by enzymatic proteolysis, altering the peptide backbone can help reduce their rate of degradation. The highly charged side chain groups on peptidomimetics provide greater binding affinity and selectivity of the receptors towards these peptidomimetics which will reduce unwanted side effects and improve the therapeutic effects. As a result of their properties, peptidomimetics are of high interest as bioactive agents and as drugs having pharmacological activities.

N-Substituted glycine oligomers (NSG), otherwise referred to as α -peptoids, belonged to peptidomimetics class and are a readily accessible class of synthetic, non-natural peptide mimic of modular design into which a plethora of structural elements can be readily incorporated.⁴² The first NSG reports came from Zuckermann *et al.* in 1992.⁴³ They are mimics of α -peptides in which the side chains are attached to the backbone N^α -amide nitrogen instead of C^α -atom. The schematic comparison of peptides and peptoids, provided in Figure 4, shows the similarities in the spacing of the side chains and the carbonyl groups, and the differences in the chirality of the two monomers.

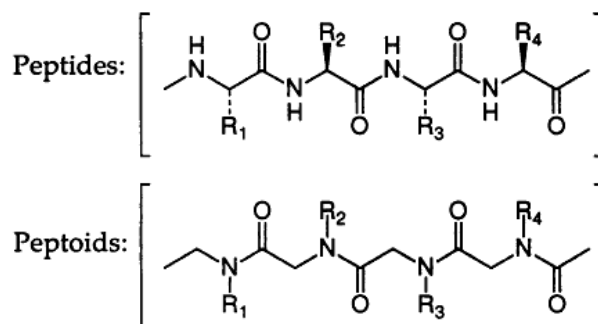


Figure 4. Schematic comparison between peptides and peptoids showing the similarity of spacing of the side chains, and the lack of stereochemistry of the peptoid monomers.

NSG's were originally anticipated as a source of lead structure development in the pharmaceutical industry through the preparation of combinatorial libraries of short oligomers.⁴⁴

Hence, focused on tetrapeptide peptide 26 we decided to synthesize the peptoid analogue (compound **41**, Figure 5).

Recently, the peptoid was tested to verify if it inhibits GRK2 kinase activity. It appears not inhibit notably GRK2 activity compared to peptide 2. Specifically, peptoid 41 causes a $20.5 \pm 3.2\%$ inhibition of GRK2 activity instead of 49.6 ± 6.3 for peptide 2 (data not shown).

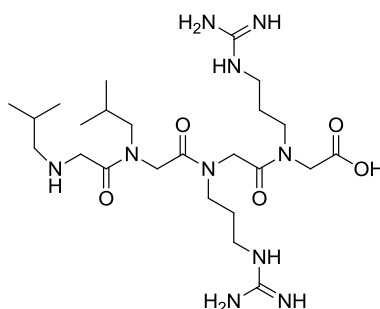


Figure 5. Structure of compound 41.

3. Chemistry

3.1 General procedure for synthesis

The synthesis of peptides (**1-18**, **25-30**) was performed according to the solid phase approach using standard Fmoc methodology in a manual reaction vessel.⁴⁵ The first amino acid, was linked onto the Rink resin (100–200 mesh, 1% DVB, 0.75 mmol/g) previously deprotected by a 25% piperidine solution in *N,N*-dimethylformamide (DMF) for 30 min.

The following protected amino acids were then added stepwise. Each coupling reaction was accomplished using a 3-fold excess of amino acid with HBTU and HOBt in the presence of DIPEA. The N^α-Fmoc protecting groups was removed by treating the protected peptide resin with a 25% solution of piperidine in DMF.

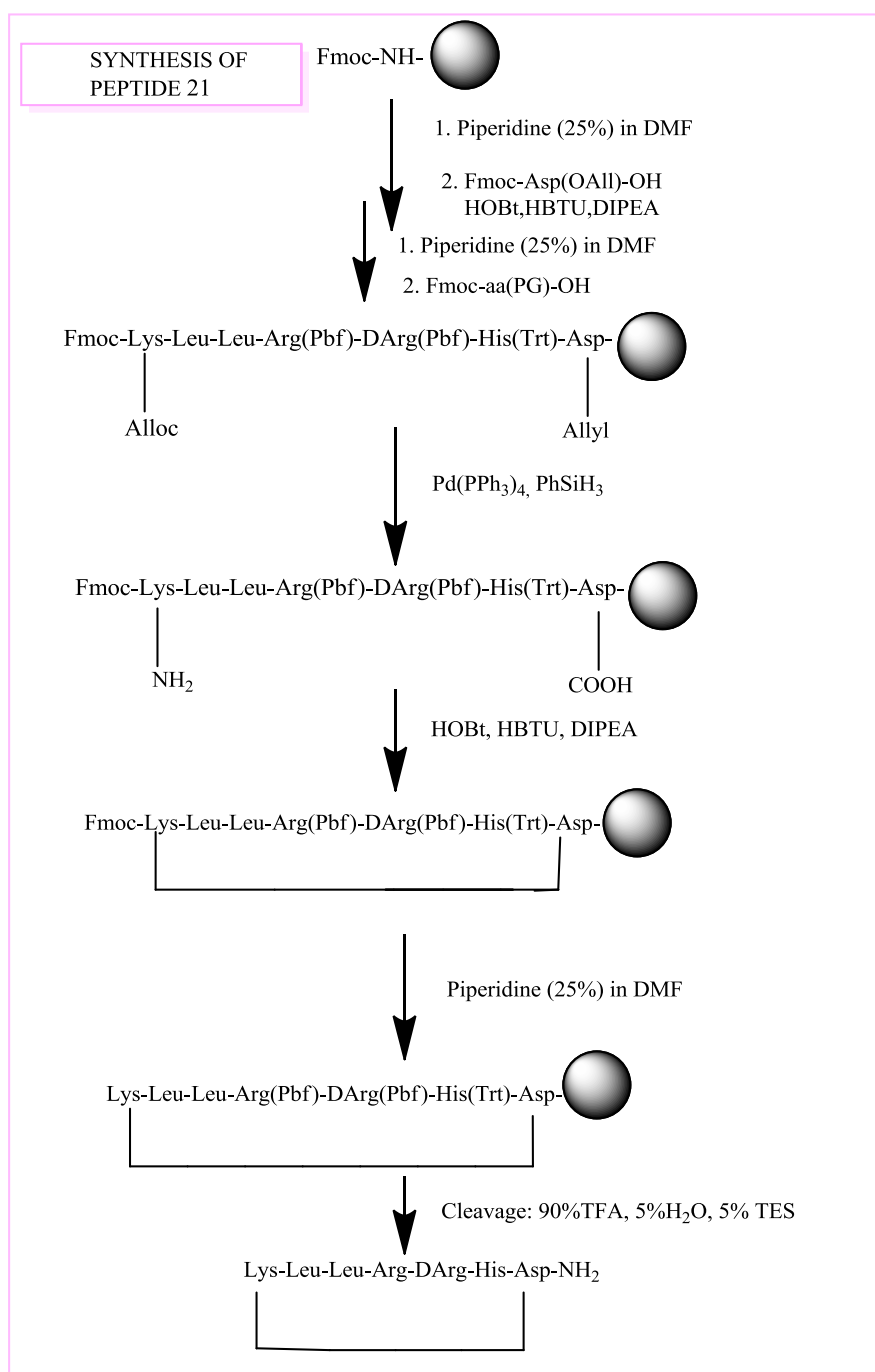
In addition, after each step of deprotection and after each coupling step, Kaiser test was performed to confirm the complete removal of the Fmoc protecting group, respectively, and to verify that complete coupling has occurred on all the free amines on the resin.

The N-terminal Fmoc group was removed as described above, and the peptide was released from the resin with trifluoroacetic acid (TFA)/triisopropylsilane(iPr₃SiH)/H₂O (90:5:5) for 3 h. The resin was removed by filtration, and the crude peptide was recovered by precipitation with cold anhydrous ethyl ether to give a white powder and then lyophilized.

3.2 Synthesis of lactam analogues (peptides 21-24, 32-40)

The corresponding linear peptides were synthesized as described above. The preparation of cyclic peptides, **21-24**, **32-40** through a side-chain-to-side-chain cyclization, was carried out after removal of the Allyl/Alloc protection according to strategy reported by Grieco et al. (Scheme 1).⁴⁶

Structure, inhibition activities, and analytical data of peptides are in Table 3 and Table 5.



Scheme 1. Synthesis and folding of peptide 21.

3.3 Synthesis of head-to-tail cyclic peptides (peptides 19-20, 31)

The title peptides were synthesized using a 2-chlorotrityl chloride resin. The first N^α -Fmoc amino acid and DIPEA were dissolved in dry dichloromethane containing, if necessary, a small amount of dry DMF. This was added to the resin and stirred for 30-120 min. Other N^α -Fmoc amino acids were sequentially coupled as previously described. The final cleavage with AcOH/MeOH/DCM (1:1:8) resulted in protected peptides.⁴⁷

General procedure for cyclization: A solution of the linear protected peptide was added at room temperature to a reaction flask containing a solution of HOBt, HBTU and DIPEA in DMF. The mixture was stirred for 24 h at room temperature and monitored by TLC.

3.4 Synthesis of peptoid (compound 41)

In the solid-phase synthesis of peptoid-peptide hybrids, two different approaches can be used to introduce an N-alkylglycine (peptoid residue) on the growing peptide chain: (i) the N-substituted glycine derivative, suitably protected at the tertiary nitrogen atom, can be separately prepared and directly utilized as building block in the solid phase procedure (monomer method),^{48,49} or (ii) the peptoid residue is built during the peptide chain elongation by a combination of two submonomers, an R-haloacetic acid and a primary amine (submonomer method).⁴³ In both cases to achieve a N-Arg peptoid residue, a suitable NG-protected-3-guanidinopropanamine has to be synthesized in advance.⁵⁰ To speed up the synthesis of N-Arg containing peptoid-peptide hybrids, we optimized a procedure based on the submonomer method, which makes possible a direct assembling of the functionalized peptoid residue starting from commercially available reagents.

For the synthesis of compound **41**, the peptoid residue is built during the peptide chain elongation by a combination of two submonomers, an R-haloacetic acid and a primary amine (submonomer method).

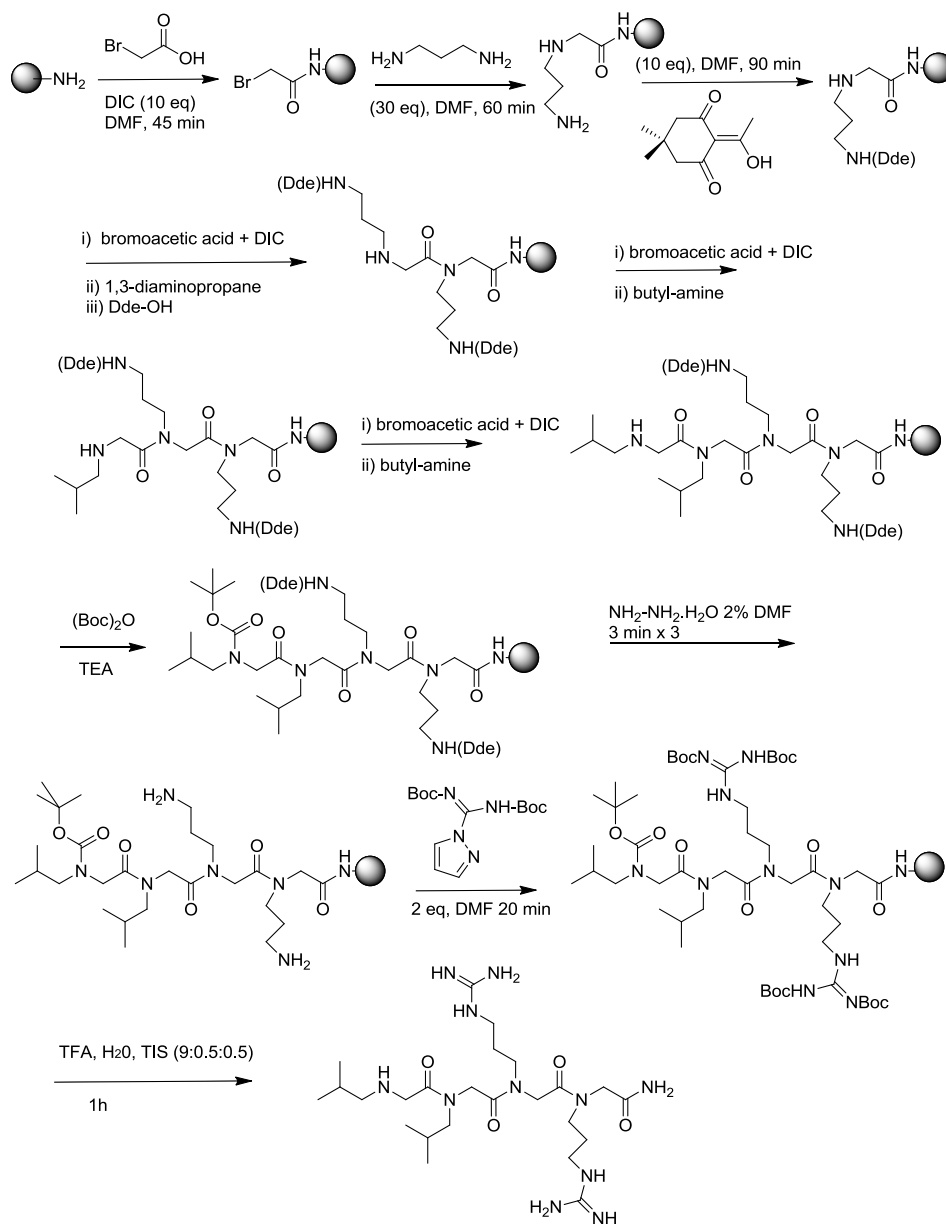
Bromoacetic acid was coupled to the NH_2 -peptide resin in the presence of $\text{N,N}'$ -diisopropylcarbodiimide (DIC).

Initially the Rink resin was deprotected by a 25% piperidine solution in N,N-dimethylformamide (DMF) for 30 min.

Bromoacetic acid was then coupled to the NH₂-peptide resin in the presence of N,N'-diisopropylcarbodiimide (DIC), and the halogen was displaced with a large excess of 1,3-diaminopropane. The resulting N-(3-aminopropyl)glycine (a precursor of NArg) was then selectively protected at the side chain amino function by reaction with 2-acetyl-5,5-dimethyl-1,3-cyclohexanedione (Dde-OH).⁵¹

Further elongation of the peptide chain was carried out according to the standard protocol,⁵² with the addition of Bromo acetic acid and the appropriate amine. The last N-alkylglycine residue was Boc protected with Boc anhydride which is orthogonal to the Dde group. This one was removed from the peptoid side chain by treatment with 2% hydrazine in DMF, and the resulting δ -amino function was on-resin guanidinylated with N,N'-di-Boc-1H-pyrazole-1-carboxamide. Simultaneous deprotection and cleavage of peptides from the resin gave the peptoid-peptide hybrids in high yield (70-80%).

The synthesis is illustrated in Scheme 2:



Scheme 2. Synthesis of compound 41.

3.5 Synthesis of labeled peptides (F1-2, F1-22)

The starting peptides 2 and 22 were synthesized as described above. Then Fmoc-deprotected, resin-bound peptides, were reacted with 5(6)-carboxyfluorescein, N,N' -diisopropyl carbodiimide and 1-

hydroxybenzotriazol at RT. Completeness of N-terminal acylation was confirmed using the Kaiser test.

3.6 Purification and Characterization

All crude peptides were purified by RP-HPLC on a preparative C18-bonded silica column using a Shimadzu SPD 10A UV/VIS detector, with detection at 215 and 254 nm.

All peptides were characterized with analytical RP-HPLC and peptides molecular weights were determined by ESI mass spectrometry and LC-MS in a LC-MS 2010 instrument (Shimadzu) fitted with a C-18 column. All analogues showed >97% purity when monitored at 215 nm. Homogeneous fractions, as established using analytical HPLC, were pooled and lyophilized.

4. Results and discussion

4.1 Inhibitory activity of peptides 3-18

The first part of the work focused on a SAR study and a NMR conformational analysis of peptides **1** and **2** which are able to selectively inhibit GRK2.^{32, 34} Ala scan results (Table 2) indicated that, while C-terminal residues are important for the activity of both peptides, N-terminal residues ²Leu and ³Leu are important only for the shorter peptide **1**. Since the conformational preferences in solution of the two peptides are very similar, a possible explanation of the different SAR observed is that hydrophobic interaction of residues ²Leu and ³Leu with the target are borrowed by ⁸Ile in peptide **2** (⁸Ile is lacking in peptide **1**). ⁴Arg side chain is of little importance for the activity of both the peptides, in contrast, replacement of ⁵Arg with Ala completely abolishes the inhibitory activity.

Since in the original sequence, the amino acid in position 5 is a *D*-enantiomer, ⁵*D*-Arg was substituted by *D*-Ala, in order to discern the real role of molecular orientation from the effects of the amino acid side chain on the inhibitory activity. We found that substitution with a neutral *D*-amino acid

such as Alanine does not change the inhibitory properties of peptides 1 and 2, thus suggesting an important role for the chirality of amino acid 5 rather than for the side chain.

Interestingly, both side chains of ⁴Arg and ⁵D-Arg can be replaced by a neutral amino acid when the chirality is retained. Indeed, peptide **17** (D-Ala derivative of peptide 2) showed the highest GRK2 inhibition potency of the series. These peptides retain specificity for the GRK2 since they were equally effective on GRK2 using two different substrates. Also, they keep selectivity since they are ineffective in inhibition GRK5 activity on the same substrates. Peptide 1, 2, 17 ability to increment basal and βAR stimulated cAMP production in HEK-293 cells is consistent with their effective inhibition of GRK2 (Figure 6). However, the low entity of those increments is likely due to the difficulty of the peptides to cross the cell membrane. The slight higher activity of peptide 2 compared to 1 roughly parallels its higher GRK2 inhibition potency.

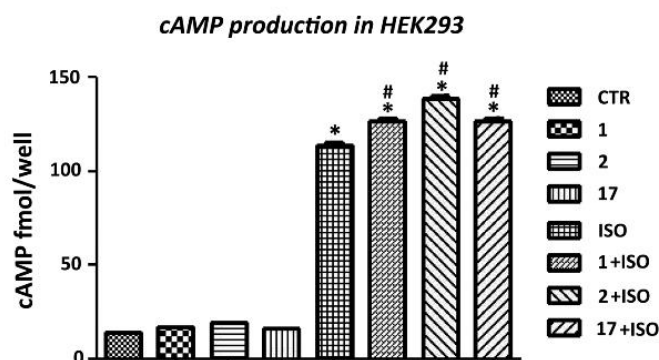


Figure 6. cAMP production in HEK-293 cells treated with 1, 2 and 17 as determined by enzyme immunoassay. ISO: Isoproterenol. Each data point represents the mean±SEM of 3 independent experiments; * = p<0.0001 vs Ctr; # = p<0.01 vs Iso. 89x57mm (600 x 600 DPI).

Differently, slight higher activity of peptide 2 compared to 17 would indicate that, even if ⁵D-Arg is dispensable for GRK2 interaction (Table 2), it can improve the permeating properties of the peptide.

NMR analysis of peptides 1, 2, 16, and 17 was performed in water and DPC micelle solutions. The last is a membrane mimetic medium and was

chosen since GRK2 phosphorylation of GPCRs occurs close to the plasma membrane. Peptides conformational preferences are similar since they have similar diagnostic NMR parameters. Peptides structures in DPC micelles are characterized by two β -turns that involve ^1Gly to ^4Arg and ^2Leu to $^5\text{D-Ala}$ (or $^5\text{D-Arg}$), followed by a short extended region encompassing residues 6 and 7 (Figure 7). The NMR structures of the peptides in DPC are very similar to the X-ray structure of the fragment encompassing the HJ loop of the GRK2 (pdb entry 3CIK)⁵³ which, indeed, was the starting point for the design of the peptides 1 and 2. Figure 7 shows the superposition of the NMR structure of 17 with that of the fragment 383-390 of the GRK2. Equivalent backbone atoms of 17 and GRK2 superimpose to an RMSD of 0.17 Å. It can be also observed the good overlapping of the unchanged side chains which occupies similar space regions. Therefore, the isolated peptide keeps the 3D structure of the protein segment and likely competes with the activation functions of this loop.^{30, 31}

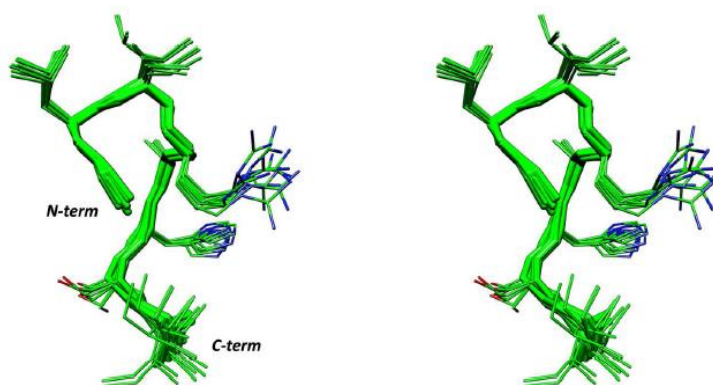


Figure 7. Stereoview of the 10 lowest energy conformers of 17. Structures were superimposed using the backbone heavy atoms. Heavy atoms are shown with different colours (carbon, green; nitrogen, blue; oxygen, red). Hydrogen atoms are not shown for clarity. 150x91mm (300 x 300 DPI).

This result could explain the selectivity observed for these peptides towards GRK2 compared to GRK5. In fact, GRK5 HJ loop corresponding sequence is MIEGQS (CLUSTAL Omega alignment; www.ebi.ac.uk/Tools/msa/clustalo) which compared to the GRK2 sequence LLRGHS has, *inter alia*, a very different charge content (-1 vs +1/+2).

4.2 Inhibitory activity of cyclic peptides (peptides 19-24)

Once we demonstrated that peptides 1 and 2, selectively inhibit GRK2 *in vitro* we decided to focused on these compounds to identify more potent and selective inhibitors of GRK2.³⁴

Peptides 1 and 2 are the not acylated derivatives of compounds KRX-683₁₀₇ and KRX-683₁₂₄, respectively (Table 1), in turn derived from the fragment 383-390 of the HJ loop of GRK2 (Table 1).³²

Conformational similarity of these peptides to the protein fragment within the crystal structure of GRK2,⁵³ prompted us to design novel analogues of peptides 1 and 2 based on head-to-tail and side chain-to-side chain cyclization, according to the HJ loop structure (Figure 2). Hence, the lactam were introduced as a conformational constraint to stabilize the putative 3D active conformation. The utility of backbone or side chain cyclization has been well established in peptides, and it has been demonstrated to increase biological activity and selectivity since they are usually more stable in metabolism than the parent linear molecules.⁵⁴ In this context, lactam bridges are preferable over disulfide ones due to their chemical stability.⁵⁵

All cyclic peptides retain the ability to inhibit GRK2 (Table 3) demonstrating the validity of the design strategy. Potency fluctuations were observed upon the insertion of ⁸Ile in cyclic analogues.

Probably, conformational restraints imposed by the cyclization also affect exocyclic Ile residue spatial orientation which, in turn, influences the inhibitory activity. Cyclic peptide **22** is the most active in the GRK2 inhibition overcoming of about 10% its precursor (peptide 2). Interestingly, peptides also retain selectivity towards GRK2 since they don't affect GRK5 kinase activity on rhodopsin levels. To bring our observation to a biological setup, we tested the effects of GRK2 inhibitors in cells on the beta adrenergic receptors density. Indeed, it is known that GRK2 inhibition can change the affinity state of the beta adrenergic receptor by preventing desensitization,⁵⁶ furthermore recent evidences suggest that also the total number of β adrenergic receptors is under the control of GRK2 activity,⁵⁷ thus indicating that the kinase also

control down regulation, the major and most effective mechanism of regulation of β AR signaling.

Interestingly, peptide **22** results to be more effective than the lead compound **2** to increase β 2AR density (Figure 8A). Similar results are obtained in cAMP production studies. In fact, **22** increases both basal and β 2AR stimulated cAMP production in cells (Figure 8B).

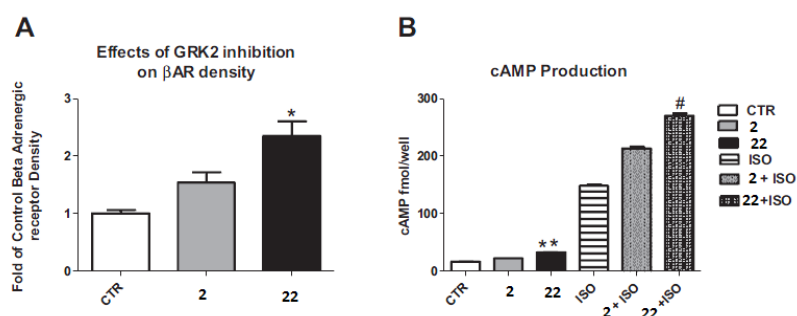


Figure 8. (A) β 2-adrenergic receptors density in HEK-293 cells treated with peptides **2** and **22** (1 mM for 1 h). Each data point represents the mean \pm SEM of 3 independent experiments; * p-value \leq 0.05. (B) cAMP production in HEK-293 cells treated with **2** and **22** as determined by cAMP immunoassay. ISO: Isoproterenol, 0.1 mM. Each data point represents the mean \pm SEM of 3 independent experiments; **p < 0.0001 vs Ctr; #p < 0.01 vs ISO.

These results are particularly important since they indicated these peptides are able to penetrate the cell membrane by itself without the need of acylation (as for KRX-683₁₂₄), conjugation with cell penetrating peptides, etc. To confirm this important suggestion, we measured the internalization of both fluorescently labeled peptides (FI-2 and FI-22, respectively).

As observed in Figure 9A and B, both peptides are able to cross cell membrane with the linear compound FI-2 incorporated to cells more effectively than compound FI-22.

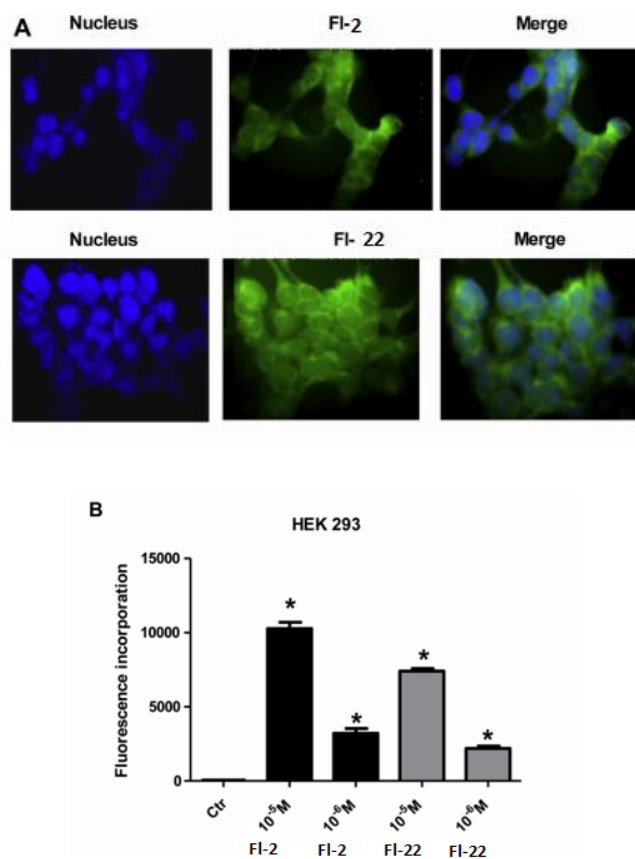


Figure 9. (A) Incorporation of fluorescently labeled peptides into β 2HEK-293 cells. The cells were incubated with 1 mM FI-2 (upper panel) and FI-22 (lower panel) for 1 h. Images were obtained by confocal microscopy. (B) Quantification of 3 experiments measuring fluorescence incorporation of the cells incubated with either FI-2 or FI-22, at either 10 mM or 1 Mm $p < 0.01$ vs Control (Ctr).

Probably, peptide 22 highest potency in the inhibition of GRK2 kinase activity is the predominant factor determining the observed significant increase of β 2 adrenergic receptor density and cAMP production.

Promising compound 22 was also investigated for its conformational preferences. NMR analysis of peptide 22 was performed in water and DPC micelle solutions. It is well-known that water is the best medium to be used for the structural study of peptides. Unfortunately it favors the prevailing of disordered and flexible conformations so that the building of a 3D model is often precluded.

Mixtures made up of water and organic solvents are the most used media to produce environmental constraints. In particular, alcohols and fluoro alcohols are known to stabilize peptide secondary structures.⁵⁸ Micelle solutions are membrane mimetic environments and are largely used for conformational studies of peptide hormones and antimicrobial peptides.⁵⁹ In this case, a micellar solution of DPC was chosen since GRK2 phosphorylation of GPCRs occurs close to the plasma membrane. Peptide **22** structure in DPC micelles is characterized by two β -turns that involve ¹Gly to ⁴Arg and ²Leu to ⁵D-Arg, followed by a short extended region encompassing residues 6 and 7 (Figure 10). Compared to the linear parent peptides, compound **22** shows a lower conformational flexibility (in fact, the backbone heavy atoms RMSD decreases from 0.31 to 0.20 Å, compared to the linear analogue).³⁴

More interestingly, the NMR structures of peptide **22** are very similar to the crystal structure of the fragment encompassing the HJ loop of the GRK2 (pdb entry 3CIK).⁵³ Figure 9 shows the superposition of the NMR structure of **22** with that of the fragment 383-390 of the GRK2. Equivalent backbone atoms of **22** and GRK2 superimpose to an RMSD of 0.17 Å. It can be also observed the good overlapping of the unchanged side chains which occupies similar space regions. Also, ⁸Ile side chain is well overlapped with that of Pro390, supporting the positive contribution of this residue on peptide activity. Therefore, the isolated peptide keeps the 3D structure of the protein segment and likely competes with the activation functions of this loop.³¹

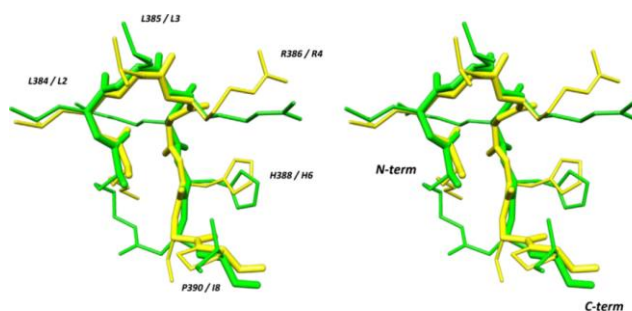


Figure 10. Stereoview of **22** lowest energy conformer (green) and fragment 383-390 of GRK2 (1, yellow, pdb entry 3CIK). The structures are superimposed using the backbone heavy atoms.

4.3 Inhibitory activity of peptides 25-28

The effectiveness of these peptides to inhibit GRK2 kinase activity was assessed by in vitro assay using GRK2 purified protein and the G protein-coupled receptor rod outer segments (ROS) as a substrate (Figure 10) in presence of [γ - 32 P]- adenosine triphosphate (ATP).

Peptide 26 was compared with peptide lead 1, with the same peptide synthesized with CPP (Cell Penetrating Peptide), two lactam cyclic peptides (21 and 23), another tetrapeptide (compound 25) and a tripeptide 27.

It showed that peptide **26**, $^1\text{Leu}^2\text{Leu}^3\text{Arg}^4\text{DArg}$, inhibits GRK2 activity more than lead compound 1 (50.5% versus 47.6%) (Figure 11).

Next, to verify whether these peptides selectively inhibit GRK2, we repeated the activity assay substituting GRK5 to GRK2 purified protein. GRK2 selective inhibition is suggested by the evidence that all peptides don't affect GRK5 kinase activity on rhodopsin phosphorylation levels.

Starting from these interesting data, we designed a peptidomimetic derived from tetrapeptide 26 with the aim to synthesize small molecules in the future.



Figure 11. Inhibitory GRK2 kinase activity for peptides 21, 23, 25, 26 and 27 in vitro assay using GRK2 purified protein and the G protein-coupled receptor rod outer segments (ROS) as a substrate in presence of [γ - 32 P]- adenosine triphosphate (ATP).

Focused on peptide 2, we compared the lead compound, two lactam cyclic peptides (22 and 24), the head-to tail peptide (peptide 20) with tetrapeptide 28, $^1\text{DArg}^2\text{His}^3\text{Ser}^4\text{Ile}$, obtained from N- and C-terminal deletions of peptide 2. This compound inhibits GRK2 of 35.4% instead of 47.6% for peptide lead (Figure 12).

In conclusion, starting from peptides lead, 1 and 2, to design more stable and active peptides some improvement are required. Both deletions and/or cyclization lead to a more active peptides than peptide lead.

The advantage in case of deletion is in a fast and economic synthesis and then we have the possibility to design peptidomimetics and small molecules starting from three-four amino acids.

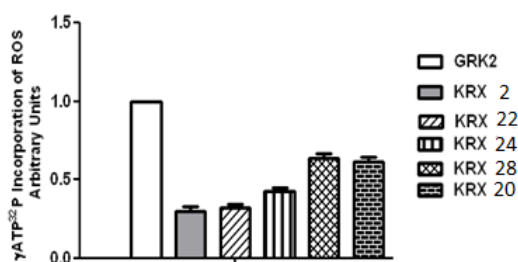


Figure 12. Inhibitory GRK2 kinase activity for peptides 20, 22, 24 and 28 in vitro assay using GRK2 purified protein and the G protein–coupled receptor rod outer segments (ROS) as a substrate in presence of [γ -³²P]- adenosine triphosphate (ATP).

4.4 Effects of GRK2 inhibition on β AR density: a comparison between peptides 22 and 26

To confirm the effectiveness of GRK2 inhibition in a cellular setup, we tested the effects of GRK2 inhibitors in cells on beta adrenergic receptors density in HEK-293 cells stably overexpressing the β_2 adrenergic receptor (β_2 AR).¹¹ In HEK-293 cells, incubation with compound 2, the cyclic peptide 22 (1 mM) and the tetrapeptide 26 results in the increase in β_2 AR density, consistent with an effective inhibition of GRK2 (Figure 13). Interestingly, peptide 22 results to be more effective than the others. Peptide 26 and 2 increase the β_2 AR density in the same manner.

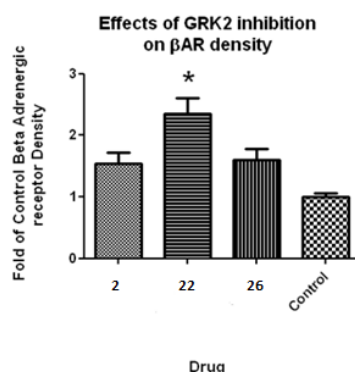


Figure 13. (A) β_2 -adrenergic receptors density in HEK-293 cells treated with peptides 2, 22, 26 (1 mM for 1 h). Each data point represents the mean \pm SEM of 3 independent experiments; * p-value ≤ 0.05 .

For all the other compounds (**34-41**) inhibitory activity assays are in progress.

5. Conclusion

GRK2 is involved in the regulation of many pivotal cell functions, and is therefore a key player in human health and disease, such as in several relevant cardiovascular, inflammatory or cancer pathologies. Hence, modulation of its activity could be exploited with therapeutic purposes.

The present study describes the design, synthesis, and biological evaluation of a series of linear and cyclic peptides which are able to selectively inhibit GRK2.

Starting from peptides **1** and **2**, this study: i) found the (in)dispensable residues which can be replaced in an attempt to improve peptide properties (GRK2 interaction, membrane permeation); ii) determined their conformational preferences which can help the design of novel peptides and peptidomimetics with enhanced conformational stability; iii) found that a restricted conformation increases inhibitory activity and lead to a more stable compound.

In particular, cyclic peptide 22 demonstrated to increase the inhibitory potency of the linear parent 2. Our results showed that 22 also increased, more effectively than 2, the density of β adrenergic receptors and the β AR stimulated cAMP production in cardiac cells, further confirming the GRK2 control on regulation of β AR signaling. These findings confirm that conformational-based chemical modification of the linear fragment encompassing the HJ loop of the GRK2 is an effective approach to identify structures able to modulate GRK2 activity through inhibition.

6. Experimental section

6.1 Synthesis of linear derivatives (peptides 1-18, 25-30)

The synthesis of GRK2 analogues was performed according to the solid phase approach using standard Fmoc methodology in a manual reaction vessel.⁴³ N^{α} -Fmoc-protected amino acids, Rink amide-resin, N-hydroxy-benzotriazole (HOBt), 2-(1H-benzotriazole-1-yl)-1,1,3,3-tetramethyluronium hexafluoro-phosphate (HBTU), N,N-diisopropylethyl-amine (DIPEA), Piperidine and Trifluoroacetic acid were purchased from Iris Biotech (Germany). Peptide synthesis solvents, reagents, as well as CH_3CN for high performance liquid chromatography (HPLC) were reagent grade and were acquired from commercial sources and used without further purification unless otherwise noted. The first amino acid, N^{α} Fmoc-Xaa-OH (Xaa = Ile, Ser(tBu), Ala, DArg(Pbf), His(Trt)) was linked on to the Rink resin (100–200 mesh, 1% DVB, 0.75 mmol/g) previously deprotected by a 25% piperidine solution in N,N-dimethylformamide (DMF) for 30 min.

The following protected amino acids were then added stepwise: N^{α} -Fmoc-Ala-OH, N^{α} -Fmoc-His($N_{(im)}$ trityl(Trt))-OH, N^{α} -Fmoc-DArg(2,2,4,6,7-pentamethyldihydro benzofuran-5-sulfonyl (Pbf))-OH (or N^{α} -Fmoc-DAla-OH), N^{α} -Fmoc-Arg(Pbf)-OH, N^{α} -Fmoc-Leu-OH, N^{α} -Fmoc-Gly-OH, N^{α} -Fmoc-Ser(tBu)-OH. Each coupling reaction was accomplished using a 3-fold excess of amino acid with HBTU and HOBt in the presence of DIPEA (6 eq.).

The N^α-Fmoc protecting groups was removed by treating the protected peptide resin with a 25% solution of piperidine in DMF (1x 5 min and 1x 25 min).

The peptide resin was washed three times with DMF, and the next coupling step was initiated in a stepwise manner. The peptide resin was washed with dichloromethane (DCM) (3×), DMF (3×), and DCM (3×), and the deprotection protocol was repeated after each coupling step.

In addition, after each step of deprotection and after each coupling step, Kaiser test was performed to confirm the complete removal of the Fmoc protecting group, respectively, and to verify that complete coupling has occurred on all the free amines on the resin.

The N-terminal Fmoc group was removed as described above, and the peptide was released from the resin with trifluoroacetic acid (TFA)/triisopropylsilane (iPr₃SiH)/H₂O (90:5:5) for 3 h. The resin was removed by filtration, and the crude peptide was recovered by precipitation with cold anhydrous ethyl ether to give a white powder and then lyophilized.

6.2 Synthesis of head-to-tail cyclic peptides (peptides 19-20, 31)

The title peptides were synthesized using a 2-chlorotrityl chloride resin. The first N^αFmoc-Xaa-OH (Xaa = Ile, Ser(tBu), DArg(Pbf), (0.6-1.2 equiv relative to the resin for 2-chlorotrityl resin) and DIPEA (4 equiv relative to amino acid) were dissolved in dry dichloromethane (DCM) (approx. 10 mL per gram of resin) containing, if necessary, a small amount of dry DMF (enough to facilitate dissolution of the acid). This was added to the resin and stirred for 30-120 min. After stirring, the resin was washed with 3×DCM/MeOH/DIPEA (17:2:1), 3×DCM, 2×DMF and 2×DCM. Other N^α-Fmoc amino acids (4 equiv) were sequentially coupled as previously described. The final cleavage with AcOH/ MeOH/DCM (1:1:8) resulted in protected peptides.^{36,47}

6.2.1 General procedure for cyclization

A solution of the linear protected peptide (0.03 mmol) in DMF (6.5 mL) was added at room temperature to a reaction flask containing a solution of N-

hydroxybenzotriazole (HOBt) (3 equiv, 12 mg, 0.09 mmol), HBTU (3 equiv, 34 mg, 0.09 mmol) and DIPEA (5 equiv, 0.26 mL, 1.5 mmol) in DMF (1 mL). The mixture was stirred for 24 h at room temperature and monitored by TLC. The mixture was concentrated under reduced pressure, and the residue was dissolved in ethyl acetate (AcOEt). The organic phase was washed twice with 5% aqueous sodium bicarbonate (NaHCO₃), dried over sodium sulfate (Na₂SO₄), and filtered. The solvent was removed by reduced pressure to give the final crude protected peptide.

6.3 Synthesis of lactam analogues (peptides 21-24, 32-40)

The corresponding linear peptides were synthesized as described above and the amino acids N^α-Fmoc-Asp(Allyl)-OH, N^α-Fmoc-Glu(Allyl)-OH and N^α-Fmoc-Lys(Alloc)-OH, N^α-Fmoc-Orn(Alloc)-OH, N^α-Fmoc-Dap(Alloc)-OH and N^α-Fmoc-Dab(Alloc)-OH were used as lactam precursors. After linear assembly, the N γ -Alloc and the Allyl groups were removed according to the following procedure: 200 mg of peptide resin was washed with dichloromethane (DCM) under Ar and a solution of PhSiH₃ (24 equiv) in 2 mL of DCM was added. Subsequently a solution of Pd(PPh₃)₄ (0.25 equiv) in 6 mL of DCM was added and the reaction was allowed to proceed under Ar for 30 min. The peptide resin was washed with DCM (3x), DMF (3x) and DCM (4x), and the deprotection protocol was repeated (3x). The macrocyclic lactam ring formation was mediated by addition of HBTU (6 equiv), HOBt (6 equiv) and DIPEA (12 equiv) for 2 h.^{36,46} The process was repeated if necessary (Kaiser test used to monitor completion). The N-terminal Fmoc group was removed and the peptide was released from the resin as described above.

6.3.1 Side-chain deprotection

The protected cyclopeptide (0.02 mmol) was treated with 10 mL of a solution of TFA/triisopropylsilane (TIS)/H₂O 95: 2.5: 2.5 at room temperature. After 24 h, the reaction mixture was evaporated in vacuo, and the residue was

washed with diethyl ether (Et₂O) and concentrated in vacuo, yielding the side chain-deprotected cyclopeptide as a trifluoroacetate salt (quant.).

6.4 Synthesis of peptoid 41

For on-resin assembling of N^K-protected N-aminoalkylglycine residue, a 1 M solution of bromoacetic acid in DMF (10 equiv) and DIC (10 equiv) was added to the N^α-deprotected peptide resin. After the mixture was stirred for 45 min, the resin was washed with DMF (6 times) and a solution of the selected diamine (1,3-diaminopropane and butyl-amine, 30 eq) in DMF was added. After 2 h of reaction, the resin was collected by filtration and washed with DMF. The primary amino group on the resulting peptoid residue was protected by reaction with a 0.5 M solution of Dde-OH (10 equiv, 90 min) in DMF, and the assembling of the peptide chain was resumed. The last N-alkylglycine residue was Boc protected with Boc anhydride. Different from the Fmoc group, the Boc is stable to the basic conditions required to remove the Dde group.

For on-resin guanidinylation of peptoid-peptide hybrids, the peptoid-peptide hybrid, still attached to the solid support, was repetitively treated with 2% hydrazine in DMF (3 times for 3 min) to remove the Dde group from the peptoid side chain.

After the usual washing cycles, the resulting N-aminoalkylglycine residue was guanidylated by reaction with 2 equiv of N,N'-bis-Boc-1-guanylpiperazine (0.03 M in DMF); the reaction was performed at 35 °C and was complete in less than 2 h.⁴⁸

Cleavage of peptides from the resin and removal of the acid labile protecting groups were simultaneously achieved by treatment of the final peptide-peptoid hybrid resin with a TFA-H₂O-triisopropylsilane (TIS) mixture (95:2.5:2.5 by volume) for 90-120 min at room temperature. Peptides were precipitated by addition of cold diethyl ether and dried overnight under vacuum. Crude peptides were obtained in 70-80% yield.

6.5 Synthesis of labeled peptides (FI-2, FI-22)

The starting peptides 2 and 22 were synthesized as described above. Then Fmoc-protected, resin-bound peptides, were reacted with 3 equiv of 5(6)-carboxyfluorescein, N,N'-diisopropyl carbodiimide, and 1-hydroxybenzotriazol, each in DMF for 16 h in 10-mL syringes on a shaker at RT. Reactions were stopped by washing the resins three times each with DMF, methanol, dichloromethane, and diethyl ether. Completeness of N-terminal acylation was confirmed using the Kaiser test.

6.6 Purification and characterization

All crude peptides were purified by RP-HPLC on a preparative C18-bonded silica column (Phenomenex, Jupiter Proteo 90Å, 100 mm × 21.2 mm, 10µm) using a Shimadzu SPD 10A UV/VIS detector, with detection at 210 and 254 nm. The column was perfused at a flow rate of 15 mL/min with solvent A (10%, v/v, water in 0.1% aqueous TFA), and a linear gradient from 10 to 90% of solvent B (80%, v/v, acetonitrile in 0.1% aqueous TFA) over 15 min was adopted for peptide elution. Analytical purity and retention time (t_R, Tables 2-5) of each peptide were determined using HPLC conditions in the above solvent system (solvents A and B) programmed at a flow rate of 1 mL/min using a linear gradient from 10 to 90% B over 15 min, fitted with Phenomenex, Aeris XB-C18 column (150 mm × 4.60 mm, 3.6 µm).

All analogues showed >97% purity when monitored at 215 nm. Homogeneous fractions, as established using analytical HPLC, were pooled and lyophilized.

At the same time, LC-MS was performed in a LC-MS 2010 instrument (Shimadzu) fitted with a C-18 column (Phenomenex, Aeris XB-C18 column (150 mm × 4.60 mm, 3.6 µm) eluted with a 10-90% linear gradient of B into A for all compounds.

To check and to have a confirmation of peptides molecular were used ESI mass spectrometry. ESI-MS analysis in positive ion mode, were made using a Finnigan LCQ ion trap instrument, manufactured by Thermo Finnigan (San

Jose, CA, USA), equipped with the Excalibur software for processing the data acquired. The sample was dissolved in a mixture of water and methanol (50/50) and injected directly into the electrospray source, using a syringe pump, which maintains constant flow at 5 mL/min. The temperature of the capillary was set at 220 °C.

6.7 NMR Spectroscopy

The samples for NMR spectroscopy were prepared by dissolving the appropriate amount of peptide to obtain a concentration 1-2 mM in 0.55 mL of $^1\text{H}_2\text{O}$ (pH 5.5), 0.05 ml of $^2\text{H}_2\text{O}$ for water samples, 200 mM DPC- d_{38} for micelle samples.³⁴ NMR spectra were recorded on a Varian INOVA 700 MHz spectrometer equipped with a z-gradient 5 mm triple-resonance probe head. All the spectra were recorded at a temperature of 25°C. The spectra were calibrated relative to 3 (trimethylsilyl)propionic acid (TSP, 0.00 ppm) as internal standard. One-dimensional (1D) NMR spectra were recorded in the Fourier mode with quadrature detection. Water suppression was achieved by using the double-pulsed field gradient spin-echo (DPFGSE) scheme.⁶⁰ 2D double quantum filtered correlated spectroscopy (DQF-COSY),⁶¹ TOCSY,⁶² and NOESY⁶³ spectra were recorded in the phase-sensitive mode using the method of States.⁶⁴ Data block sizes were 2048 addresses in t_2 and 512 equidistant t_1 values. Before Fourier transformation, the time domain data matrices were multiplied by shifted \sin^2 functions in both dimensions. A mixing time of 70 ms was used for the TOCSY experiments. NOESY experiments were run with mixing times in the range of 100-200 ms. The qualitative and quantitative analyses of DQF-COSY, TOCSY, and NOESY spectra, were obtained using the interactive program package XEASY.⁶⁵ $^3J_{\text{HN-H}\alpha}$ coupling constants were obtained from 1D ^1H NMR and 2D DQF-COSY spectra. Many $^3J_{\text{HN-H}\alpha}$ coupling constants were difficult to measure in DPC solution probably because of a combination of small coupling constants and broad lines. The temperature coefficients of the amide proton chemical shifts were calculated from 1D ^1H NMR and 2D TOCSY experiments performed at different temperatures by means of linear regression.

6.7.1 Structural Determinations

The NOE-based distance restraints were obtained from NOESY spectra collected with a mixing time of 200 ms. The NOE cross peaks were integrated with the XEASY program and were converted into upper distance bounds using the CALIBA program incorporated into the program package VDYANA. Cross peaks which overlapped more than 50% were treated as weak restraints in the DYANA calculation. For each examined peptide, an ensemble of 100 structures was generated with the simulated annealing of the program DYANA. An error-tolerant target function (tf-type=3) was used to account for the peptide intrinsic flexibility of the peptide. The annealing procedure produced 100 conformations from which 20 structures were chosen, whose interprotonic distances best fitted NOE derived distances, and then refined through successive steps of restrained and unrestrained EM calculations using the Discover algorithm (Accelrys, San Diego, CA) and the consistent valence force field (CVFF)⁶⁶ as previously described. Graphical representation were carried out with the the UCSF Chimera package.⁶⁷ RMS deviation analysis between energy minimized structures were carried out with the program MOLMOL.⁶⁸

6.8 In Vitro Methods

6.8.1 GRK Activity in Rhodopsin Phosphorylation Assays

To evaluate the effect of all synthesized peptides on GRK2 activity we assessed GRK2 or GRK5 purified proteins by light-dependent phosphorylation of rhodopsin-enriched rod outer segment membranes (ROS) using [γ -³²P]-ATP as previously described.^{17,69} Briefly, 50 ng of active GRK2 or GRK5 were incubated with ROS membranes in presence or absence of inhibitor peptides in reaction buffer (25 mL) containing 10 mM MgCl₂, 20 mM Tris-Cl, 2 mM ethylenediaminetetraacetic acid (EDTA), 5 mM ethylene glycol tetraacetic acid (EGTA), and 0.1 mM ATP and 10 Ci of [γ -³²P]-ATP. After incubation with white light for 15 minutes at room temperature, the reaction was

quenched with ice-cold lysis buffer and centrifuged for 15 minutes at 13000g. The pelleted material was resuspended in 35 μ L protein gel loading dye, electrophoresed and resolved on SDS-PAGE 4-12% gradient (Invitrogen), stained with Coomassie blue, destained, vacuum dried, and exposed for autoradiography. Phosphorylated rhodopsin was visualized by autoradiography of dried gels and quantified using a PhosphorImager (Molecular Dynamics). Alternatively, the pellet was resuspended in 100 μ L of ice-cold lysis buffer and the level of [γ - 32 P]-ATP incorporation into ROS was determined by liquid scintillation counter.

6.8.2 MBP Kinase assay

50 ng of active GRK2 or GRK5 were assayed on 100 ng of purified MBP in presence or absence of peptides 1-30. Phosphorylation reactions were initiated by adding 20 mM ATP, 1 mM CaCl₂, 20 mM MgCl₂, 4 mM Tris, pH 7.5, and 10 Ci of [γ - 32 P]-ATP (specific activity 3000 Ci/mmol) and prolonged for 30 min at 37°C. Laemmli buffer was added to stop the reaction.

Sample were processed as above described.¹¹

6.8.3 cAMP synthesis

HEK 293 overexpressing β 2AR were plated in 96-well plates (10,000 cells/well) and serum starved overnight. Cells were incubated in a fresh medium in the presence 2 and 22 peptides 1 μ M for one hour and then stimulated with non selective β adrenergic receptor agonist Isoproterenol 10 μ M for 15 min. The cAMP quantification was evaluated by enzyme immunoassay, using an EIA commercial kit (RPN 2255 GE Healthcare Bio-Sciences AB, Uppsala, Sweden). The cAMP content present in HEK- 293 cell was expressed in fmoles per well. All values are presented as mean \pm SEM of three independent experiments. One-way ANOVA was performed to compare the different groups. A significance level of $P < 0.05$ was assumed for all statistical evaluations.

Statistics were computed with GraphPad Prism Software (GraphPad Software Inc., version 4, San Diego, CA, USA).

6.9 β -Adrenoreceptor radioligand binding

Cultured Embryonic Kidney cells overexpressing β_2 adrenergic receptor (β_2 HEK-293) were treated with peptides 2 and 22 1 mM for one hour. Membrane fraction was prepared by homogenization of whole cell in ice-cold buffer (25 mM Tris-HCl (pH 7.5), 5 mM EDTA, 5 mM EGTA, 1 mM phenylmethylsulfonyl fluoride, 2 mg/mL each leupeptin and aprotinin) as previously described.¹¹

Total β AR density was determined by incubating 60 mg of sarcolemmal membranes with a saturating concentration of [¹²⁵I]cyanopindolol and 20 mmol/L alprenolol to define nonspecific binding.

Assays were conducted at 37 °C for 60 min and then filtered over GF/C glass fiber filters (Whatman) that were washed and counted in a gamma counter.⁵⁶ All values are presented as mean \pm SEM of three independent experiments. One-way ANOVA was performed to compare the different groups. A significance level of P <0.05 was assumed for all statistical evaluations. Statistics were computed with GraphPad Prism Software (GraphPad Software Inc., version 4, San Diego, CA, USA).

6.10 Internalization studies

β_2 HEK-293 overexpressing human β_2 AR cells were plated in 4-well ibidi plate (10,000 cells/well) and serum starved overnight.

The cells were then incubated with fluorescently labeled peptides (Fl-2 and Fl-22) 1 mM for 60 min at 37°C. After washing twice with PBS cell images were taken by using an Eclipse E1000 Fluorescence Microscope (Nikon) and acquired by using Sigma Scan Pro software (Jandel). Images were optimized for contrast in Adobe Photoshop, but no further manipulations were made.

Alternatively HEK-293 cells were plated in 24-well plates (20,000 cells/well) and serum starved overnight The cells were then incubated with

fluorescently labeled peptides (Fl-2 and Fl-22) at the concentration of 10 and 1 mM for 60 min at 37°C. The fluorescence incorporation was quantified on a Tecan Genios plate reader with a 485 nm excitation filter and a 510 nm emission filter using a gain setting of 1.0. The background signal from cells untraced was subtracted. All values are presented as mean \pm SEM of three independent experiments. One-way ANOVA was performed to compare the different groups. A significance level of $P < 0.05$ was assumed for all statistical evaluations. Statistics were computed with GraphPad Prism Software (GraphPad Software Inc., version 4, San Diego, CA, USA).

¹ Pitcher, JA.; Freedman, NJ.; Lefkowitz, RJ. G Protein-coupled receptor kinases. *Annu Rev Biochem* **1998**, 67, 653-692.

² Ferguson, S. Evolving concepts in G protein-coupled receptor endocytosis: The role in receptor desensitization and signalling. *Pharmacol Rev* **2001**, 53, 1-24.

³ Reiter, E.; Lefkowitz, RJ. GRKs and beta-arrestins: roles in receptor silencing, trafficking and signaling. *Trends Endocrinol Metab* **2006**, 17, 159-165.

⁴ a) Moore, CA.; Milano, SK.; Benovic, JL. Regulation of Receptor Trafficking by GRKs and Arrestins. *Annu Rev Physiol* **2007**, 69, 451-482; (b) Hupfeld, CJ.; Olefsky, JM. Regulation of Receptor Tyrosine Kinase Signaling by GRKs and β -Arrestins. *Annu Rev Physiol* **2007**, 69, 561-577.

⁵ Ribas, C.; Penela, P.; Murga, C.; Salcedo, A.; Garcia-Hoz, C.; Juradopueyo, M.; Aymerich, I.; Mayor, Jr. F. The G protein-coupled receptor kinase (GRK) interactome: role of GRKs in GPCR regulation and signaling. *Biochim Biophys Acta* **2007**, 1768, 913-922.

⁶ a) Oppermann, M.; Diverse-Pierluissi, M.; Drazner, MH.; Dyer, SL.; Freedman, NJ.; Peppel KC.; Lefkowitz, RJ. Monoclonal antibodies reveal receptor specificity among G-protein coupled receptor kinases. *Proc Natl Acad Sci U.S.A.* **1996**, 93, 7649-7654; (b) Willets, JM.; Challiss RA J.; Nahorski, SR. Non-visual GRKs: are we seeing the whole picture? *Trends Pharmacol Sci* **2003**, 24, 626-633.

⁷ Inglesef, J.; Freedman, NJ.; Koch, WJ.; Lefkowitz, RJ. Structure and mechanism of the G protein-coupled receptor kinases. *J Biol Chem* **1993**, 268, 23735-23738.

⁸ Penela, P.; Murga, C.; Ribas, C.; Lafarga, V.; Mayor, Jr. F. The complex G protein coupled receptor kinase 2 (GRK2) interactome unveils new physiopathological targets. *Br J Pharmacol* **2010**, 160, 821-832.

⁹ Jurado-Pueyo, M.; Campos, PM.; Mayor, Jr. F.; Murga C. GRK2-dependent desensitization downstream of G proteins. *J Recept Signal Transduct Res* **2008**, 28, 59-70.

¹⁰ Evron, T.; Daigle, TL.; Caron, MG; GRK2: multiple roles beyond G protein-coupled receptor desensitization. *Trends Pharmacol Sci* **2012**, 33, 154-164.

¹¹ Cipolletta, E.; Campanile, A.; Santulli, G.; Sanzari, E.; Leosco, D.; Campiglia, P.; Trimarco, B.; Iaccarino, G. The G protein coupled receptor kinase 2 plays an essential role in beta-adrenergic receptor-induced insulin resistance. *Cardiovasc Res* **2009**, 84, 407-415.

¹² Matkovich, SJ.; Diwan, A.; Klanke, JL.; Hammer, DJ.; Marreez, Y.; Odley, AM.; Brunskillm EW.; Koch, WJ.; Schwartz, RJ.; Dorn, GW. Cardiac-Specific Ablation of G-Protein Receptor Kinase 2 Redefines Its Roles in Heart Development and β -Adrenergic Signaling. *Circ Res* **2006**, 99, 996-1003.

¹³ Penela, P.; Rivas, V.; Salcedo, A.; Mayor, Jr. F. G protein-coupled receptor kinase 2 (GRK2) modulation and cell cycle progression. *Proc Natl Acad Sci U S A* **2010**, 107, 1118-1123.

¹⁴ Penela, P.; Ribas, C.; Aymerich, I.; Mayor, Jr. F. New roles of G protein-coupled receptor kinase 2 (GRK2) in cell migration. *Cell Adh Migr* **2009**, 3, 19-23.

¹⁵ Ferguson, SS. Phosphorylation-independent attenuation of GPCR signaling. *Trends Pharmacol Sci* **2007**, 28, 173-179.

¹⁶ Metaye, T.; Gibelin, H.; Perdrisot, R.; Kraimps, JL. Pathophysiological roles of G-protein-coupled receptor kinases. *Cell Signal* **2005**, 17, 917-928.

¹⁷ Iaccarino, G.; Barbato, E.; Cipolletta, E.; De Amicis, V.; Margulies, KB.; Leosco, D.; Trimarco, B.; Koch, WJ. Elevated myocardial and lymphocyte GRK2 expression and activity in human heart failure. *Eur Heart J* **2005**, 26, 1752-1758.

¹⁸ Vroon, A.; Kavelaars, A.; Limmroth, V.; Lombardi, MS.; Goebel, MU.; Van Dam, AM.; Caron, MG.; Schedlowski, M.; Heijnen, CJ. G Protein-Coupled Receptor Kinase 2 in Multiple Sclerosis and Experimental Autoimmune Encephalomyelitis. *J Immunol* **2005**, 174, 4400-4406.

¹⁹ Dorsam, RT.; Gutkind, JS. G-protein-coupled receptors and cancer. *Nat Rev Cancer* **2007**, 7, 79-94.

²⁰ a) Iaccarino, G.; Koch, WJ. Therapeutic potential of G-protein coupled receptor kinases in the heart. *Expert Opinion on Investig Drugs* **1999**, 8, 545-554; b) Rengo, G.; Lymperopoulos, A.; Leosco, D.; Koch WJ. GRK2 as a novel gene therapy target in heart failure. *J Mol Cell Cardiol* **2011**, 50, 785-792.

²¹ Ho, J.; Cocolakis, E.; Dumas, VM.; Posner, BI.; Laporte, SA.; Lebrun, JJ. The G protein-coupled receptor kinase-2 is a TGFbeta-inducible antagonist of TGFbeta signal transduction. *Embo J* **2005**, 24, 3247-3258.

²² Metaye, T.; Levillain, P.; Kraimps, JL.; Perdrisot, R. Immunohistochemical detection, regulation and antiproliferative function of G-protein-coupled receptor kinase 2 in thyroid carcinomas. *J Endocrinol* **2008**, 198, 101-110.

²³ Poppel, K.; Jacobson, A.; Huang, X.; Murray, JP.; Oppermann, M.; Freedman, NJ. Overexpression of G protein-coupled receptor kinase-2 in smooth muscle cells attenuates mitogenic signaling via G protein coupled and platelet-derived growth factor receptors. *Circulation* **2000**, 102, 793-799.

²⁴ Wan, KF.; Sambhi, BS.; Tate, R.; Waters, C.; Pyne, NG. The inhibitory γ subunit of the type 6 retinal cGMP phosphodiesterase functions to link c-Src and G-protein-coupled receptor kinase 2 in a signaling unit that regulates p42/p44 mitogen-activated protein kinase by epidermal growth factor. *J Biol Chem* **2003**, 278, 18658-18663.

²⁵ Bliziotis, M.; Gunness, M.; Zhang, X.; Nissenson, R.; Wiren, K. Reduced G-protein-coupled-receptor kinase 2 activity results in impairment of osteoblast function. *Bone* **2000**, 27, 367-373.

²⁶ Metaye, T.; Gibelin, H.; Perdrisot, R.; Kraimps, JL. Pathophysiological roles of G-protein-coupled receptor kinases. *Cell Signal* **2005**, 17, 917-928.

²⁷ Salcedo, A.; Mayor, Jr. F.; Penela, P. Mdm2 is involved in the ubiquitination and degradation of G-protein-coupled receptor kinase 2. *Embo J* **2006**, 25, 4752-4762.

²⁸ Iino, M.; Furugori, T.; Mori, T.; Moriyama, S.; Fukuzawa, A., Shibano, T. Rational Design and Evaluation of New Lead Compound Structures for Selective bArk1 Inhibitors. *J Med Chem* **2002**, 45, 2150-2159.

²⁹ Takeda Pharmaceuticals Company Limited, Ikeda, S., kaneko, M., Fujiwara, S. World patent WO2007034846.

³⁰ Winstel, R.; Ihlenfeldt, HG.; Jung, G.; Krasel, C.; Lohse, MJ. Peptide inhibitors of G protein-coupled receptor kinases. *Biochem Pharmacol* **2005**, 70, 1001-1008.

³¹ Anis, Y.; Leshem, O.; Reuveni, H.; Wexler, I.; Ben Sasson, R.; Yahalom, B.; Laster, M.; Raz, I.; Ben Sasson, S.; Shafrir, E.; Ziv, E. Antidiabetic effect of novel modulating peptides of G-protein-coupled kinase in experimental models of diabetes. *Diabetologia*, **2004**, 47, 1232-1244.

³² Niv, MY.; Rubin, H.; Cohen, J.; Tsurulnikov, L.; Licht, T.; Peretzman-Shemer, A.; Cnàan, E.; Tartakovsky, A.; Stein, I.; Albeck, S.; Weinstein, I.; Goldenberg-Furmanov, M.; Tobi, D.; Cohen, E.; Laster, M.; Ben-Sasson, SA.; Reuveni, H. Sequence-based design of kinase inhibitors applicable for therapeutics and target identification. *J Biol Chem* **2004**, 279, 1242-1255.

³³ Mayer, G.; Wulffen, B.; Huber, C.; Brockmann, J.; Flicke, B.; Neumann, L.; Hafenbradl, D.; Kleb, B.M.; Lohse, M.J.; Krasel, C.; Blind, M. An RNA molecule that specifically inhibits G-protein-coupled receptor kinase 2 in vitro. *RNA* **2008**, 14, 524-534.

³⁴ Gomez-Monterrey, I.; Carotenuto, A.; Cipolletta, E.; Sala, M.; Vernieri, E.; Limatola, A.; Bertamino, A.; Musella, S.; Grieco, P.; Trimarco, B.; Novellino, E.; Iaccarino, G.; Campiglia, P. SAR study and conformational analysis of a series of novel peptide G protein-coupled receptor kinase 2 (GRK2) inhibitors. *Biopolymers* **2014**, 101, 121-128.

³⁵ Kishimoto, A.; Nishiyama, K.; Nakanishi, H.; Uratsujig, Y.; Nomura, H.; Takeyama, Y.; Nishizuka, Y. Studies on the phosphorylation of myelin basic protein by protein kinase C and adenosine 3':5'-monophosphate-dependent protein kinase. *J Biol Chem* **1985**, 260, 12492-12499.

³⁶ Carotenuto, A.; Cipolletta, E.; Gomez-Monterrey, I.; Sala, M.; Vernieri, E.; Limatola, A.; Bertamino, A.; Musella, S.; Sorriento, D.; Grieco, P.; Trimarco, B.; Novellino, E.; Iaccarino, G.; Campiglia, P. Design, synthesis and efficacy of novel G protein-coupled receptor kinase 2 inhibitors. *Eur J Med Chem* **2013**, 69, 384-392.

³⁷ Wishart, D.S.; Sykes, B.D.; Richards, F.M. The Chemical Shift Index: a fast method for the assignment of protein secondary structure through NMR spectroscopy. *Biochemistry* **1992**, 31, 1647-1651.

³⁸ Hruby, V.J.; Bonner, G.G. Design of Novel Synthetic Peptides Including Cyclic Conformationally and Topographically Constrained Analogs. *Methods in Mol Biol* **1994**, 35, 201-240.

³⁹ Cerminara, I.; Chiumminto, L.; Funicello M.; Guarnaccio A.; Lupattelli, P. Heterocycles in Peptidomimetics and Pseudopeptides: Design and Synthesis. *Pharmaceuticals* **2012**, 5, 297-316.

⁴⁰ Grauer, A.; Konig, B. Peptidomimetics-A versatile route to biologically active compounds. *Eur J Org Chem* **2009**, 5099-5113.

⁴¹ Edmonds, M.K.; Abell, A.D. Design and synthesis of a conformationally restricted *trans* peptide isostere based on the bioactive conformations of saquinavir and nelfinavir. *J Org Chem* **2001**, 66, 3747-3752.

⁴² Culf, A.S.; Ouellette, R.J. Solid-Phase Synthesis of N-Substituted Glycine Oligomers (α -Peptoids) and Derivatives. *Molecules* **2010**, 15, 5282-5335.

⁴³ Zuckermann, R.N.; Kerr, J.M.; Kent, S.B.H.; Moos, W.H. Efficient method for the preparation of peptoids [oligo(N-substituted glycines)] by submonomer solid-phase synthesis. *J Am Chem Soc* **1992**, 114, 10646-10647.

⁴⁴ Patch, J.A.; Kirshenbaum, K.; Seurnyck, S.L.; Zuckermann, R.N.; Barron, A.E. Versatile Oligo (N-Substituted) Glycines: The Many Roles of Peptoids in Drug Discovery. *Pseudopeptides in Drug Discovery* **2004**, 1-31.

⁴⁵ Atherton, E.; Sheppard, RC. Solid-Phase Peptide Synthesis: A Practical Approach. *IRL Press: Oxford, U.K.* **1989**.

⁴⁶ Grieco, P.; Gitiu PM.; Hruby, VJ. Preparation of 'side-chain-to-side-chain' cyclic peptides by allyl and alloc strategy: potential for library synthesis. *J Pept Res* **2001**, *57*, 250-256.

⁴⁷ Chen, X.; Park, R.; Shahinian, AH.; Bading, JR.; Conti, PS. Pharmacokinetics and tumor retention of ¹²⁵I-labeled RGD peptide are improved by PEGylation. *Nucl Med Biol* **2004**, *31*, 11-19.

⁴⁸ Gobbo, M.; Benincasa, M.; Bertoloni, G.; Biondi, B.; Dosselli, R.; Papini, E.; Reddi, E.; Rocchi, R.; Tavano, R.; Gennaro, R. Substitution of the Arginine/Leucine Residues in Apidaecin Ib with Peptoid Residues: Effect on Antimicrobial Activity, Cellular Uptake, and Proteolytic Degradation. *J Med Chem* **2009**, *52*, 5197-5206.

⁴⁹ Simon, RJ.; Kania, RS.; Zuckermann, RN.; Huebner, VD.; Jewell, DA.; Banville, S.; Wang, Ng, S.; L.; Rosenberg, S.; Marlowe, CK.; Spellmeyer, DC.; Tan, R.; Frankel, AD.; Santi, DV.; Cohen, FE.; Bartlett, PA. Peptoids: a modular approach to drug discovery. *Proc Natl Acad Sci U.S.A.* **1992**, *89*, 9367-9371.

⁵⁰ Uno, T.; Beausoleil, E.; Goldsmith, RA.; Levine, BH.; Zuckermann, RN. New submonomers for poly N-substituted glycines (peptoids). *Tetrahedron Lett* **1999**, *40*, 1475-1478.

⁵¹ Bycroft, BW.; Chan, WC.; Chhabra, SR.; Dome, ND. A novel lysine-protecting procedure for continuous solid phase synthesis of branched peptides. *J Chem Soc Chem Commun* **1993**, 778-779.

⁵² Robinson, S.; Roskamp, EJ. Solid phase synthesis of guanidines. *Tetrahedron* **1997**, *53*, 6697-6705.

⁵³ Tesmer, JJ .G.; Tesmer, VM.; David T.; Lodowski, DT.; Steinhagen, H.; Huber, J. Structure of human G protein-coupled receptor kinase 2 in complex with the kinase inhibitor balanol. *J Med Chem* **2010**, *53*, 1867-1870.

⁵⁴ Gilon, C.; Mang, C.; Lohof, E.; Friedler, A.; Kessler, H. Synthesis of Peptides and Peptidomimetics. *Eds.: M. Goodman, A. Felix, L. Moroder, C. Toniolo; Thieme Verlag, Stuttgart, New York* **2003**, 215-271.

⁵⁵ (a) Hargittai, B.; Solé, NA.; Groebe DR.; Abramson, SN.; Barany, G. Chemical syntheses and biological activities of lactam analogues of alpha-conotoxin SI. *J Med Chem* **2000**, *43*, 4787-4792; (b) Grieco, P.; Carotenuto, A.; Patacchini, R.; Maggi, CA.; Novellino, E.; Rovero, P. Design, synthesis, conformational analysis, and biological studies of urotensin-II lactam analogues. *Bioorg Med Chem* **2002**, *10*, 3731-3739.

⁵⁶ Iaccarino, G.; Barbato, E.; Cipolletta, E.; Esposito, A.; Fiorillo, A.; Koch, WJ.; Trimarco, B. Cardiac betaARK1 upregulation induced by chronic salt deprivation in rats. *Hypertension* **2001**, *38*, 255-260.

⁵⁷ Perino, A.; Ghigo, A.; Ferrero, E.; Morello, F.; Santulli, G.; Baillie, GS.; Damilano, F.; Dunlop, AJ.; Pawson, C.; Walser, R.; Levi, R.; Altruda, F.; Silengo, L.; Langeberg, LK.; Neubauer, G.; Heymans, S.; Lembo, G.; Wymann, MP.; Wetzker, R.; Houslay, MD.; Iaccarino, G.; Scott, JD.; Hirsch, E. Integrating cardiac PIP₃ and cAMP signaling through a PKA anchoring function of p110 γ . *Mol Cell* **2011**, 42, 84-95.

⁵⁸ (a) Shiraki, K.; Nishikawa, K.; Goto, Y. Trifluoroethanol-induced stabilization of the alpha-helical structure of beta-lactoglobulin: implication for nonhierarchical protein folding. *J Mol Biol* **1995**, 254, 180-194; (b) Gomez-Monterrey, I.; Sala, M.; Rusciano, MR.; Monaco, S.; Maione, AS.; Iaccarino, G.; Tortorella, P.; D'Ursi, AM.; Scrima, M.; Carotenuto, A.; De Rosa, G.; Bertamino, A.; **Vernieri, E.**; Grieco, P.; Novellino, E.; Illario, M.; Campiglia, P. Characterization of a selective CaMKII peptide inhibitor. *Eur J Med Chem* **2013**, 62, 425-434; (c) Carotenuto, A.; Alcaro, MC.; Saviello, MR.; Peroni, E.; Nuti, F.; Papini, AM.; Novellino, E.; Rovero, P. Designed glycopeptides with different β -turn types as synthetic probes for the detection of autoantibodies as biomarkers of multiple sclerosis. *J Med Chem* **2008**, 51, 5304-5309.

⁵⁹ (a) Di Cianni, A.; Carotenuto, A.; Brancaccio, D.; Novellino, E.; Reubi, JC.; Beetschen, K.; Papini, AM.; Ginanneschi, M.; Novel octreotide dicarbanalogues with high affinity and different selectivity for somatostatin receptors. *J Med Chem* **2010**, 53, 6188-6197; (b) Grieco, P.; Carotenuto, A.; Auriemma, L.; Saviello, MR.; Campiglia, P.; Gomez-Monterrey, I.; Marcellini, L.; Luca, V.; Barra, D.; Novellino, E.; Mangoni, ML. The effect of D-amino acids substitution on the selectivity of temporin L towards target cells: identification of a potent anti-Candida peptide. *Biochim Biophys Acta* **2013**, 1828, 652-660.

⁶⁰ Hwang, TL.; Shaka, A. Water Suppression that Works. Excitation Sculpting Using Arbitrary Waveforms and Pulsed Field Gradients. *J Magn Reson* **1995**, 112, 275-279.

⁶¹ Piantini, U.; Sorensen, O.; Ernst RR. Multiple quantum filters for elucidating NMR coupling networks. *J Am Chem Soc* **1982**, 104, 6800-6801.

⁶² Braunschweiler, L.; Ernst, RR. Coherence transfer by isotropic mixing: application to proton correlation spectroscopy. *J Magn Reson* **1983**, 53, 521-528.

⁶³ Jeener, J.; Meier, BH.; Bachman, P.; Ernst RR. Investigation of exchange processes by two-dimensional NMR spectroscopy. *J Chem Phys* **1979**, 71, 4546-4553.

⁶⁴ States, DJ.; Haberkorn, RA.; Ruben DJ. A Two-Dimensional Nuclear Overhauser Experiment with Pure Absorption Phase in Four Quadrants. *J Magn Reson* **1982**, 48, 286-292.

⁶⁵ Bartels, C.; Xia, T.; Billeter, M.; Guntert, P.; Wuthrich, K. The program XEASY for computer-supported NMR spectral analysis of biological macromolecules. *J Biomol NMR* **1995**, 6, 1-10.

⁶⁶ Maple, JR.; Dinur, U.; Hagler, AT. Derivation of force fields for molecular mechanics and dynamics from ab initio energy surfaces. *Proc Natl Acad Sci USA*. **1988**, 85, 5350-5354.

⁶⁷ Pettersen, EF.; Goddard, TD.; Huang, CC.; Couch, GS.; Greenblatt, DM.; Meng, EC.; Ferrin, TE. UCSF Chimera--a visualization system for exploratory research and analysis. *J Comput Chem* **2004**, 25, 1605-1612.

⁶⁸ Koradi, R.; Billeter, M.; Wuthrich, K. MOLMOL: A program for display and analysis of macromolecular structures. *J Mol Graph* **1996**, 14, 51-55.

⁶⁹ Cho, M-C.; Rao, M.; Koch, WJ.; Thomas, SA.; Palmiter, RD.; Rockman, HA. Enhanced Contractility and Decreased β -Adrenergic Receptor Kinase-1 in Mice Lacking Endogenous Norepinephrine and Epinephrine. *Circulation* **1999**, 99, 2702-2707.

CHAPTER 4

Characterization of a selective CaMKII peptide inhibitor

Abstract Analogues of potent CaMKinase II inhibitor, CaM-KNtide, were prepared to explore new structural requirements for the inhibitory activity. The full potency of CaMKII inhibition by CaM-KIIN α is contained within a minimal region of 17 amino acids (peptide 5, KRPPKLGQIGRAKRVVI). Fusion with the tat sequence generated the cell-penetrating inhibitor version tat-5. This tat-5 fusion peptide maintained selectivity for CaMKII over CaMKI and CaMKIV, and appeared to slightly further enhance potency (IC₅₀ ~30 nM). Within a breast cancer cell line and in primary human fibroblasts, tat-5 inhibited the Erk signaling pathway and proliferation without any measurable cytotoxicity.

Keywords Protein kinase Ca²⁺/calmodulin-dependent protein kinase, CaMKinase II inhibitor, CaM-KNtide analogues, cell growth inhibition.

Abbreviations CaMK, Ca²⁺/calmodulin-dependent protein kinase; CaM-KNtide, CaMKinase II inhibitor; CaM, calmodulin; ATP, adenosine triphosphate; PKA, phosphokinase A; PKC, phosphokinase C; RP-HPLC, reversed-phase high performance liquid chromatography; Ant, 16-amino-acid sequence from the *Drosophila* Antennapedia; Tat, 35-amino-acid sequence from the HIV Tat protein; MTT, 3-(4,5-dimethylthiazol-2-yl)-2,5-diphenyltetrazolium bromide; DAPI, 4,6-diamidino-2-phenylindole; CD, circular dichroism; HFA, hydrofluoroalkane; RMSD, root-meansquare deviation; Fmoc, 9-fluorenyl-methoxycarbonyl; DCM, dichloromethane; DIEA, N,N-diisopropylethylamine; DMF, N,N-dimethylformamide; TIS, triisopropylsilane; CH₃CN, acetonitrile; HOBt, N-hydroxy-benzotriazole; HBTU, 2-(1H-benzotriazole-1-yl)-1,1,3,3-tetramethyluronium hexafluoro phosphate; ESI-MS, electrospray ionization mass spectrometry; DMEM, Dulbecco's modified eagle medium; EDTA, ethylenediaminetetraacetic acid; EGTA, ethylene glycol tetraacetic acid; SDS, sodium dodecyl sulfate; CaCl₂, calcium chloride; HEPES, 4-(2-hydroxyethyl)-1-piperazineethanesulfonic acid; BSA, bovine serum albumin; NaOH, sodium hydroxide; PBS, phosphate buffered saline. * Abbreviations used for amino acids follow the rules of the IUPAC-IUB Commission of Biochemical Nomenclature in *J Biol Chem* **1972**, 247, 977-983. Amino acid symbols denote L-configuration.

1. Introduction

Calmodulin (CaM) kinases are a large family of Ser/Thr protein kinases that include kinases with broad substrate spectrum and with high substrate selectivity.¹ As the name implies, CaM kinases (CamKs) are generally activated by binding of Ca²⁺/CaM to their regulatory region. Among CaMKs, CaMKII transduces elevated Ca²⁺ signals in cells to a number of target proteins ranging from ion channels to transcriptional activators.²

1.1 Ca²⁺/Calmodulin-dependent protein kinase II (CaMKII)

Ca²⁺/Calmodulin-dependent protein kinase II (CaMKII) constitutes a family of closely related multifunctional serine/threonine kinases that transduces elevated Ca²⁺ signals in cells to a number of target proteins ranging from ion channels to transcriptional activators.^{1,2} The enzyme consists of 8-12 subunits in a combination of various isoforms (α , β , γ and δ). The α and β isoforms are predominantly expressed in the nervous system, whereas the γ and δ isoforms are ubiquitous.³ Local changes in Ca²⁺ concentration induce activation of CaMKII by binding to calmodulin (CaM).⁴ Binding of the Ca²⁺/CaM complex to an autoregulatory region of the enzyme disrupts auto-inhibitory interactions, allowing substrates and ATP to gain access to the catalytic domain.

Simultaneous Ca²⁺/CaM binding to adjacent subunits within the same holoenzyme, stimulates autophosphorylation at Thr286. This CaMKII autophosphorylation markedly enhances the avidity of CaMKII for Ca²⁺/CaM (from nanomolar to picomolar affinity), but confers significant “autonomous” CaMKII activity even in the event of Ca²⁺/CaM dissociation (Ca²⁺-independent activity). In the absence of Ca²⁺/CaM, CaMKII undergoes autophosphorylation at Thr305/306 and Ser314, which blocks Ca²⁺/CaM binding, thereby inactivating the enzyme.⁵ Likewise other signaling enzymes, CaMKII has important regulatory consequences in many physiological processes. Among processes regulated by CaMKII are neuronal growth and functions related to brain development,⁶ synaptic plasticity⁷ as well as the formation and maintenance of memory,⁸ cell proliferation⁹ and apoptosis,¹⁰ proper function of the immune system,¹¹ and the central control of energy

balance.¹² CaMKII also regulates diverse cellular functions that are important for myocardial adaptation to stress, including Ca^{2+} homeostasis,¹³ membrane excitability,¹⁴ cell survival,¹⁵ and gene transcription.¹⁶ On the other hand, different studies demonstrated that the misregulation or dysfunction of this enzyme is involved in certain pathological conditions, such as Alzheimer,¹⁷ Parkinson,¹⁸ cerebral ischemia,¹⁹ cancer^{20,21,22} and cardiovascular diseases including hypertrophy and other types of ischemia/reperfusion injury^{23,24} obesity and diabetes.²⁵ Current knowledge about CaMKII control on physiological or pathological functions is largely based on experiments with pharmacological inhibitors.^{26,27} This prompted an intensive research in this area. Over the past two decades, a number of relatively potent and selective CaMKII inhibitors have been reported.

2. Aim of work

CaMKII inhibitors such as KN62,²⁸ KN93,²⁹ and peptides derived from the auto inhibitory region of CaMKII, such as AIP³⁰ or AC3-I,³¹ are useful tools for examining the functional significance of Ca^{2+} /CaMKII in the periphery and in the CNS system. Nevertheless, these compounds showed low potency and absence of highly specific inhibition. Thus, auto inhibitory region-derived peptides also inhibit other CaM-kinases and PKC,³² while KN62/KN93 cannot discriminate between CaMKII and CaMKIV and also inhibit voltage-gated K^+ and Ca^{2+} channels.^{33,34} A natural inhibitor of CaMKII, protein CaM-KIIN, provides a promising alternative in the research of selective inhibition.³⁵ Two different isoforms of CaM-KIIN, named CaM-KIIN α and CaMKIIN β , are found in the brain. These proteins show 80% similarity with 70% identity into their amino acid sequences and are 95% identical in their inhibitory domain, differing by only one residue (S12 in CaM-KIIN α versus A12 in CaM-KIIN β).³⁵ The inhibitory protein CaM-KIIN β is highly selective for inhibition of CaMKII with little effect on CaMKI, CaMKIV, CaMKK, PKA, or PKC. A 27-residue peptide derived from it, (CaM-KNtide KRPPKLGQIGRSKRVIEDDRIDDVLK), retains the same selectivity and has a similar IC₅₀ of 50 nM for both the total and the Ca^{2+} -independent

activities of CaMKII. Recently, Vest et al. has identified a new peptide with an active sequence of 21 residues named CN21 (KRPPKLGQIGRSKRVIEDDR).³³ Recently, Coultrap and Bayer reported that the compound named CN19 (KRPPKLGQIGRSKRVIED) represents the minimal region of CaMKIIN α that retains full potency and specificity for CaMKII inhibition.^{36,37} As part of our current interest in the study of CaMKII-dependent cell signaling,³⁸ we directed our efforts toward the identification of novel CaMKII peptide inhibitors.³⁹

2.1 Selective CaMKII peptide inhibitors

Focused on the inhibitory region of CaM-KIIN β we designed different CaM-KNtide analogues and evaluated the inhibitory activity and specificity. The starting⁴⁰ 69 fragment of CaM-KIIN β (CaMKNtide β) and CaM-KNtide α differs by only one amino acid (A12 to S12). This modification could prevent the S12 phosphorylation of substrate reducing interferences with CaMKII inhibition, analogously to what happens with the natural peptides and in agreement with Coultrap and Bayer hypothesis.

Moreover, we describe the selectivity data for the more potent derivative characterized (peptide 17), as well as the structural results obtained using CD and NMR techniques. Finally, the biological effects of this fragment, conveniently conjugated to cell-permeating peptide tat, on the tumor cells growth inhibition, cytotoxic data and the activation of cell proliferation signaling pathway were also discussed.

2.2 The first series of inhibitors (peptides scramble and 1-7)

As first series, we synthesized a scramble analogue of the CaM-KNtide β sequence and seven peptides that cover the entire CaM-KNtide β sequence. Each short peptide had the sequence shifted of five residues, both from N- and C-terminal side (compounds **1-7**, Table 1).

Table 1. Structure and inhibitory activity of compounds CaM-KNtide, and peptides **1-7**.

Frag.	Peptide	Sequence	Inhib. (%±SD)	HPLC		ESI MS	
				k'	Found	Calculated	
1-27	CaM-KNtide β	KRPPKLGQIGRAKRVVIEDDRIDDVLK	94.8±5.0	3.27	3115.30	3115.70	
	Scramble	IDGVIAQGDLPVDKEPKRLRKRDIRKRV	13.3±6.2	3.27	3115.82	3115.70	
6-27	1	LGQIGRAKRVVIEDDRIDDVLK	< 5	2.69	2509.22	2508.90	
11-27	2	RSKRVVIEDDRIDDVLK	< 5	2.49	2057.23	2056.30	
17-27	3	VIEDDRIDDVLK	13.0±9.1	2.52	1429.70	1429.50	
1-22	4	KRPPKLGQIGRAKRVVIEDDRI	56.0±14.0	2.78	2544.62	2544.04	
1-17	5	<u>KRPPKLGQIGRAKRVVI</u>	<u>76.0±4.1</u>	3.12	1916.64	1915.40	
1-12	6	KRPPKLGQIGRA	< 5	2.75	1321.04	1320.60	
1-7	7	KRPPKLG	< 5	2.08	796.21	795.01	

$k' = [(\text{peptide retention time} - \text{solvent retention time}) / \text{solvent retention time}]$.
Peptide concentration 5 μM .

The shortest peptide that retained good inhibition of CaMKII (>75%) was the fragment containing amino acids 1-17 (peptide **5**, named now CN17 β). All further truncations at the C-terminus by 4 amino acids or more (peptides **6** and **7**) and any truncation at the N-terminus by 5 amino acids or more (peptides **1-3**) showed minimal or no inhibition.

CN17 β seems to be slightly more potent than the corresponding analogue S12 (KRPPKLGQIGRSKRVI, termed CN17 α), described by Vest et al., which inhibit <70% CaMKII activity at 5 μM . These results confirmed that CaM-KNtide β sequence containing an Ala residue at position 12 was an effective starting point to develop novel agents with CaMKII inhibitor activity.

2.3 A truncation study at both the N- and C-terminals of the fragment 1-17 (peptides 8-16)

Subsequently, a truncation study at both the N- and C-terminals of the fragment 1-17 was performed in order to obtain additional information on the

minimum active sequence. Also, CN19 was synthesized and tested for comparative purpose.³⁶ In our experimental conditions, CN19 lost about 40% of the CaM-KNtide activity (Tables 1 and 2) while Coultrap and Bayer found that it retained full potency and specificity for CaMKII inhibition.^{36,37} The discrepancy between our results and those obtained by Coultrap and Bayer on CN19 inhibition potency could be explained considering that the experimental conditions used in CaMKII activity assays are not exactly matching.

Table 2. Structure and inhibitory activity of compounds CaM-KNtide, and peptides **8-16**.

Frag.	Peptide	Sequence	Inhib. (%±SD)	HPLC	ESI MS	
				k'	Found	Calculated
1-19	CN19	KRPPKLGQIGRSKRVVIED	54.0±1.0	3.17	2176.23	2175.28
1-17	5	KRPPKLGQIGRAKRVVI	76.0±4.1	3.12	1916.64	1915.40
2-17	8	RPPKLGQIGRAKRVVI	< 5	3.01	1788.40	1788.23
3-17	9	PPKLGQIGRAKRVVI	< 5	3.08	1632.72	1632.04
4-17	10	PKLGQIGRAKRVVI	< 5	2.57	1535.03	1534.93
5-17	11	KLQIGRAKRVVI	< 5	2.54	1437.98	1437.81
6-17	12	LGQIGRAKRVVI	< 5	2.58	1309.72	1309.60
1-16	13	KRPPKLGQIGRAKRVV	10.2±2.0	2.61	1803.77	1803.25
1-15	14	KRPPKLGQIGRAKRV	18.0±9.0	2.60	1704.30	1704.13
1-14	15	KRPPKLGQIGRAKR	< 5	2.09	1605.11	1604.98
1-13	16	KRPPKLGQIGRAK	< 5	2.34	1449.99	1448.79

$k' = [(peptide\ retention\ time - solvent\ retention\ time) / solvent\ retention\ time]$. Peptide concentration 5 μ M.

2.4 Alanine scanning approach of fragment 1-17 (peptides 17-32)

Further truncation of compound CN17 β significantly reduced CaMKII inhibition (compounds **8-16**, Table 2), suggesting a bioactive role for both the

N- and C-terminal sequences. These results demonstrate that a satisfactory inhibitory activity is contained in 1-17 fragment of the CaM-KNtide β .

For this reason, we decided to check the contribution of the various amino acid residues to the inhibitory activity of CN17 β through an L-Ala scanning analysis (peptides **17-32**, Table 3).

Table 3. Structure and inhibitory activity of compounds CaM-KNtide, and peptides **17-32**.

Pep.	Sequence	Inhib. (% \pm SD)	HPLC	ESI MS	
			k'	Found	Calculated
5	KRPPKLGQIGRAKRVI	76.0\pm4.4	3.15	1916.64	1915.40
17	ARPPKLGQIGRAKRVI	13.5\pm2	3.20	1859.32	1858.30
18	KAPPKLGQIGRAKRVI	< 5	3.17	1832.72	1830.29
19	KRAPKLGQIGRAKRVI	78.4\pm4	3.13	1890.09	1889.36
20	KRPAKLGQIGRAKRVI	13.2\pm2	3.13	1890.75	1889.36
21	KRPPALGQIGRAKRVI	7.0\pm2	4.71	1859.96	1858.30
22	KRPPKAGQIGRAKRVI	< 5	3.35	1876.40	1874.33
23	KRPPKLAQIGRAKRVI	26.1\pm4	3.18	1931.16	1929.43
24	KRPPKLGAIQIGRAKRVI	34.4\pm3	3.16	1860.22	1858.35
25	KRPPKLGQAQIGRAKRVI	< 5	3.15	1874.58	1873.32
26	KRPPKLGQIARAKRVI	21.6\pm2	3.15	1931.22	1929.43
27	KRPPKLGQIGAAKRVI	13.0\pm2	3.19	1831.12	1830.29
28	KRPPKLGQIGRAARVI	33.7\pm1	3.17	1860.14	1859.31
29	KRPPKLGQIGRAKAVVI	69.0\pm2	3.16	1830.95	1831.30
30	KRPPKLGQIGRAKRAVI	24.2\pm2	3.16	1889.21	1888.35
31	KRPPKLGQIGRAKRVAI	74.2\pm1	3.14	1888.16	1888.30
32	KRPPKLGQIGRAKRVA	48.7\pm3	4.71	1875.52	1874.32

$k' = [(peptide\ retention\ time - solvent\ retention\ time) / solvent\ retention\ time]$. Peptide concentration 5 μ M.

Data indicate a different sensitivity of our CN17 β to Ala substitutions, compared to results obtained by Coultrap and Bayer with the same mutation in the peptide CN19.^{36,37} Only one mutant enhanced the potency of CN17 β versus the three mutants 19, 28, and 29, which increased significantly the

potency of CN19.³⁶ In our case, compound 19 increased slightly the inhibitor activity of CN17 β while peptide 28 reduced its potency of more than 2.5 fold, indicating an important role for residue ¹³Lys in the CN17 β - CaMKII binding. Finally, mutant R14 maintained the inhibitor efficacy.

2.5 Cell penetrating peptide (ant-CN17 β , tat-CN17 β)

With the aim to improve the ability to penetrate cell, CN17 β was fused with two well known penetrating peptides (Ant: RQIKIWFQNRRMKWKKGGC and Tat: RKKRRQRRRPPQC) leading to peptides ant-CN17 β and tat-CN17 β , respectively (Table 4).

Table 4. Structure compounds CaM-KNtide and peptides **tat-CN17 β** and **ant-CN17 β** .

Peptide	Sequence	HPLC ^a k'	ESI-MS (M+H)	
			Calcd	Found
CN17β	KRPPKLGQIGRAKRVVI	3.12	1916.64	1915.40
ant-CN17β	ant- KRPPKLGQIGRAKRVVI	3.72	4362.35	4363.56
tat-CN17β	tat- KRPPKLGQIGRAKRVVI	3.75	3663.48	3664.23

$k' = [(peptide\ retention\ time - solvent\ retention\ time) / solvent\ retention\ time]$.

To test whether these fusion peptides were able to inhibit CaMKII activity, we performed an in vitro kinase assay.

3. Chemistry

3.1 General procedure for synthesis

Peptides were synthesized according to the solid-phase approach using standard Fmoc methodology in a manual reaction vessel.⁴¹ The first amino acid, N ^{α} Fmoc-Xaa-OH, was linked onto the Wang resin (100–200 mesh, 1% DVB, 1.1 mmol/g) and was attached to Wang resin using HOBt/HBTU as an activating agent (3eq.) and a catalytic amount of DMAP. The following

protected amino acids were then added stepwise. The N^α-Fmoc protecting groups were removed by treating the protected peptide resin with a 25% solution of piperidine in DMF (1 × 5min and 1 × 25min) and the deprotection protocol was repeated after each coupling step.

In addition, after each step of deprotection and after each coupling step, Kaiser test was performed to confirm the complete removal of the Fmoc protecting group, respectively, and to verify that complete coupling has occurred on all the free amines on the resin. Then Kaiser test was performed to confirm the acetylation reaction.

The N-terminal Fmoc group was removed as described above, and the peptide was released from the resin with TFA/iPr₃SiH/H₂O (90 : 5 : 5) for 3 h.

The resin was removed by filtration, and the crude peptide was recovered by precipitation with cold anhydrous ethyl ether to give a white powder and then lyophilized.

3.2 Purification and Characterization

All crude peptides were purified by RP-HPLC on a preparative C18-bonded silica column using a Shimadzu SPD 10A UV/VIS detector, with detection at 215 and 254 nm. All peptides were characterized with analytical RP-HPLC and peptides molecular weights were determined by ESI mass spectrometry and LC-MS in a LC-MS 2010 instrument (Shimadzu) fitted with a C-18 column. All analogues showed >97% purity when monitored at 215 nm. Homogeneous fractions, as established using analytical HPLC, were pooled and lyophilized.

4. Results and Discussion

The first part of the work focused on a SAR study of entire CaM-KNtideβ sequence designed a scramble analogue of the CaM-KNtideβ sequence and seven peptides that cover the entire sequence. Each short peptide had the sequence shifted of five residues, both from N- and C-terminal side (compounds **1-7**, Table 1).

The shortest peptide that retained good inhibition of CaMKII (>75%) was the fragment containing amino acids 1-17 (peptide **5**, named now CN17 β). Starting from these data, CN17 β was considered the peptide lead.

Two different approaches were used to identify more potent and selective compounds: i) a truncation study at both N- and C-terminals of the fragment 1-17; ii) Alanine scanning approach.

Interestingly, further truncation of compound CN17 β significantly reduced CaMKII inhibition (compounds **8-16**, Table 2), suggesting a bioactive role for both the N- and C-terminal sequences. In particular all peptides showed an inhibitory activity < 5% except compounds 13 and 14 that showed 10.2% and 18.0% of inhibitory activity respectively.

These results suggested that a satisfactory inhibitory activity is contained in 1-17 fragment of the CaM-KNtide β . For this reason we decided to apply the Alanine scanning approach to peptide lead.

The involvement of the N-terminal, internal or C-terminal amino acids in the CN17 β activity can be summarized as follows: (a) in the N-terminal fragment (KRPPK) ²Arg is critical for inhibitory activity; ¹Lys, ⁴Pro and ⁵Lys are important and significantly contribute to the potency of CN17 β , while the substitution of ³Pro by Ala leads to the analogue 19 with a slightly increase potency; (b) the internal hexapeptide Leu-Gly-Glu-Ile-Gly-Arg sequence is important for activity. The residues ⁶Leu and ⁹Ile result to be critical for the inhibitory activity of CN17 β while the contribution of ⁸Glu is lower; (c) in the C-terminal fragment (KRVVI), ¹³Lys and ¹⁵Val are important for biological activity while ¹⁴Arg and ¹⁶Val contribute to a lesser extent to the activity.

4.1 Biological effects of cell permeating tat-CN17 β

With the aim to improve the ability to penetrate cell, CN17 β was fused with two well known penetrating peptides (Ant: RQIKIWFQNRRMKWKKGGC and Tat: RKKRRQRRRPPQC) leading to peptides ant-CN17 β and tat-CN17 β , respectively. To test whether these fusion peptides were able to inhibit CaMKII activity, we performed an in vitro kinase assay.

The results of the concentration response curve for tat-CN17 β , ant-CN17 β , and the CaM-KNtide β are shown in Figure 1.

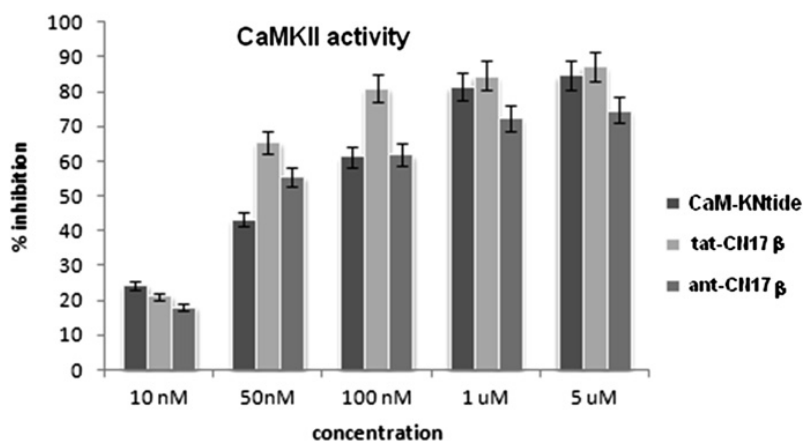


Figure 1. Dose-response curves for CaM-KNtide and peptides tat-CN17 β and ant-CN17 β . Data are indicated as percent of inhibition over untreated; error bars represent \pm standard deviation (SD).

CaM-KNtide β exhibited an apparent IC₅₀ of 50 nM toward CaMKII, while tat-CN17 β and ant-CN17 β showed approximately IC₅₀ of 30 and 40 nM, respectively. Indeed, for CaM-KNtide β and tat-CN17 β the inhibitory effect was maximal at 1 μ M (~95% inhibition) and didn't change even at the highest concentration of 5 μ M. At this last concentration, ant-CN17 β exhibited a minor percentage of inhibition (76.2%). Similarly to the results described by Vest et al.,^{33a} the fusion of CN17 β with tat led to an increment of both potency and selectivity of the resulting peptide, while after the fusion with ant, the peptide retained the inhibitory activity and selectivity (Figure 2).

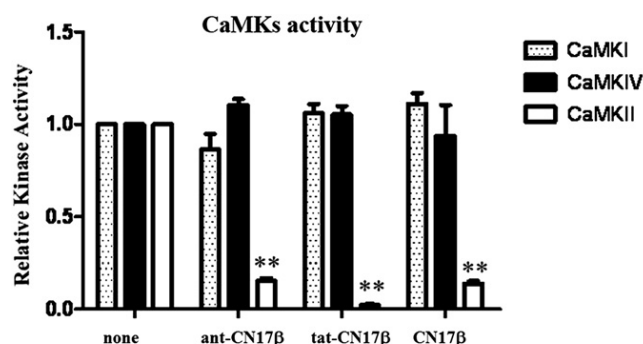


Figure 2. Inhibitory activity and selectivity of peptides ant-CN17 β , tat-CN17 β , and CN17 β at 5 μ M. Data are indicated as fold decrease; error bars represent \pm standard deviation (SD); **p-value < 0.01.

In fact, as shown, neither peptide ant-CN17 β nor tat-CN17 β inhibit CaMKI (6.1% or -) or CaMKIV (-). The antennapedia cell-penetrant motif used in this study has been previously shown to bind calmodulin and affect CaMKII activity indirectly.^{33a} Anyway, since the selective inhibitory activity for CaMKII was observed for both the conjugate peptides ant-CN17 β and tat-CN17 β , with the best results obtained with tat-CN17 β , this indicates that the CN17 β sequence is responsible for the activity.

4.1.1 Proliferation

As described above, CaMKII plays a pivotal role in the cell pathways regulating proliferation, and its inhibition can reduce cardiovascular hyperplasia⁴² and tumor cell growth.⁴³ We investigated the possibility that cell permeating compound tat-CN17 β inhibited the proliferation of both tumor and vascular cell lines. We determined the effect of our compound on a breast cancer MCF7 and a colon cancer HT29 cell lines, on primary rat vascular smooth muscle VSMC cells, and on primary human fibroblasts.

DNA duplication was assessed by the uptake of tritiated thymidine (3HT).⁴⁴ In this assay we used also the selective CaMKII inhibitor ant-CaNtide (ant-fused CaM-KNtide) as reference peptide.

As observed in Figure 3A, both ant-CaNtide and tat-CN17 β reduced 3HT uptake, but the percent of inhibition depends upon the cell line used. Tat-

CN17 β was more effective than ant-CaNtide. Antiproliferative effect is clearly correlated to the proliferation rate of the cell line, indeed immortalized tumor lines MCF7 and HT29 are more affected than primary normal cells. We also investigated whether the inhibition of cell proliferation was correlated to a cytotoxic effect of tat-CN17 β in our cell models.⁴⁵ Cell viability was measured using PrestoBlue™ Cell Viability Reagent (Invitrogen Inc, San Diego, CA). As shown in Figure 3B, at the same concentration, none of the peptides in the study modified the cell viability in any of cell lines we tested. These results suggest that the mechanism underlying the inhibitory activity of our peptides involves the proliferation signaling without promoting cellular death process in the time assay.

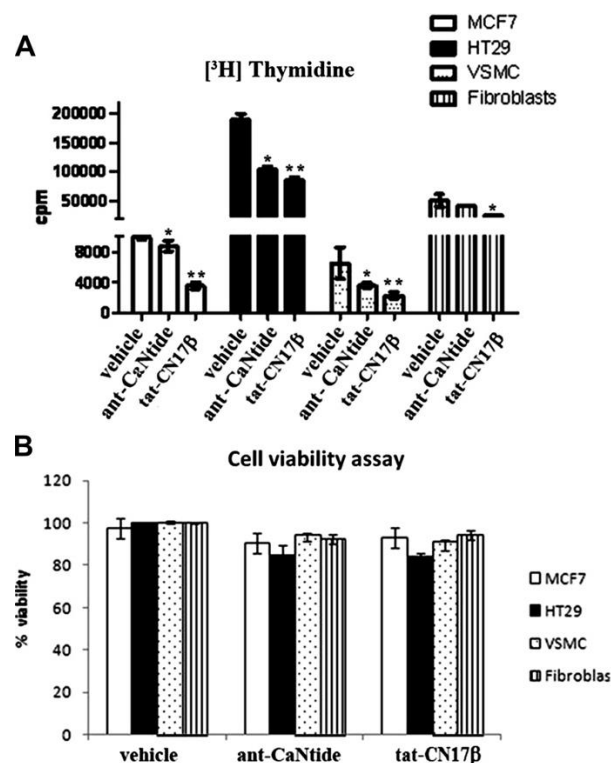


Figure 3. A) Antiproliferative and (B) cytotoxic activities of ant-CaNtide and tat-CN17 β at 5 μ M. Results are presented as total incorporated counts per minute (cpm). Average \pm SD values from n = 4 experiments are shown. *p-value \leq 0.05. **p-value \leq 0.01.

4.1.2 Signal transduction

CaMKII is involved in the activation of the most important signaling pathway regulating cell proliferation: the Ras/Raf/MEK/ERK signaling pathway. Illario et al. demonstrated the existence of a cross-talk between Ca^{2+} /CaM/CaMKII and Ras/Raf/MEK/ERK pathways.⁴⁶ Accordingly, ant-CaNtide is able to significantly affect CaMKII-mediated cell proliferation, by down regulating ERK activation. As tat-CN17 β affected cell proliferation, we investigated whether it is also able to interfere with ERK activation. With this aim, we evaluated the expression of Erk, phospho(p)Erk, CaMKII, and phospho(p)CaMKII in cardiomyoblast (H9C2) and colon cancer (HT-29) cell lines by western blot (Figure 4A and B). Cells were serum starved over night in 0.5% DMEM/BSA and treated for 30 min with 10% of FBS, with or without CaMKII inhibitor tat-CN17 β . As shown in Figure 4A and B, serum stimulation induced both CaMKII and ERK activation, which was altered by treatment with different concentrations of tat-CN17 β . Densitometry measurements of immunoblots analyzing the levels of depicting pCaMKII and pERK in H9C2 and HT29 cells were performed using Image J software (NIH) (Figure 4C, D). In H9C2 cells (Figure 4A, C), ERK phosphorylation was down-regulated in a dose-dependent manner, whereas in HT-29 cells tat-CN17 β at 100 nM induced the maximal down-regulation of ERK phosphorylation (Figure 4B, D). These results suggest that the peptide interferes with cell proliferation by regulating, at least, the Ras/Raf/MEK/ERK signaling pathway.

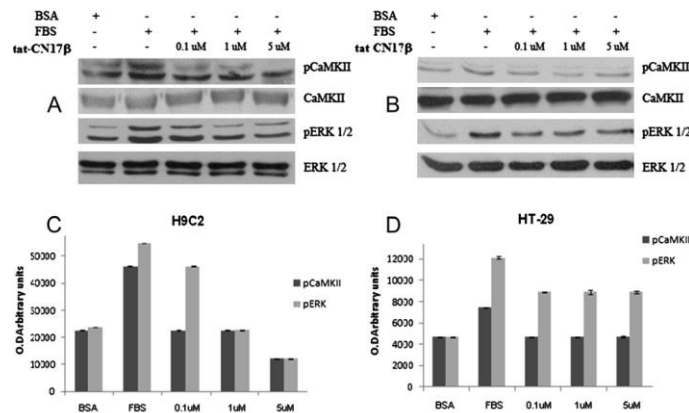


Figure 4. Immunoblots for Erk, phospho(p)Erk, CaMKII, and phospho(p)CaMKII in (A) H9C2 and (B) HT-29 cells stimulated with serum and treated with 0.1, 1, and 5 μ M tat-CN17 β for 30 min. The respective densitometry analysis (C) and (D) are shown. Signal densities of bands represent individual and average values \pm SD from 3 experiments.

4.2 CaMKII activity in cells

The ability of peptides ant-CN17 β and tat-CN17 β to permeate the membranes allowed us to measure CaMKII activity in cells. To this purpose, the cardiomyoblast-like, H9C2, cells were starved for 12 h, and then stimulated for 30 min with 10% FBS in absence or presence of 5 μ M of indicated peptides. Endogenous CaMKII was immunoprecipitated, and its activity was measured by kinase assay using AC2. The ant-CaNtide was also tested as reference peptide.

As shown in Figure 5 all tested peptides significantly inhibited activation of endogenous CaMKII. Tat-CN17 β and ant-CN17 β inhibited the CaMKII activity of 58 and 52%, respectively, and they seem to be moderately more potent than ant-CaNtide, which inhibits 39% of the CaMKII activity. According to these results, and analogously to that described by Vest et al. about tat-CN21,^{33a} the shorter derivative tat-CN17 β becomes a powerful, readily accessible, and easy to-use tool for studying cellular CaMKII functions.

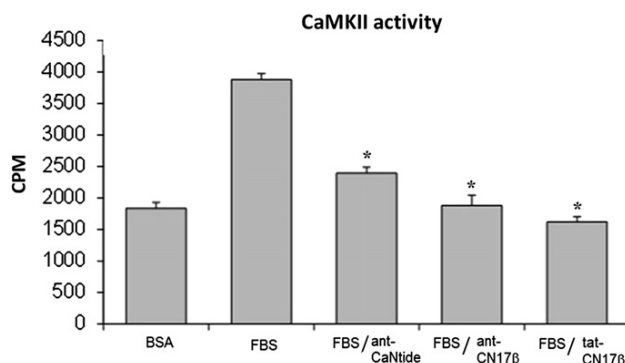


Figure 5. Inhibition of endogenous CaMKII activation by ant-CaNtide, ant-CN17 β , tat- CN17 β peptides as determined by kinase assay. Results are presented as total incorporated counts per minute (cpm). Average \pm SD values from $n= 4$ experiments are shown. * p -value ≤ 0.05 .

4.3 Conformational studies

To drive the next design steps, we also carried out a study on the conformational preferences of the CN17 β . A preliminary screening of the conformational preferences of CN17 β as a function of the solvent system was performed by means of CD spectroscopy (data not shown). CD spectra were recorded in water solution and in a water/HFA mixture (50:50, v/v) as structuring medium.^{47,48}

Quantitative analysis of CD curves was carried out using both SELCON3 and ContinLL algorithm on DICHROWEB⁴⁹ website.

The most common conformation of CN17 β in water is random coil ($\approx 80\%$ of the total conformer population). In water/HFA (50:50, v/v) mixture, turn helical structures ($\approx 65\%$) and minor amounts of β -strand and unordered conformations (respectively $\approx 15\%$ and 20% of the total conformer population) are observable.

NMR spectra were acquired in water/HFA (50:50, v/v) the same solvents used for the CD measurement. Chemical shift assignments of the proton spectra of CN17 β in water/HFA mixture were achieved via the standard systematic application of DQF-COSY,⁵⁰ TOCSY⁵¹ and NOESY experiments,⁵² using the SPARKY software package⁵³ according to the

procedure of Wüthrich.⁵⁴ Analysis of sequential and medium range NOE connectivities reveals the presence of regular secondary structures. In particular NH-NH ($i, i + 1$), α -N($i, i + 3$) and α - β ($i, i + 3$) NOEs involve ⁵Lys-¹¹Arg residues, whereas strong sequential α -N($i, i + 1$) connectivities are observable along the ¹¹Arg¹⁶Val fragment.

The structural calculations of CN17 β in water/HFA solution (50:50 v/v) based on sequential and medium range NOE data were performed using DYANA and Amber 5.0 softwares.^{55,56} Figure 6 shows the superposition of the best 20 NMR structures of CN17 β overlapped at level of ⁵Lys-¹⁰Gly backbone atoms.

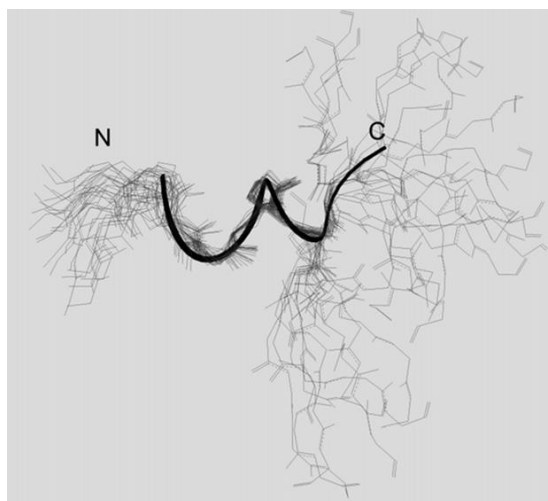


Figure 6. NMR structure bundle (20 low energy conformers) of CN17 β overlapped at level of ⁵Lys¹⁰Gly backbone atoms (RMSD \leq 0.54). NMR structures were calculated using DYANA software on the basis of NOESY spectra recorded at 600 MHz (T = 300 K) in water/HFA solution (50:50 v/v).

The bundle reveals a high structural similarity (backbone RMSD \leq 0.54 Å) in the overlapped region, suggesting that NMR structures are defined with high precision in this region. Analysis of CN17 β NMR structures using PDBSUM on-line server⁵⁷ leads to identify the prevalence of regular α -helices in the ⁶Leu¹¹Arg segment and γ -turn conformations in the ³Pro⁵Leu segment. The crystal structure of the 21-residue segment of CaM-KNtide, the parent peptide of compound 5, is characterized by α -helical conformation in the

⁶Leu¹¹Arg segment.⁴⁰ The remaining residues assume extended conformation to interact with a large surface of CaMKII structure. According to previous crystallographic studies, CaMKII structure exhibits three docking sites—docking site A, B and C e to interact with R1 portion of the regulatory segment.⁴⁰ Analogously to R1, these docking sites are contacted by CaMKNtide residues: in particular the basic residues ²Arg and ⁵Lys occupy docking sites C and B, hydrophobic ⁶Leu and ⁹Ile occupy docking site B and ¹¹Arg and ¹⁵Val occupy docking site A. The comparison of our best NMR structure of CN17β with the crystal structure of CaM-KNtide bound to the kinase domain of CaMKII (Figure 7), indicates that the two structures have similar α-helical arrangement in the ⁵Lys¹¹Arg segment. ⁵Lys, ⁶Leu and ⁹Ile residues, belonging to the α-helix and involved in interaction with CaMKII, share a common orientation of the side chains. Other indispensable residues for CaMKII inhibitory activity (¹Lys, ²Arg, and ¹⁵Val; Ala scan, see above) do not overlap well by comparing the two structures. Anyway, they belong to the terminal regions of the peptide which are highly flexible in water/HFA solution. It is likely that the peptide initially binds CaMKII through the core residues ⁵Lys, ⁶Leu and ⁹Ile and then ¹Lys, ²Arg, and ¹⁵Val assume the appropriate binding conformation by induced fitting. The design of novel CaM-KNtide based inhibitors should point to restrict the conformational space of the indispensable but flexible residues to fit the active conformation of the peptide in the complex.

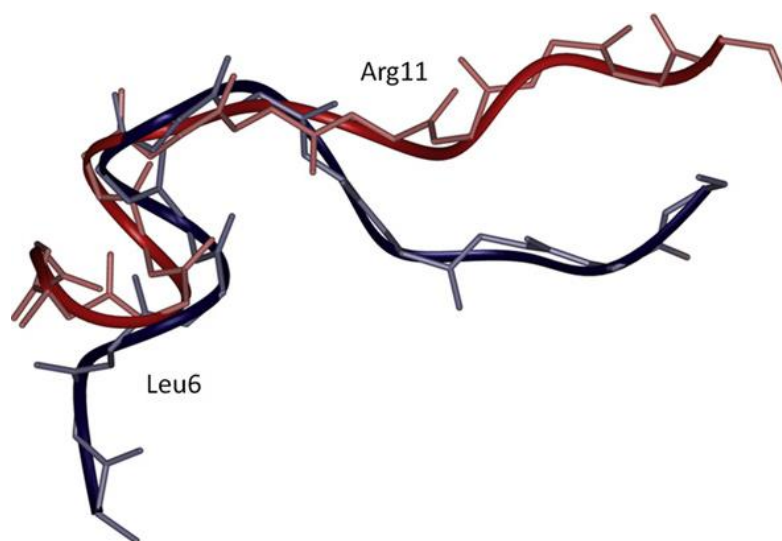


Figure 7. Structural comparison of the NMR-derived lowest energy conformation of CN17 β (dark blue) in water/HFA solution (50:50 v/v) and 21-residue segment of CaMKNtide (CN21) crystal structure (red) complexed to CaMKII enzyme (pdb code 3KL8). The structures are superimposed at level of backbone heavy atoms of $^6\text{Leu}^{11}\text{Arg}$ residues. (For interpretation of the references to color in this figure legend, the reader is referred to the web version of this article.)

5. Conclusion

CaMKII is involved in the regulation of many pivotal cell functions, such as proliferation, and is therefore a key player in pathological processes, like oncogenesis. Hence, modulation of its activity could be exploited with therapeutic purposes. The present study describes the finding of a small CN17 β , the 1-17 fragment of CaM-KNtide β , that selectively inhibits CaMKII. The fusion of CN17 β with penetrations led to the conjugate peptides, ant-CN17 β and tat-CN17 β , which maintained usable inhibitory potency and selectivity of action compared to the parent peptide.

Tat-CN17 β demonstrated to retain inhibitory potency, and to be more active than full length ant-CaNtide, to inhibit the proliferation of different cell lines, in particular of a breast cancer cell line and of primary human fibroblasts even if its sequence was 16 residues shorter. Our results indicated that tat-

CN17 β inhibits cell growth and interferes with the Ras/Raf/MEK/ERK signaling pathway, through the inhibition of endogenous CaMKII.

Finally, conformational analysis of parent CN17 β gave important information on the design of novel analogues. Our data outline a promising perspective: the availability of a small peptide as a tool to modulate complex signal transduction pathways, and interfere with their homeostasis in disease, as well as the generation of specific, more stable and cell targeted peptides.

6. Experimental section

6.1 Peptide synthesis

The synthesis of CaM-KNtide β analogues was performed according to the solid phase approach using standard Fmoc methodology in a manual reaction vessel.⁴¹ N $^{\alpha}$ -Fmoc-protected amino acids, Wang resin, HOBt, HBTU, DIEA, DMAP, piperidine and trifluoroacetic acid were purchased from Iris Biotech (Germany). Peptide synthesis solvents, reagents, as well as CH₃CN for HPLC were reagent grade and were acquired from commercial sources and used without further purification unless otherwise noted. The corresponding first amino acid, N $^{\alpha}$ -Fmoc-Lys(Boc)-OH, N $^{\alpha}$ -Fmoc-Val-OH, N $^{\alpha}$ -Fmoc-Ile-OH, N $^{\alpha}$ -Fmoc-Ala-OH, N $^{\alpha}$ -Fmoc-Gly-OH, N $^{\alpha}$ -Fmoc-Asp(tBu)-OH, N $^{\alpha}$ -Fmoc-Arg(Pbf)-OH) was linked on to the resin previously deprotected by a 25% piperidine solution in DMF for 30 min. The following protected amino acids were then added stepwise: N $^{\alpha}$ -Fmoc-Leu-OH, N $^{\alpha}$ -Fmoc-Val-OH, N $^{\alpha}$ -Fmoc-Asp(tBu)-OH, N $^{\alpha}$ -Fmoc-Glu(OtBu)-OH, N $^{\alpha}$ -Fmoc-Arg(Pbf)-OH, N $^{\alpha}$ -Fmoc-Ile-OH, N $^{\alpha}$ -Fmoc-Ala-OH, N $^{\alpha}$ -Fmoc-Gly-OH, N $^{\alpha}$ -Fmoc-Gln(trt)-OH, N $^{\alpha}$ -Fmoc-Pro-OH, N $^{\alpha}$ -Fmoc-Trp(Boc)-OH, N $^{\alpha}$ -Fmoc-Phe-OH, N $^{\alpha}$ -Fmoc-Met-OH, N $^{\alpha}$ -Fmoc-Cys(trt)-OH.

Each coupling reaction was accomplished using a 3-fold excess of amino acid with HBTU and HOBt in the presence of DIEA (6 eq.). The N $^{\alpha}$ -Fmoc protecting groups were removed by treating the protected peptide resin with a 25% solution of piperidine in DMF (1 \times 5 min and 1 \times 25 min). The peptide

resin was washed three times with DMF, and the next coupling step was initiated in a stepwise manner.

The peptide resin was washed with DCM (3×25), DMF ($3\times$), and DCM ($3\times$), and the deprotection protocol was repeated after each coupling step.

The N-terminal Fmoc group was removed as described above, and the peptide was released from the resin with TFA/TIS/H₂O (90:5:5) for 3 h. The resin was removed by filtration, and the crude peptide was recovered by precipitation with cold anhydrous ethyl ether to give a white powder and then lyophilized.

6.2 Purification and characterization of CaMKII inhibitors

All crude peptides were purified by RP-HPLC on a preparative C18-bonded silica column (Phenomenex, Jupiter 300Å, 100 mm \times 21.2 mm, 10 μ m,) using a Shimadzu SPD 10A UV–Vis detector, with detection at 210 nm and 254 nm. The column was perfused at a flow rate of 15 mL/min with solvent A (10%, v/v, water in 0.1% aqueous TFA), and a linear gradient from 10% to 90% of solvent B (80%, v/v, acetonitrile in 0.1% aqueous TFA) over 15 min was adopted for peptide elution. Analytical purity and retention time (t_R) of each peptide were determined using HPLC conditions in the above solvent system (solvents A and B) programmed at a flow rate of 1 mL/min using a linear gradient from 10% to 90% B over 15 min, fitted with C-18 column Phenomenex, Aeris XB-C18 column (150 mm \times 4.60 mm, 3.6 μ m). All analogues showed >97% purity when monitored at 215 nm. Homogeneous fractions, as established using analytical HPLC, were pooled and lyophilized.

At the same time, analytical reversed-phase HPLC was performed on C-18 Phenomenex column Aeris XB-C18 column (150 mm \times 4.60 mm, 3.6 μ m) in a model LC-2010 system (Shimadzu, Kyoto, Japan).

Elution was done with linear 10–90% gradients of solvent B into A (Solvent A was 0.1% TFA in water; solvent B was 0.1% TFA in CH₃CN) over 15 min at 1 mL/min flow rate, with UV detection at 220 nm for all peptides.

To check and to have a confirmation of peptides molecular weights were used ESI mass spectrometry. ESI-MS analysis in positive ion mode, were

made using a Finnigan LCQ ion trap instrument, manufactured by Thermo Finnigan (San Jose, CA, USA), equipped with the Excalibur software for processing the data acquired. The sample was dissolved in a mixture of water and methanol (50/50) and injected directly into the electrospray source, using a syringe pump, which maintains constant flow at 5 $\mu\text{L}/\text{min}$. The temperature of the capillary was set at 220 $^{\circ}\text{C}$.

6.3 Cell culture

Cardiomyoblasts H9C2, human breast cancer MCF-7, human colon adenocarcinoma grade II HT29, primary cultures of VSMCs obtained from thoracic aortas of WKY rats, primary cultures of fibroblasts obtained from human gum were maintained in DMEM with 10% fetal bovine serum. All media were supplemented with 100 units/mL penicillin and 100 $\mu\text{g}/\text{mL}$ streptomycin.

6.4 CaMKII activity assay

In all CaMKII assays, purified or endogenous CaMKII was incubated with $\text{Ca}^{2+}/\text{CaM}$; EGTA was used as a negative control.

Active recombinant full-length alpha CaMKII (Signal Chem, La Jolla) was incubated for 30 min at 30 $^{\circ}\text{C}$ with 1 mmol/L CaCl_2 and 1 $\mu\text{mol}/\text{L}$ CaM in 10 μl of a reaction mixture (50 mmol/L HEPES pH 7.5, 10 mmol/L MgCl_2 , 0.5 mmol/L dithiothreitol (DTT), 100 nmol/L microcystin, 0.1 mmol/L non-radiolabeled ATP).⁵⁸ In a second reaction step, an aliquot from the first reaction was incubated with 200 μM of Autocamtide-2 as a substrate for CaMKII and the different peptides at concentration of 5 μM , in presence of 0.2 $\mu\text{Ci}/\text{mL}$ of Easy Tides Adenosine 50-triphosphate [$\gamma^{32}\text{P}$]-ATP (Perkin Elmer) for 30 min at 30 $^{\circ}\text{C}$; EGTA was added to quantify CaMKII autonomous activity. ^{32}P -incorporation was determined by spotting 20 μl of the reaction to Whatman P-81 phosphocellulose paper, and subsequently washing in 75 mM phosphoric acid.

Dried filters were counted on a Beckman LS 6000 scintillation counter.

6.5 CaMKI and CaMKIV activity assay

CaMKI and CaMKIV phosphorylation assays were performed at 30 °C in a standard solution consisting of 50 mM Hepes (pH 7.5), 10 mM MgCl₂, 1 mM CaCl₂, 1 mM dithiothreitol, 0.1% Tween 80, 0.5 mg/mL bovine serum albumin, and 25 μM of CaM, 50 ng of CaMKK2, ATP (~50 cpm/pmol), and activated CaMKI (ENZO life sciences) or CaMKIV (ENZO life sciences) in a final volume of 50 μl.⁵⁹ The reactions were initiated by the addition of enzyme to a final concentration of 1 nM and terminated after 5 or 10 min. In a second reaction step, an aliquot from the first reaction was incubated with 200 μM of ADR1G as a substrate for CaMKI or 200 μM of γ-peptide as a substrate for CaMKIV and 5 mM of peptides ant-CN17β, tat-CN17β and CN17β in presence of 0.2 μCi/μl of Easy Tides Adenosine 50-triphosphate [³²P]-ATP (Perkin Elmer) for 30 min at 30 °C. Reactions were terminated by spotting 20 μl on Whatman P-81 phosphocellulose filters followed by extensive washing in 75 mM phosphoric acid. The dried filters were counted on a Beckman LS 6000 scintillation counter.

6.6 [³H]Thymidine incorporation

To determine DNA synthesis, cells (MCF-7, HT29, VSMC, primary fibroblasts) were placed in a 24-well plate and serum-starved for 12 h in DMEM, 0.5% BSA. To test the effects of CaMKII's inhibitors on cell proliferation 5 μM of ant-CaNtide and tat-CN17β were added to wells. A total of 0.5 μCi [³H]thymidine was then added to the plates. After 24 h, the plates were gently washed with PBS and then with 10% trichloroacetic acid (TCA), and incubated 10 min with 20% TCA at 4 °C. The plates were washed with 5% TCA, and cells were lysed with 0.2% SDS, 0.5 N NaOH for 15 min at 4 °C. The lysates were then resuspended in 5 mL scintillation fluid and counted in a β-counter (Becton Dickinson, Franklin Lakes, NJ, USA).

6.7 Cell viability assay

This assay was performed using PrestoBlue™ Cell Viability Reagent (Invitrogen Inc, San Diego, CA). PrestoBlue™ reagent is a resazurin-based solution that functions as a cell viability indicator by using the reducing power of living cells to quantitatively measure the proliferation of cells. The PrestoBlue™ reagent contains a cell-permeant compound that is blue in color and virtually not fluorescent. When added to cells, the PrestoBlue™ reagent is modified by the reducing environment of the viable cell, turns red in color and becomes highly fluorescent. This change in fluorescence is detected as measurement of absorbance, referred to the two controls (medium alone, and untreated cells). This reagent was used to evaluate cell viability in presence or absence of CaMKII inhibitors. Briefly, MCF7, HT29, VSMC, primary fibroblasts cells were plated into 96 multi-well at a density of 2000 cells/well in quadruplicate. CaMKII inhibitor, ant-CaNtide and tat-CN17β, were added to each well at a concentration of 5 μM for 24 h. Then 10 μl of reagent were added to each well, and the plates were returned to cell culture incubator for 2 h at dark. The absorbance in each well was measured at 570 nm in a microplate plate reader, and was referred to the absorbance of the two controls, that were used to calibrate the plate reader.

6.8 Western blot analysis

H9C2 and HT-29 were serum starved over night with DMEM/0.5% BSA. Cells were stimulated with 10% of FBS for 30 min and treated with different concentration of tat-CN17β for 30 min. At the end of the stimulation, cells were lysed in ice-cold RIPA/SDS buffer [50 mmol/L TrisHCl (pH 7.5), 150 mmol/L NaCl, 0.01 g/L NP-40, 0.0025 g/L deoxycholate, 2 mmol/L Na₃VO₄, 0.2 g/L sodium dodecylsulfate].

Protein concentration was determined using BCA assay kit (Pierce). Equal amounts of total cellular extracts or immunocomplexes were electrophoresed on 4-12% SDS-PAGE gel (NOVEX) and transferred to a nitrocellulose filter (Immobilon P; Millipore Corporation, Bedford, MA). The membranes were

blocked in Tris buffered saline containing 0.002 g/L Tween 20 (TBST) and 0.05 g/L nonfat dry milk. After blocking, the membranes were washed three times in TBST and then incubated overnight at 4° C in TBST containing 5% BSA with primary specific antibody: total CaMKII and ERK 1/2 (1:1000, Santa Cruz, CA), phospho-tyrosine p44/p42 ERK (1:1000 Santa Cruz, CA) and phospho-CaMKII antibody (pT286) (Invitrogen). The blots were washed three times in TBST incubated in appropriate HRP-conjugated secondary antibodies (1:2000, Santa Cruz, CA) diluted in TBST containing 5% nonfat dry milk and incubated for 1 h at room temperature. After 3 additional washes with TBST, immunoreactive bands were visualized by enhanced chemiluminescence using the ECL-plus detection kit (Amersham Biosciences) and quantified by using ImageQuant software (Amersham Biosciences).

6.9 Sample preparation for CD and NMR analysis

To record CD and NMR experiments in water/HFA solution (50:50 v/v) CN17 β was added to an aqueous solution (pH 5.4, phosphate buffer 25 mM). This yielded final concentrations of 0.15 mM for CD experiments. For NMR samples, a H₂O/D₂O (90:10 v/v) mixture was used. To exclude potential aggregation, we recorded the 1D proton spectra of CN17 β at a concentration range spanning 1.0-0.1 mM. At a peptide concentration of 1.0 mM there were not any noticeable effects of aggregation. Therefore, our NMR analyses were carried at sample concentrations of 1 mM.

6.10 CD analysis

All CD spectra were recorded using a JASCO J810 spectropolarimeter at room temperature and with a cell path length of 1 mm. CD spectra were performed at 25 °C using a measurement range from 260 to 190 nm, 1-nm bandwidth, 4 accumulations and a 10 nm/min scanning speed. Spectra were corrected for solvent contribution. For an estimation of secondary structure content, CD spectra were analyzed using both the ContinLL and SELCON3 algorithms from the DICHROWEB website.⁴⁹

6.11 NMR analysis

NMR spectra were collected using a Bruker DRX-600 spectrometer at 300 K. 1D NMR spectra were recorded in the Fourier mode with quadrature detection. The water signal was suppressed by low-power selective irradiation in the homo-gated mode. DQFCOSY, TOCSY, and NOESY^{45,47} experiments were run in the phase-sensitive mode using quadrature detection in ω_1 via time-proportional phase increases of the initial pulse. Data block sizes were 2048 addresses in t_2 and 512 equidistant t_1 values. Prior to Fourier transformation, the time domain data matrices were multiplied by shifted sin 2 functions in both dimensions. A mixing time of 70 ms was used for the TOCSY experiments. NOESY experiments were run with mixing times in the range of 100-300 ms. Qualitative and quantitative analyses of DQF-COSY, TOCSY, and NOESY spectra were achieved using SPARKY software.⁵³

6.12 NMR structure calculations

Peak volumes were translated into upper distance bounds with the CALIBA routine from the DYANA software package.⁵⁵ The requisite pseudoatom corrections were applied for non-stereospecifically assigned protons at prochiral centers and for the methyl group. After discarding redundant and duplicated constraints, the final list of experimental constraints was used to generate an ensemble of 100 structures by the standard DYANA protocol of simulated annealing in torsion angle space implemented (using 6000 steps). No dihedral angle or hydrogen bond restraints were applied. The best 20 structures that had low target function values (0.83-1.19) and small residual violations (maximum violation = 0.38 Å) were refined by in vacuo minimization in the AMBER 1991 force field using the SANDER program of the AMBER 5.0 suite.⁵⁶ To mimic the effect of solvent screening, all net charges were reduced to 20% of their real values. Moreover, a distance-dependent dielectric constant ($\epsilon = r$) was used. The cut-off for non-bonded interactions was 12 Å. NMR-derived upper bounds were imposed as semi-parabolic penalty functions, with force constants of 16 kcal/mol Å². The

function was shifted to be linear when the violation exceeded 0.5 Å. The best 10 structures after minimization had AMBER energies ranging from -441.4 to -391.1 kcal/mol.

¹ Hook, SS.; Means, AR. Ca²⁺/CaM-dependent kinase: from activation to function. *Annu Rev Pharmacol Toxicol* **2001**, 414, 71-505.

² Soderling, TR.; Chang, B.; Brickey, D. Cellular signaling through multifunctional Ca²⁺/calmodulin dependent protein kinase II. *J Biol Chem* **2002** 76, 3719-3722.

³ Braun, AP.; Schulman, H. The multifunctional calcium/calmodulin-dependent protein kinase: from form to function. *Annu Rev Physiol* **1995**, 57, 417-445.

⁴ Meyer, T.; Hanson, PI.; Stryer, L.; Schulman, H. Calmodulin trapping by calcium calmodulin-dependent protein kinase. *Science* **1992**, 256, 1199-1202.

⁵ Hudmon, A.; Schulman, H. Structure-function of the multifunctional Ca²⁺/calmodulin-dependent protein kinase II. *Biochem J* **2002**, 364, 593-611 (and references therein).

⁶ Wu, GY.; Cline, HT. Stabilization of dendritic arbor structure in vivo by CaMKII. *Science* **1998**, 279, 222-226.

⁷ Colbran, RJ.; Brown, AM. Calcium/calmodulin-dependent protein kinase II and synaptic plasticity. *Curr Opin Neurobiol* **2004**, 14, 318-322.

⁸ (a) Giese, KP.; Fedorov, NB.; Filipkowski, RK.; Silva, AJ. Autophosphorylation at Thr286 of the alpha calcium-calmodulin kinase II in LTP and learning. *Science* **1998**, 279, 870-873; (b) Lisman, J.; Schulman, H.; Cline, H. The molecular basis of CaMKII function in synaptic and behavioural memory. *Nat Rev Neurosci* **2002**, 3, 175-190; (c) Lee, YS.; Silva, AJ. The molecular and cellular biology of enhanced cognition. *Nat Rev Neurosci* **2009**, 10, 126-140; (d) Buard, I.; Coultrap, SJ.; Freund, RK.; Lee, YS.; Dell'acqua, ML.; Silva, AJ.; Bayer, KU. CaMKII "autonomy" is required for initiating but not for maintaining neuronal long-term information storage. *J Neurosci* **2010**, 30, 8214-8220; (e) Sanhueza, M.; Fernandez-Villalobos, G.; Stein, IS.; Kasumova, G.; Zhang, P.; Bayer, KU.; Otmakhov, N.; Hell, JW.; Lisman, J. Role of the CaMKII/NMDA receptor complex in the maintenance of synaptic strength. *J Neurosci* **2011**, 31, 9170-9178.

⁹ (a) Kahl, CR.; Means, AR. Regulation of cell cycle progression by calcium/calmodulin-dependent pathways. *Endocr Rev* **2003**, 24, 719-736; (b) Yuan, K.; Chung, LWK.; Siegal, GP.; Zayzafoon, M. Alpha-CaMKII controls the growth of human osteosarcoma by regulating cell cycle progression. *Lab Invest* **2007**, 87, 938-950; (c) Rusciano, M.; Salzano, M.; Monaco, S.; Sapio, M.; Illario,

M.; De Falco, V.; Santoro, M.; P.; Pastore, L.; Fenzi, G.; Rossi, G.; Vitale, M. The Ca²⁺/calmodulin dependent kinase II (CaMKII) is activated in papillary thyroid carcinoma and mediates cell proliferation stimulated by RET/PTC. *Endocr Relat Cancer* **2010**, *17*, 113-123.

¹⁰ Olofsson, MH.; Havelka, AM.; Brnjic, S.; Shoshan, MC.; Linder, S. Charting calcium-regulated apoptosis pathways using chemical biology: role of calmodulin kinase II. *BMC Chem Biol* **2008**, *8*, 2.

¹¹ (a) Herrmann, TL.; Morita, CT.; Lee, K.; Kusner, DJ. Calmodulin kinase II regulates the maturation and antigen presentation of human dendritic cells. *J Leukoc Biol* **2005**, *78*, 1397-1407; (b) Bui, JD.; Calbo, S.; Hayden-Martinez, K.; Kane, LP.; Gardner, P.; Hedrick, SM. A role for CaMKII in T cell memory. *Cell* **2000**, *100*, 457-467.

¹² (a) Erickson, J.; Patel, R.; Hart, G.; Bers, D. Specific intracellular glycosylation directly modulates CamKII activity during hyperglycemia. *Circulation* **2010**, *122*, A20245; (b) Illario, M.; Monaco, S.; Cavallo, AL.; Esposito, I.; Formisano, P.; D'Andrea, L. Cipolletta, E.; Trimarco, B.; Fenzi, G.; Rossi, G.; Vitale, M. Calcium-calmodulin dependent kinase II (CaMKII) mediates insulin-stimulated proliferation and glucose uptake. *Cell Signal* **2009**, *21*, 786-792.

¹³ Grueter, CE.; Abiria, SA.; Wu, Y.; Anderson, ME.; Colbran, RJ. Differential regulated interactions of calcium/calmodulin-dependent protein kinase II with isoforms of voltage-gated calcium channel beta subunits. *Biochemistry* **2008**, *47*, 1760-1767.

¹⁴ Wagner, S.; Dybkova, N.; Rasenack, ECL.; Jacobshagen, C.; Fabritz, L.; Kirchhof, P.; Maier, SKG.; Zhang, T.; Hasenfuss, G.; Brown, JH.; Bers, DM.; Maier, LS. Ca²⁺/calmodulin-dependent protein kinase II regulates cardiac Na⁺ channels. *J Clin Invest* **2006**, *116*, 3127-3138.

¹⁵ Erickson, JR.; Joiner, MA.; Guan, X.; Kutschke, W.; Yang, J.; Oddis, CV.; Ryan, K.; Bartlett, RK.; Lowe, JS.; O'Donnell, SE.; Aykin-Burns, N.; Zimmerman, MC.; Zimmerman, K.; Ham, AL.; Weiss, RM.; Spitz, DR.; Shea, MA.; Colbran, RJ. Mohler, PJ.; Anderson, ME. A dynamic pathway for calcium-independent activation of CamKII by methionine oxidation. *Cell* **2008**, *133*, 462-474.

¹⁶ Maier, LS.; Bers, DM. Role of Ca²⁺/calmodulin-dependent protein kinase (CaMK) in excitation-contraction coupling in the heart. *Cardiovasc Res* **2007**, *73*, 631-640.

¹⁷ Yoshimura, Y.; Ichinose, T.; Yamauchi, T.; Phosphorylation of tau protein to sites found in Alzheimer's disease brain is catalyzed by Ca²⁺/calmodulin-dependent protein kinase II as demonstrated tandem mass spectrometry. *Neurosci Lett* **2003**, *353*, 185-188.

- ¹⁸ Picconi, B.; Gardoni, F.; Centonze, D.; Mauceri, D.; Cenci, MA.; Bernardi, G.; Calabresi, P.; Di Luca, M. Abnormal Ca²⁺/Calmodulin-dependent protein kinase II function mediates synaptic and motor deficits in experimental Parkinsonism. *J Neurosci* **2004**, 24, 5283-5291.
- ¹⁹ Coultrap, SJ.; Vest, RS.; Ashpole, NM.; Hudmon, A.; Bayer, KU. CaMKII in cerebral ischemia. *Acta Pharmacol Sin* **2011**, 32, 861-872.
- ²⁰ Tombes, RM.; Krystal, GW. Identification of novel human tumor cell-specific CaMK-II variants. *Biochim Biophys Acta* **1997**, 1355, 281-292.
- ²¹ Yang, BF.; Xiao, C.; Roa, WH.; Krammer, PH.; Hao, C. Calcium/calmodulin dependent protein kinase II regulation of c-FLIP expression and phosphorylation in modulation of Fas-mediated signaling in malignant glioma cells. *J Biol Chem* **2003**, 278,7043-7050.
- ²² Rokhlin, OW.; Taghiyev, AF.; Bayer, KU.; Bumcrot, D.; Koteliansk, VE.; Glover, RA.; Cohen, MB. Calcium/calmodulin-dependent kinase II plays an important role in prostate cancer cell survival, *Cancer Biol Ther* **2007**, 6, 732-742.
- ²³ Zhang, T.; Brown, JH. Role of Ca²⁺/calmodulin-dependent protein kinase II in cardiac hypertrophy and heart failure. *Cardiovasc Res*. **2004**, 63, 476-486.
- ²⁴ Zhang, R.; Khoo, MSC.; Wu, Y.; Yang, Y.; Grueter, CE.; Ni, G.; Price Jr., EE.; Thiel, W.; Guatimosin, S.; Song, LS.; Madu, EC.; Shah, AN.; Vishnivetskaya, TA.; Atkinson, JB.; Gurevich, VV.; Salama, G.; Lederer, WJ.; Colbran, RJ.; Anderson, ME. Calmodulin kinase II inhibition protects against structural heart disease. *Nat Med* **2005**, 11, 409-417.
- ²⁵ Højlund, K.; Birk, JB.; Klein, DK.; Levin, K.; Rose, AR.; Hansen, BF.; Nielsen, JN.; Beck-Nielsen, H.; Wojtaszewski, JFP. Dysregulation of glycogen synthase COOH- and NH₂-terminal phosphorylation by insulin in obesity and type 2 Diabetes Mellitus. *J Clin Endocrinol Metab* **2009**, 94, 4547-4556.
- ²⁶ Anderson, M.; Braun, A.; Wu, Y.; Lu, T.; Wu, Y.; Schulman, H.; Sung, RJ. KN-93, an inhibitor of multifunctional Ca²⁺/Calmodulin-dependent protein kinase, decreases early after depolarizations in rabbit heart. *J Pharmacol Exp Ther* **1998**, 287, 996-1006.
- ²⁷ Vest, RS.; O'Leary, H.; Coultrap, SJ.; Kindy, MS.; Bayer, KU. Effective post-insult neuroprotection by a novel Ca²⁺/Calmodulin-dependent protein kinase II (CaMKII) inhibitor. *J Biol Chem* **2010**, 285, 20675-20682.
- ²⁸ Tokumitsu, H.; Chijiwa, T.; Hagiwara, M.; Mizutani, A.; Terasawa, M.; Hidaka, H. KN-62, 1-[N,O-bis(5-isoquinolinesulfonyl)-N-methyl-L-tyrosyl]-4-phenylpiperazine, a specific inhibitor of Ca²⁺/calmodulin-dependent protein kinase II. *J Biol Chem* **1990**, 265, 4315-4320.

- ²⁹ Sumi, M.; Kiuchi, K.; Ishikawa, T.; Ishii, A.; Hagiwara, M.; Nagatsu, T.; Hidaka, H. The newly synthesized selective Ca²⁺/calmodulin dependent protein kinase II inhibitor KN-93 reduces dopamine contents in PC12h cells. *Biochem Biophys Res Commun* **1991**, 181 968-975.
- ³⁰ Ishida, A.; Kameshita, I.; Okuno, S.; Kitani, T.; Fujisawa, H. A novel highly specific and potent inhibitor of calmodulin-dependent protein kinase II. *Biochem Biophys Res Commun* **1995**, 212, 806-812.
- ³¹ Braun, AP.; Schulman, H. A non-selective cation current activated via the multi-functional Ca(2+)-calmodulin-dependent protein kinase in human epithelial cells. *J Physiol* **1995**, 488, 37-55.
- ³² (a) Hvalby, O.; Hemmings, HG.; Paulsen, O.; Czernik, AJ.; Nairn, AC.; Godfraind, JM.; Jensen, V.; Raastad, M.; Storm, JF.; Andersen, P.; Greengard, P. Specificity of protein kinase inhibitor peptides and induction of long-term potentiation. *Proc Natl Acad Sci U. S. A.* **1994**, 91, 4761- 4765; (b) Smith, MK.; Colbran, RJ.; Soderling, TR. Specificities of autoinhibitory domain peptides for four protein kinases: implications for intact cell studies of protein kinase functions. *J Biol Chem* **1990**, 265, 1837-1840.
- ³³ (a) Vest, RS.; Davies, KD.; O'Leary, H.; Port, JD.; Bayer, KU. Dual mechanism of a natural CaMKII inhibitor. *Mol Biol Cell* **2007**, 18, 5024-5033; (b) Enslin, H.; Sun, P.; Brickey, D.; Soderling, SH.; Klamov, E.; Soderling, TR. Characterization of Ca²⁺/calmodulin-dependent protein kinase IV. Role in transcriptional regulation. *J Biol Chem* **1994**, 269, 15520-15527.
- ³⁴ (a) Li, G.; Hidaka, H.; Wollheim, CB. Inhibition of voltage-gated Ca²⁺ channels and insulin secretion in HIT cells by the Ca²⁺/calmodulin-dependent protein kinase II inhibitor KN-62: comparison with antagonists of calmodulin and L type Ca²⁺ channels. *Mol Pharmacol* **1992**, 42, 489-498; (b) Ledoux, J.; Chartier, D.; Leblanc, N. Inhibitors of calmodulin-dependent protein kinase are nonspecific blockers of voltage-dependent K⁺ channels in vascular myocytes. *J Pharmacol Exp Ther* **1999**, 290, 1165-1174.
- ³⁵ (a) Chang, BH.; Mukherji, S.; Soderling, T. Characterization of a calmodulin kinase II inhibitor protein in brain. *Proc Natl Acad Sci U. S. A.* **1998**, 95, 10890-10895; (b) Chang, BH.; Mukherji, S.; Soderling, T. Calcium/calmodulin-dependent protein kinase II inhibitor protein: localization of isoforms in rat brain. *Neuroscience* **2001**, 102 767-777.
- ³⁶ Coultrap, SJ.; Bayer, KU. Improving a natural CaMKII inhibitor by random and rational design. *PLoS One* **2011**, 6, e25245.
- ³⁷ Coultrap, SJ.; Buard, I.; Kulbe, JR.; Dell'Acqua, ML.; Bayer, KU. CaMKII autonomy is substrate-dependent and further stimulated by Ca²⁺/calmodulin. *J Biol Chem* **2010**, 285, 17930-17937.

- ³⁸ Cipolletta, E.; Monaco, S.; Maione, AS.; Vitiello, L.; Campiglia, P.; Pastore, L.; Franchini, C.; Novellino, E.; Limongelli, V.; Bayer, KU.; Means, AR.; Rossi, G.; Trimarco, B.; Iaccarino, G.; Illario, M. Calmodulin-dependent kinase II mediates vascular smooth muscle cell proliferation and is potentiated by extracellular signal regulated kinase. *Endocrinology* **2010**, 151, 2747-2759.
- ³⁹ Gomez, IM.; Sala, M.; Rusciano, MR.; Monaco, S.; Maione, AS.; Iaccarino, G.; Tortorella, P.; D'Ursi, AM.; Scrima, M.; Carotenuto, A.; De Rosa, G.; Bertamino, A.; **Vernieri, E.**; Grieco, P.; Novellino, E.; Illario, M.; Campiglia, P. Characterization of a selective CaMKII peptide inhibitor. *European Journal of Medicinal Chemistry* **2013**, 62, 425-434.
- ⁴⁰ Chao, LH.; Pellicen, P.; Deindl, S.; Barclay, LA.; Schulman, H.; Kuriyan, J. Intersubunit capture of regulatory segments is a component of cooperative CaMKII Activation. *Nat Struct Mol Biol* **2010**, 17, 264-272.
- ⁴¹ Atherton, E.; Sheppard, RC. Solid-phase Peptide Synthesis: A Practical Approach. *IRL, Oxford*. **1989**.
- ⁴² Lu, YM.; Shioda, N.; Han, F.; Kamata, A.; Shirasaki, Y.; Qin, ZH.; Fukunaga, K. DY- 9760e inhibits endothelin-1-induced cardiomyocyte hypertrophy through inhibition of CaMKII and ERK activities. *Cardiovasc Ther* **2009**, 27, 17-27.
- ⁴³ Wang, C.; Li, N.; Liu, X.; Zheng, Y.; Cao, X. A novel endogenous human CaMKII inhibitory protein suppresses tumor growth by inducing cell cycle arrest via p27 stabilization. *J Biol Chem* **2008**, 283, 11565-11574.
- ⁴⁴ Denizot, F.; Langa, R. Rapid colorimetric assay for cell growth and survival: modifications to the tetrazolium dye procedure giving improved sensitivity and reliability. *J Immunol Methods* **1986**, 89, 271-277.
- ⁴⁵ Mosmann, T. Rapid colorimetric assay for cellular growth and survival: application to proliferation and cytotoxicity assays. *J Immunol Methods* **1983**, 65, 55-63.
- ⁴⁶ (a) Illario, M.; Cavallo, AL.; Bayer, KU.; Di Matola, T.; Fenzi, G.; Rossi, G.; Vitale, M. Calcium/calmodulin-dependent protein kinase II binds to Raf-1 and modulates integrin-stimulated ERK activation. *J Biol Chem* **2003**, 278, 45101-45108; (b) Illario, M.; Cavallo, AL.; Monaco, S.; Di Vito, E.; Mueller, F.; Marzano, LA.; Troncone, G.; Fenzi, G.; Rossi, G.; Vitale, M. Fibronectin-induced proliferation in thyroid cells is mediated by alpha-beta3 integrin through Ras/Raf-1/MEK/ERK and calcium/CaMKII signals. *J Clin Endocrinol Metab* **2005**, 90, 2865-2873.
- ⁴⁷ Rajan, R.; Awasthi, SK.; Bhattacharjya, S.; Balaram, P. Teflon-coated peptides: hexafluoroacetone trihydrate as a structure stabilizer for peptides. *Biopolymers* **1997**, 42, 125-128.

- ⁴⁸ (a) Picone, D.; D'Ursi, A.; Motta, A.; Tancredi, T.; Temussi, PA. Conformational preferences of [Leu5]enkephalin in biomimetic media. Investigation by ¹H NMR. *Eur J Biochem* **1990**, 192, 433-439; (b) D'Ursi, AM.; Albrizio, S.; Greco, G., Mazzeo, S.; Mazzoni, MR.; Novellino, E.; Rovero, P. Conformational analysis of the Gas protein C-terminal region. *J Pept Sci* **2002**, 8, 476-488.
- ⁴⁹ Whitmore, L.; Wallace, B. DICHROWEB, an online server for protein secondary structure analyses from circular dichroism spectroscopic data. *Nucleic Acids Res* **2004**, 32 W668.
- ⁵⁰ Piantini, U.; Sorensen, O.; Ernst, R. Multiple quantum filters for elucidating NMR coupling networks. *J Am Chem Soc* **1982**, 104, 6800-6801.
- ⁵¹ Bax, A.; Davis, D. MLEV-17-based two-dimensional homonuclear magnetization transfer spectroscopy. *J Magn Reson* **1985**, 65, 355-360.
- ⁵² Jeener, J.; Meier, B.; Bachmann, P.; Ernst, R. Investigation of exchange processes by two-dimensional NMR spectroscopy. *J Chem Phys* **1979**, 71, 4546-4553.
- ⁵³ Goddard, T.; Kneller, D. SPARKY 3, University of California, San Francisco, **2004**.
- ⁵⁴ Wüthrich, K. NMR of Proteins and Nucleic Acids, Wiley-Interscience, **1986**.
- ⁵⁵ Guntert, P.; Mumenthaler, C.; Wuthrich, K. Torsion angle dynamics for NMR structure calculation with the new program DYANA. *J Mol Biol* **1997**, 273, 283-298.
- ⁵⁶ (a) Case, D.; Pearlman, D.; Caldwell, J.; Cheatham III, T.; Ross, W.; Simmerling, C.; Darden, T.; Merz, K.; Stanton, R.; Cheng, A.; AMBER 5, University of California, San Francisco, **1997**; (b) Pearlman, D.; Case, D.; Caldwell, J.; Ross, W.; Cheatham, T.; AMBER, a package of computer programs for applying molecular mechanics, normal mode analysis, molecular dynamics and free energy calculations to simulate the structural and energetic properties of molecules. *Comput Phys Commun* **1995**, 91, 1-41.
- ⁵⁷ Laskowski, RA.; Chistyakov, VV.; Thornton, JM. PDBsum more: new summaries and analyses of the known 3D structures of proteins and nucleic acids. *Nucleic Acids Res* **2005**, 33, D266-D268.
- ⁵⁸ Chin, D.; Winkler, KE.; Means, AR. Characterization of substrate phosphorylation and use of calmodulin mutants to address implications from the enzyme crystal structure of calmodulin-dependent protein kinase I. *J Biol Chem* **1997**, 272, 31235-31240.
- ⁵⁹ Chin, D.; Means, AR. Mechanisms for regulation of calmodulin kinase IIa by Ca²⁺/calmodulin and autophosphorylation of threonine 286. *Biochemistry* **2002**, 411, 14001-14009.

Appendix A- Automated peptide synthesizers

Solid-phase peptide synthesis (SPPS) is still often faced with challenges in the assembly of long and ‘difficult’ sequences, *e.g.* due to aggregation and steric hindrance giving rise to incomplete reactions.

These problems have only partly been solved by new coupling reagents and solid supports. Precise microwave heating has emerged as one new parameter for SPPS, in addition to coupling reagents, resins, solvents etc.¹

Fast and precise heating by microwave irradiation during solid-phase peptide synthesis (SPPS) can reduce reaction times as well as provide better purities and greater yields for the synthesis of difficult peptides.

Microwave- assisted SPPS has proven to be a useful and reliable tool for the synthesis of peptides as well as small proteins. It is particularly well suited for sequences with a high propensity to form β -sheet-type structures and for sterically difficult coupling.

Several chemical methods to suppress intramolecular aggregation have been described and include pseudo-prolines,² solvent composition,³ and chaotropic salts.⁴

Heating is likely to reduce both the inter- and intramolecular-derived self-assemblies and thereby decrease the reaction time and improve the coupling efficiency of bulky and β -branched amino acids.

Microwave irradiation is a promising tool in peptide chemistry because of the rapid and precise elevation of the temperature and the efficient temperature control during the synthesis.

A.1 Automated Peptide Synthesizers

Following Merrifield’s pioneering invention of solid-phase peptide synthesis, his group also developed the concept of automated solid-phase peptide synthesis^{5,6} and constructed the first synthesizers in the mid-1960s.^{7,8} Using one of the first synthesizers, Gutte and Merrifield synthesized Ribonuclease A, a 124 amino acid protein, using an astonishing 369 chemical reactions and 11,391 steps on the automated peptide synthesizer, relying on the synthetic chemistry and analytical methods available at that time.^{9,10} Later other laboratories and companies developed a diverse range of laboratory

synthesizers.^{11,12} The introduction of Fmoc based SPPS¹³ and more sophisticated hardware as well as software allowed for simpler designs of automated peptide synthesizers. The simplified synthesizers have over the years led to comparably robust and reliable synthesizers, which have resulted in high-quality peptides and good reproducibility.

A.2 Applications

In the last year of my PhD, my research group started to approach to automated synthesizer, in particular to SyroWaveTM (Biotage) (Figure 1) which has shown to be a very flexible instrument for SPPS due to its ability to perform either single microwave reactions or conventional parallel synthesis at RT.



Figure 1. The Biotage Syro WaveTM.

This instrument is built around a valve-free robot originally developed for parallel peptide synthesis, where the robotic arm transports reagents instead of pumping via valves. Additionally, the reaction vessel is vortexed in the microwave cavity.

This is the first example of an “X-Y” robotic microwave-assisted synthesizer developed for the assembly of long peptides. Several groups have shown that mixing is extremely important during microwave-assisted SPPS.^{14,15} Overall the use of microwave heating during SPPS will often aid the synthesis of difficult peptides and small proteins, provided that commonly occurring side reactions can be avoided.

For the synthesis of difficult sequence the introduction of state-of-the-art resins and coupling reagents has solved previous problems associated with its synthesis.

Microwave irradiation in combination with the optimal coupling reagent showed to solve most of the challenges with the assembly of peptide.

A.2.1 Optimization of automated peptide synthesizers

The possibility of a so-called microwave effect¹⁶ has been discussed but studies have indicated that the observed enhancement was purely of a thermal nature, as similar results were obtained with conventional heating.¹⁷

Another significant question is how to prevent the occurrence of epimerization. Studies on the risk of epimerization in peptides containing Cys and His residues during microwave-assisted SPPS indicated that His and Cys should be coupled at 50°C or maybe even at room temperature.

The aim of this study was to develop a general protocol for microwave accelerated solid-phase synthesis of carboxyl sequence.

Microwave irradiation in combination with the optimal coupling reagent showed to solve most of challenges with the assembly of peptide.

The synthesis of PTPRJ agonist, peptide **6** [CHHALTHAC] (see Chapter 2) was used to investigate optimal coupling conditions, especially temperature, time, solid supports and coupling reagents on the automated microwave-assisted peptide synthesizer SyroWaveTM.¹⁸

A first attempt to prepare peptide **6** by a standard Fmoc procedure using Wang resin not functionalized and the same protocol used for manual synthesis (HBTU/HOBt as coupling reagents and DMF as solvent of choice) showed a yield rather low (Figure 2).

LC-MS analysis of the crude product showed the expected peptide without Alanine-Cysteine in C-terminal (m/z 818) as the main peak but the overall quality of the material was rather low (Figure 2).

Different synthesis were planned using i) Fmoc-Cys(trt)-Wang resin avoiding the use of a catalytic amount of DMAP; ii) 2-Cl trityl resin; iii) Fmoc-Cys-(trt)-Wang resin and HOAt instead HOBt like coupling reagent.

i) The use of functionalized Wang resin allowed us to reduce the side reactions at least in part, but the yield was still low. It was necessary to optimize the synthesis protocol changing resin and/or coupling reagents.

ii) We investigated the impact of heating on 2-Cl trityl resin during the synthesis of C-terminal carboxylic acid peptides. The first *N*^α-Fmoc amino acid were dissolved in dry dichloromethane (DCM) and with this solvent it is not possible to use MW irradiation leading to a long reaction time.

We understand also that the use of microwave during couplings lead to a premature cleavage resulting in a HPLC profile with several peaks and low yield.¹⁹

iii) The purity was further optimized by substituting HBTU with other coupling reagents. Interestingly, for this particular peptide, the results for HOAt gave a superior outcome compared to other coupling reagents.

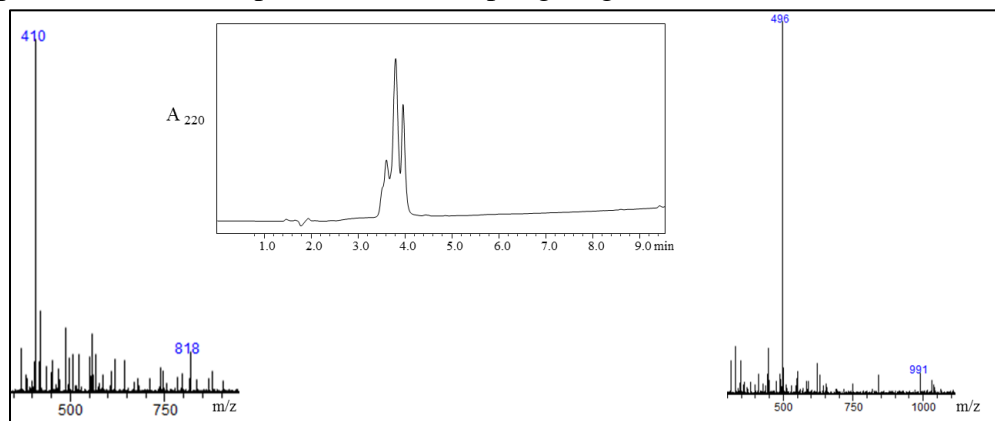


Figure 2. HPLC crude profile of peptide 6 and ESI-MS spectrum of peptide 6: $[M+2H]^{2+}$ (m/z 496), and ESI-MS spectrum of peptide 6 without $^8\text{Ala}^9\text{Cys}$: $[M+2H]^{2+}$ (m/z 410).

Summarizing, two possible synthetic approaches could be used to obtain satisfactory results: 1) manual synthesis with 2-Cl trytil resin. The steric size of 2Cl-Trt group not allow the formation of diketopiperazine (see Chapter 2); 2) automated microwave synthesis with Fmoc-Cys(trt)-Wang resin which allowed to use high temperature reducing time of synthesis and side reactions.

The protocol was optimize using HOAt as coupling reagent instead HOBt that leads to several side reactions. Moreover the preferred solvent with microwave is NMP, N-methyl pyrrolidone instead DMF, Dimethylformamide.

To ensure the completed coupling or deprotection we used all double coupling and/or double deprotection protocol which allow to repeat the reaction in the same condition twice (Table 1).

The optimal coupling condition for Histidine and Cysteine couplings (residues 1-3, 7) was 2×45 min at RT to avoid the epimerization.

Table 1. Coupling conditions for the synthesis of peptide 6, residue ⁷His⁸Ala.

N ^o Residues	Coupling reagent	Eq.	Method	
			Coupling	Deprot. Pip.40% in DMF
⁸ ALA	HOAt/NMP- HBTU/DMF	4	10min,75° C	2min, RT
			× 2	15min, RT × 2
⁷ HIS	HOAt/NMP- HBTU/DMF	4	45min, RT	2min, RT
			× 2	15min, RT × 2

All the couplings reactions were performed using DIEA as base.

¹Cys was added with the same protocol used for ⁷His.

¹ Brandt, M.; Gammeltoft, S.; Jensen, KJ. Microwave Heating for Solid-Phase Peptide Synthesis: general evaluation and application to 15-mer phosphopeptides. *Int J Pept Res Therap* **2006**, 12, 349-357.

² Wohr, T.; Wahl, F.; Nefzi, A.; Rohwedder, B.; Sato, T.; Sun, X.; Mutter, M. Pseudo-prilnes as a solubilizing, structure-disrupting protection technique in peptide synthesis. *J Am Chem Soc* **1996**, 118, 9218-9227.

³ Yamashiro, D.; Blake, J.; Hao Li, C. The use of trifluoroethanol for improved coupling in solid-phase peptide synthesis. *Tetrahedron Lett* **1976**, 17, 1469-1472.

⁴ Thaler, A.; Seebach, D.; Cardinaux, F. Lithium-salt effects in peptide synthesis. Part II. Improvement of degree of resin swelling and of efficiency of coupling in solid-phase synthesis. *Helv Chim Acta* **1991**, 74, 628-643.

⁵ Merrifield, RB. Automated synthesis of peptides. *Science* **1985**, 150, 178-185.

⁶ Merrifield, RB.; Stewart, JM. Automated peptide synthesis. *Nature* **1965**, 207, 522-523.

⁷ Merrifield, RB.; Stewart, JM.; Jernberg, N. Instrument for automated synthesis of peptides. *Anal Chem* **1966**, 38, 1905-1914.

- ⁸ Brunfeldt, K.; Halstrqm, J.; Roepstorff, P. A punched tape controlled peptide synthesizer. *Acta Chem Scand* **1969**, 23, 2830-2838.
- ⁹ Gutte, B.; Merrifield, RB. The synthesis of ribonuclease A. *J Biol Chem* **1971**, 246,1922-1941.
- ¹⁰ Cameron, LR.; Holder, JL.; Meldal, M.; Sheppard, RC. Peptide synthesis. Part 13. Feedback control in solid phase synthesis. Use of fluorenylmethoxycarbonyl amino acid 3,4-dihydro-4-oxo-1,2,3-benzotriazin-3-yl esters in a fully automated system. *J Chem Soc Perkin Transe* **1988**, 1, 2895-2901.
- ¹¹ Schnorrenberg, G.; Gerhardt, H. Fully automatic simultaneous multiple peptide synthesis in micromolar scale-rapid synthesis of series of peptides for screening in biological assays. *Tetrahedron* **1989**, 45, 7759-7764.
- ¹² Gausepohl, H.; Boulin, C.; Kraft, M.; Frank RW. Automated multiple peptide-synthesis. *Pept Res* **1992**, 5, 315-320.
- ¹³ Carpino, LA.; Han, GY. 9-Fluorenylmethoxycarbonyl function, a new base-sensitive amino-protecting group. *J Am Chem Soc* **1970**, 92, 5748-5749.
- ¹⁴ Pedersen, SL.; Sorensen, KK.; Jensen, KJ. Semi-automated microwave-assisted SPPS: optimization of protocols and synthesis of difficult sequences. *Biopolymers* **2010**, 94, 206-212.
- ¹⁵ Coantic, S.; Subra, G.; Martinez, J. Microwave-assisted solid phase peptide synthesis on high loaded resins. *Int J Pep Res Ther* **2008**, 14, 143-147.
- ¹⁶ Palasek, S.; Cox, Z.; Collins, J. Limiting racemization and aspartimide formation in microwave-enhanced Fmoc solid-phase peptide synthesis. *J Pept Sci* **2007**, 13, 143-148.
- ¹⁷ Bacsá, B.; Horvátí, K.; Bosze, S.; Andrae, F.; Kappe, CO. Solid-phase synthesis of difficult critical comparison of microwave and conventional heating technologies. *J Org Chem* **2008**, 73, 7532-7542.
- ¹⁸ Malik. L.; Tofteng, AP.; Pedersen, SL.; Sorensen, KK.; Jensen, KJ. Automated "X-Y" robot for peptide synthesis with microwave heating: application to difficult peptide sequences and protein domains. *J Pept Sci* **2010**, 16, 506-512.
- ¹⁹ Echaliér, C.; Al-Halifa, S.; Kreiter, A.; Enjalbal, C.; Sanchez, P.; Ronga, L.; Puget, K.; Verdié P.; Amblard, M.; Martinez, J.; Subra G. Heating and microwave assisted SPPS of C-terminal acid peptides on trityl resin: the truth behind the yield. *Amino Acids* **2013**, 45, 1395-1403.

Appendix B- An Optimized Fmoc Synthesis of Human Defensin 5

Current methods for solid-phase peptide synthesis (SPPS) can reliably generate a very wide range of peptides. However, peptide synthesis can be a rather time-consuming process and accelerating reactions using elevated temperatures to enhance coupling rates has been explored.¹ Furthermore, despite the many advances in the chemistry of peptide synthesis, assembly of “difficult sequences” often remains a problem, due to aggregation and steric hindrance giving rise to incomplete reactions.

These problems have only partly been solved by new coupling reagents and solid supports.

To understand how different resins and different protocols influence the efficiency of the synthesis, I focused the attention on a difficult synthesis, Human α -defensin 5 (DEF5). In particular I performed a research project in Barcelona, to Pompeu Fabra University, with the scientific support of Prof. David Andreu and Dr. Beatriz G. de la Torre.²

I used different protocols to optimize solid-phase synthesis of DEF5 using the Fmoc strategy.

B.1 Human defensin 5 (DEF5)

Human defensin 5 (DEF5) is a 32-residue cysteine-rich host-defense peptide that exhibits three disulfide bonds in the oxidized form (DEF5_{ox}) (Figure 1).

DEF5 belongs to Defensins, antimicrobial peptides (AMPs)^{3,4} that play an important role in host defense as components of the innate immune system.^{5,6}

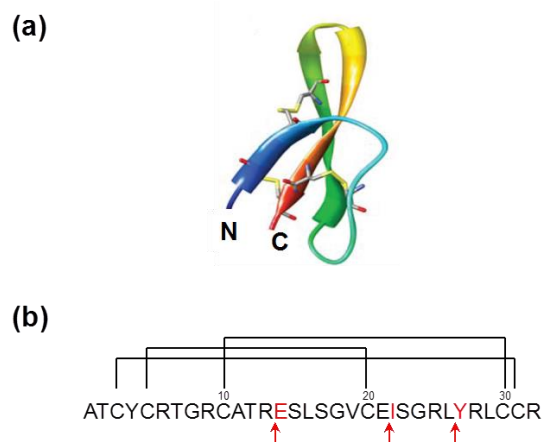


Figure 1. a) Three-dimensional structure of DEF5 showing the triple-strand β -sheet and the disulfide bridges;¹² (b) Amino acid sequence and disulfide connectivity of DEF5. Residues in red refer to points at which peptide-resin samples were taken and a mini-cleavage (arrow) performed; see text for more details.

It is stored in Paneth cell secretory vesicles as a 75-amino acid propeptide which, in response to microbial invasion, is converted into a 43-aa propeptide by the metalloproteinase matrilysin,⁷ then by trypsin proteolysis into the 32-residue mature form that is released into the intestinal lumen.⁸ DEF5 has been reported to play an important role in Crohn's disease, where loss of endogenous DEF5 is observed in the small intestinal while other Paneth cell products remain unchanged;⁹ also, a single R13H point mutation in DEF5 has been observed in patients with inflammatory bowel disease.¹⁰

A growing interest on defensin structural and functional studies has placed increasing pressure on the sources of these peptides. Most studies to date have used defensins directly purified from cell extracts and tissues, but low yield makes studies costly and highly time-consuming. The alternative of overexpressing DEF5-coding genes was for long complicated by the toxicity of the peptide toward host cells, its susceptibility to proteolytic degradation and its small size; only recently have these difficulties been partly avoided and expression of mature DEF5 achieved in moderate efficiencies in *P. pastoris*¹¹ or *E. coli* expression systems.^{12,13} Even so, a peptide of DEF5's size and complexity would ideally appear to be well within the scope of chemical synthesis methods, with their inherent expediency and flexibility. Surprisingly, however, while various synthetic accounts of "defensin like" peptides -i.e.,

around 30-residue long and with three disulfide bridges– came up in a thorough revision of the literature, only one synthesis of DEF5¹⁴ has been hitherto reported, and that by a synthetic (Boc-based) methodology that is unfeasible at many labs due to hazard restrictions to the use of anhydrous HF. It seemed worthwhile, therefore, to explore whether DEF5 could be efficiently made by the more convenient Fmoc methodology that we have successfully applied to other peptides of similar size and complexity.^{15,16} Indeed, the goal proved considerably more challenging than originally expected: a trial DEF5 synthesis run using standard Fmoc methods turned up a very unpromising product in very low yields. What follows is an account of the various synthetic improvements that have finally enabled a reasonably efficient Fmoc synthesis of DEF5. This has involved identifying problematic stretches during the sequence assembly process and introducing corrective modifications, particularly regarding the solid support and the use of Ψ-Pro dipeptide units at identified trouble spots. These improvements can be combined to produce an hexathiol DEF5 precursor clean enough to be oxidized as a crude product, with no need of purifying the intermediate, thus increasing the efficiency of the synthetic approach.

B.2 Results and discussion

The goal of this research was to find a strategy for producing DEF5, and eventually analogues thereof, by an efficient solid phase synthesis method using Fmoc chemistry. The only reports of DEF5 and DEF5 analogue synthesis published so far^{14,17} rely on Boc chemistry for chain assembly and anhydrous HF for final cleavage and deprotection, the last step being impractical for many laboratories given the safety hazards and consequent restrictions on HF use. In the search for a robust Fmoc-based synthetic route to DEF5 we have encountered a variety of hurdles that have been overcome, with reasonable success, as summarized in the workflow diagram shown in Figure 2.

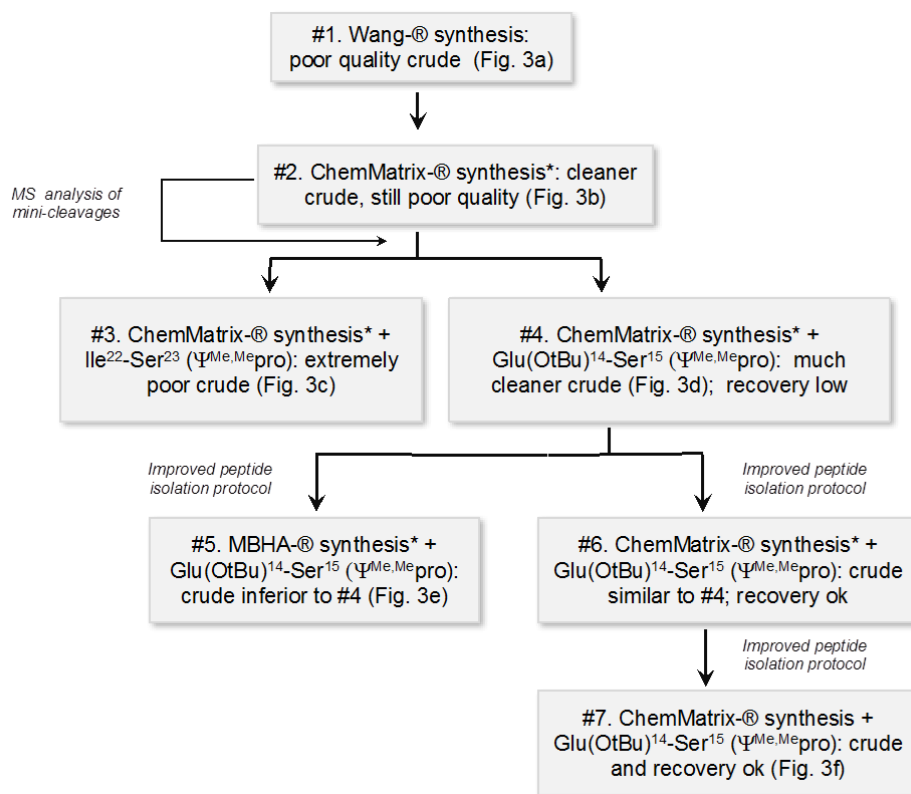


Figure 2. Workflow in the optimization of DEF5 synthesis. Asterisks in runs #2 to #6 refer to DEF5^a instead of DEF5 being used as synthetic target, for expediency reasons.

A first attempt to prepare DEF5 by a standard Fmoc procedure using Fmoc-L-Arg(Pbf)-Wang resin as starting material clearly showed that optimization would be required. UV monitoring of the sequence assembly process indicated several non-quantitative couplings and, accordingly, while LC-MS analysis of the crude product showed the expected hexathiol (MW 3588) as the main peak (Figure 3a), the overall quality of the material was rather low. In view of this, in a second trial ChemMatrix[®] resin, a PEG-based support known to minimize the aggregation phenomena¹⁸ suspected largely responsible for the poor results of the first synthesis, was used instead of polystyrene-based Wang resin. Assuming also that the synthetic problems were unrelated to the (carboxyl or amide) nature of the C-terminus, a Rink amide-functionalized ChemMatrix[®] resin, eventually furnishing DEF5 amide (DEF5^a), was chosen in order to

simplify the C-terminal attachment step. In addition, the chain elongation process was monitored by mini-cleavage of peptide resin aliquots (N-deprotected beforehand) and LC-MS analysis of the product at three pre-selected positions: (1) ^{27}Tyr , early in the synthetic process, to ensure that chain assembly was proceeding adequately or, if not, try to solve the problem by decreasing resin loading; (2) ^{22}Ile and (3) ^{14}Glu , two positions preceded each by a Ser residue, hence amenable to pseudoproline (Ψ -Pro) dipeptide replacement, a tactic to deliberately disrupt β -sheet structures causing interchain aggregation and sluggish chain growth.^{19,20} MS confirmed that synthesis was proceeding smoothly at steps (1) and (2); in both cases, the mini-cleavage afforded a highly homogeneous product with the mass expected at that stage. Mini-cleavage at (3), however, showed the (14-32) sequence to be present only in minor amounts and accompanied by various deletion peptides indicating low coupling efficiencies in the 14-23 (ESLSGVCEIS) stretch. Elongation up to the N-terminus, deprotection and cleavage gave a crude (Figure 3b) of very similar complexity to that of the mini-cleavage, only marginally cleaner than the first synthesis (Figure 3a). In view of this, two new syntheses of DEF5 amide were planned, again on ChemMatrix[®] resin, and with Ψ -Pro replacements at the above-mentioned positions. The synthesis with the Ile-Ser($\psi^{\text{Me,Me}}$ pro)-OH dipeptide replacement at positions 22-23 brought no improvement over previous runs; indeed, the main peak of the extremely poor crude (Figure 3c) could not be matched by LC-MS to the target 3587 Da mass. In contrast, replacement at positions 14-15 with Glu(OtBu)-Ser($\psi^{\text{Me,Me}}$ pro)-OH dipeptide resulted in a product with an HPLC profile (Figure 3d) significantly cleaner than any of the earlier attempts, and with the expected mass of 3587 Da for the main peak. Purification of this crude product by preparative HPLC, however, afforded a disappointingly low recovery of DEF5^a hexathiol precursor. Suspecting that the standard workup of the TFA cleavage solution, i.e., adding cold diethyl ether and centrifuging, was in this case inefficient, hence the peptide remained stuck to the resin, we resorted to a more thorough peptide isolation procedure, namely filtering-off the resin first (see Experimental section) and then treating the filtrate with chilled ether to induce peptide precipitation in the absence of resin. After centrifugation and drying, the amount of solid crude product was ca. 5 times higher than with the standard procedure. This improved isolation protocol was applied systematically henceforth (Figure 2). At this point it was clear that

Ψ -Pro replacement of the $^{14}\text{Glu}^{15}\text{Ser}$ dipeptide combined with ChemMatrix[®] resin usage had meant a significant difference in DEF5^a synthesis. To elucidate the specific contribution of the resin to the improved result, another DEF5^a synthetic run was done, this time using Rink-amide-MBHA resin, the Glu(OtBu)-Ser($\psi^{\text{Me,Me}}$ pro)-OH dipeptide at positions 14-15, and the optimized peptide isolation protocol described above. The crude product (Figure 3e) was slightly cleaner than in the first -also polystyrene-based- synthesis (Figure 3a), hence confirming the favorable effect of the ψ -Pro replacement, but nonetheless of poorer quality than when ψ -Pro and ChemMatrix[®] resin were simultaneously used, proving that only by combined usage of both modifications a substantial improvement was achieved. These advantages were again verified in the synthesis of the carboxyl (natural) sequence of DEF5, for which an aminomethyl ChemMatrix[®] resin was functionalized with the HMPP linker, loaded in manual mode with Fmoc-Arg(Pbf)-OH, then elongated as above in the synthesizer. The resulting crude (Figure 3f) was of comparable quality to the previous DEF5^a material.

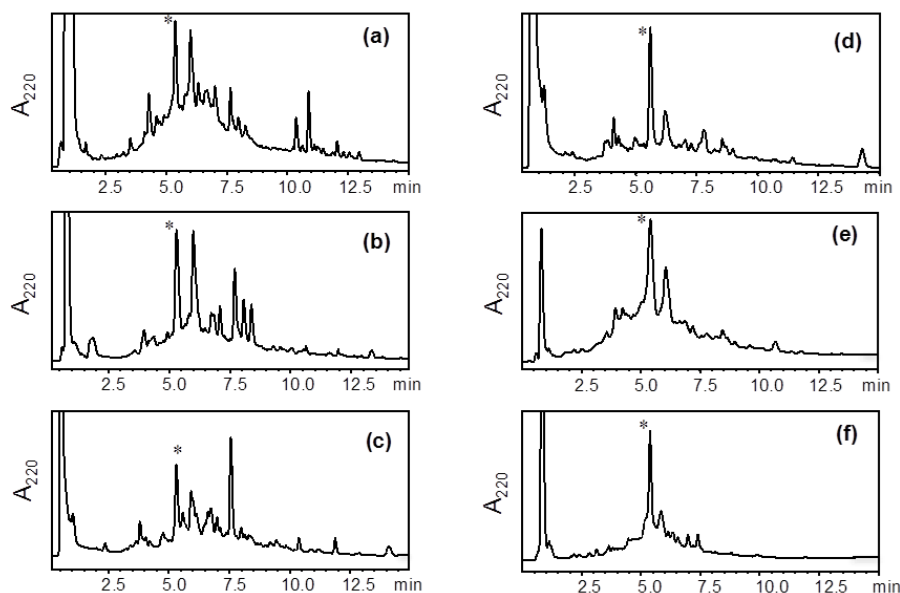


Figure 3. Optimization of DEF 5 synthesis; see workflow chart in Figure 2 for details. HPLC profiles of crude products (a) and (f) correspond to DEF5 syntheses; (b) to (e) to DEF5^a syntheses. In all instances, the asterisk-marked peak eluting at ca. 5.3 min corresponds to the hexathiol precursor of DEF5 or DEF5^a. Elution was with a linear 20 to 50% gradient of B into A over 15 min, at 1 mL/min flow rate; solvents A and B as described in the experimental.

For the final, oxidative folding step of DEF5 synthesis, an HPLC-purified hexathiol precursor was initially used. Disulfide formation in 0.1 M NH₄OAc buffer containing both reduced (GSH) and oxidized (GSSG) glutathione under N₂ atmosphere was complete after overnight reaction and led to a single folded product with the expected 3582 Da mass. Also, taking cue from the good results obtained by Wu et al. (2004) in the oxidation of the hexathiol precursor in unpurified form, we proceeded accordingly and confirmed that unpurified crude (Figure 4a) could be similarly converted to the oxidized/folded form using the above anaerobic conditions (Figure 4b). In this way, a typical synthesis run (0.1 mmol) required only a single HPLC purification step and led to highly homogeneous (>95%) folded product in amounts of ca. 15 mg. The correct folding (¹Cys⁶Cys, ²Cys⁴Cys, ³Cys⁵Cys) of our synthetic material was verified by comparison with an authentic (commercial) DEF5 sample by analytical HPLC, with both peptides found to coelute (Figure 4c).

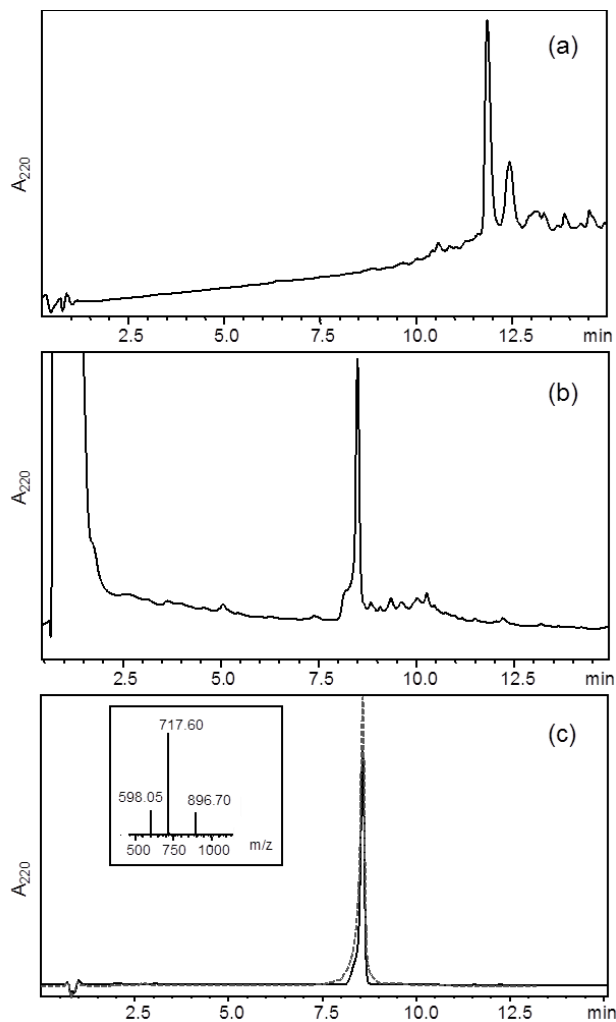


Figure 4. (a) Hexathiol precursor (run #7, Figure 2) is efficiently converted to native-folded DEF5 (b); for conditions see text. (c) HPLC-purified DEF5 (full line) coelutes with an authentic sample (broken line); inset: ESI-MS spectrum of DEF5: $[M+6H]^{6+}$ (m/z 598.05), $[M+5H]^{5+}$ (m/z 717.60) and $[M+4H]^{4+}$ (m/z 896.70) peaks are shown. In all cases, HPLC elution was with a linear 5 to 40% gradient of B into A over 15 min, at 1 mL/min flow rate; solvents A and B as described in the experimental.

B.2.1 Proteolytic Stability of both DEF5ox and DEF5red. Trypsin is a serine protease that preferentially cuts after cationic residues including Arg and Lys, and it is the processing enzyme for the DEF5 propeptide.²¹

It is accepted that the defensin disulfide array confers protease resistance, and DEF5ox (defensin 5 oxidated) is a very poor substrate for trypsin.²²

In contrast, treatment of DEF5red (defensin 5 reduced) with proteases such as trypsin results in rapid proteolytic cleavage.²³

Anyway to check this, the time course of trypsin digests of reduced and oxidized peptide was monitored by LC-MS. As expected, the DEF5red was totally degraded after 5 min digestion (data not shown). Instead, longer incubation times are required for complete proteolytic breakdown of the DEF5ox. In fact as expected the DEF5ox is quite impervious to proteolysis, with an appreciable decay only after six hours of incubation (80% degraded) and a totally digestion only after 18 hours.

In conclusion, the presence of three disulfide bonds decreases the accessibility of trypsin cleavage sites. Therefore, the complete disulfide array of native DEF5ox is essential for protease resistance.

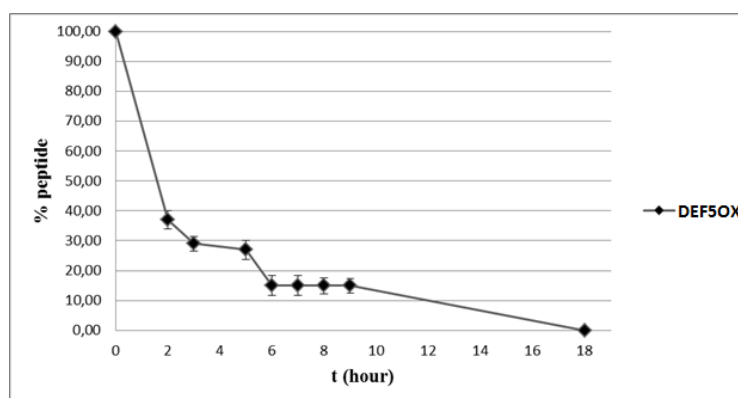


Figure 5. Stability of DEF5ox. The amount of peptide remaining after incubation for the indicated time was determined by LC-MS.

C.1 Conclusion

Results presented in this study illustrate how concomitant use of ChemMatrix[®] resin and ψ -Pro dipeptide replacement at the strategic ¹⁴Glu¹⁵Ser position transform the initially impractical production of DEF5 into a satisfactory stepwise Fmoc synthesis method. The two critical improvements in the sequence assembly process, complemented by optimized work-up after cleavage, enabled oxidative folding directly on the synthetic crude, avoiding

one intermediate purification step and thus making the global process quite efficient. This optimized synthesis paves the way to obtaining DEF5 and its analogues in sufficient quantities for structural and biological studies.

D.1 Experimental section

Chemicals

Fmoc-protected amino acids, HBTU and Fmoc-L-Arg(Pbf)-Wang resin were from Iris Biotech (Marktredwitz, Germany). Fmoc-Rink-amide ChemMatrix resin was from PCAS BioMatrix, Inc. (Saint-Jean-sur-Richelieu, Quebec, Canada). Fmoc-Rink-amide (MBHA) resin, Fmoc-Glu(OtBu)-Ser($\psi^{\text{Me,Me}}$ pro)-OH and Fmoc-Ile-Ser($\psi^{\text{Me,Me}}$ pro)-OH were from Novabiochem (Laüfelfingen, Switzerland). An authentic sample of DEF5 was purchased from Innovagen (Sweden). HPLC-grade CH₃CN and peptide synthesis-grade DMF, CH₂Cl₂, DIEA and TFA were from Carlo Erba-SdS (Sabadell, Spain). All other reagents were of the highest quality commercially available from Sigma-Aldrich (Madrid, Spain).

General peptide synthesis procedures

Peptides were assembled in an ABI433 peptide synthesizer (Applied Biosystems, Foster City, CA) running Fmoc (FastMoc) SPPS protocols at 0.1-mmol scale on either Fmoc-L-Arg(Pbf)-Wang resin, Fmoc-Rink-amide ChemMatrix resin, Fmoc-Rink-amide (MBHA) resin or aminomethyl ChemMatrix resin. Side chain functionalities were protected with tert-butyl (Glu, Ser, Thr, Tyr), N^G-2,2,4,6,7-pentamethyldihydrobenzofuran-5-sulfonyl (Arg), trityl (Cys) groups. Eight-fold excess of Fmoc-L-amino acids and HBTU, in the presence of a double molar amount of DIEA, were used for the coupling steps, with DMF as solvent. After chain assembly, full deprotection and cleavage were carried out with TFA/H₂O/EDT/TIS (94:2.5:2.5:1 v/v, 90 min, rt). Peptide isolation was initially done by the standard procedure in Fmoc chemistry, namely precipitation with cold diethyl ether and centrifugation. However, as this practice was shown to be inadequate for DEF5 (see Results and Discussion), the cleavage suspension was passed through a syringe fitted with a polyethylene porous disk to filter off the resin,

which was rinsed with an additional 1 mL of TFA; the filtrate was then poured onto cold diethyl ether to give a white precipitate that was collected by centrifugation, redissolved in 0.1M acetic acid and lyophilized.

Analysis and purification

Analytical reversed-phase HPLC was performed on C18 columns (4.6 × 50 mm, 3 μm, Phenomenex, Torrance, CA) in a model LC-2010A system (Shimadzu, Kyoto, Japan). Solvent A was 0.1% TFA in water; solvent B was 0.1% TFA in CH₃CN. Elution was done with linear 20–50% gradients of solvent B into A over 15 min at 1 mL/min flow rate, with UV detection at 220 nm for the linear peptide and with 5-40% linear gradient of B into A for oxidized peptide. LC-MS was performed in a LC-MS 2010EV instrument (Shimadzu) fitted with an XBridge column (4.6 × 150 mm, 3.5 μm, Waters, Cerdanyola del Vallès, Spain) eluted with a 20-50% linear gradient of B into A for the unfolded (reduced) peptide and with a 5-40% linear gradient of B into A for the oxidized peptide (A = 0.1% formic acid in water; B = 0.08% formic acid in acetonitrile) over 15 min at a flow rate of 1 mL/min, with UV detection at 220 nm. Preparative HPLC runs were performed on a Luna C18 column (21.2 mm × 250 mm, 10 μm; Phenomenex), using linear gradients of solvent B (0.1% in ACN) into A (0.1% TFA in water), as required, with a flow rate of 25 mL/min. Fractions of high (>95%) HPLC homogeneity and with the expected mass were combined, lyophilized, and used in subsequent experiments.

Oxidative Folding

The reduced (hexathiol) forms of DEF5 or DEF5^a were oxidized at 5 μM concentration in 0.1 M NH₄OAc, pH 7.8, 25 °C.¹⁵ The peptide, with or without previous HPLC purification (see Results and Discussion), was dissolved at the specified concentration in the above buffer containing both reduced (GSH) and oxidized (GSSG) glutathione to give a 1:100:10 peptide:GSH:GSSG ratio. The solution was then placed under inert (N₂) atmosphere and stirred overnight at 25°C. Progress of the folding reaction was monitored by analytical HPLC and, once completed, the target products were purified to homogeneity by preparative RP-HPLC and subsequently lyophilized. The

synthetic DEF5 thus folded and purified coeluted in analytical HPLC with an authentic DEF5 sample.

Proteolytic stability of DEF5

For proteolytic stability determination, peptides (1 mg/mL in 50 mM NH₄HCO₃) were incubated with trypsin (Promega) at 37°C in a 1:100 enzyme-peptide ratio. Incubation was terminated by acetic acid addition. The remaining amount of original peptide was determined by HPLC peak integration (elution conditions as above).

¹ Brandt, M.; Gammeltoft, S.; Jensen KJ. Microwave Heating for Solid-Phase Peptide Synthesis: General Evaluation and Application to 15-mer Phosphopeptides. *International Journal of Peptide Research and Therapeutics* **2006**, 12, 349-357.

² Vernieri, E.; Valle, J.; Andreu, D.; de la Torre, BG. An optimized Fmoc synthesis of human defensin 5. *Amino Acids* **2013** Dec 6. [Epub ahead of print]

³ Lehrer, RI.; Ganz, T.; Selsted, ME. Defensins: endogenous antibiotic peptides of animal cells. *Cell* **1991**, 64, 229-230.

⁴ Lehrer, RI.; Ganz, T. Defensins of vertebrate animals. *Curr Opin Immunol* **2002**, 14, 96-102.

⁵ Ganz, T.; Selsted, ME.; Szklarek, D.; Harwig, SS.; Daher, K.; Bainton, DF.; Lehrer, RI. Defensins. Natural peptide antibiotics of human neutrophils. *J Clin Invest* **1985**, 76, 1427-1435.

⁶ Ganz, T. Defensins: antimicrobial peptides of innate immunity. *Nat Rev Immunol* **2003**, 3, 710-720.

⁷ Schneider, JJ.; Unholzer, A.; Schaller, M.; Schäfer-Korting, M.; Korting, HC. Human defensins. *J Mol Med* **2005**, 83, 587-595.

⁸ Ghosh, D.; Porter, E.; Shen, B.; Lee, SK.; Wilk, D.; Drazba, J.; Yadav, SP.; Crabb, JW.; Ganz, T.; Bevins, CL. Paneth cell trypsin is the processing enzyme for human defensin-5. *Nat Immunol* **2002**, 3, 583-590.

⁹ Ishikawa, C.; Tanabe, H.; Maemoto, A.; Ito, T.; Watari, J.; Kono, T.; Fujiya, M.; Ashida, T.; Ayabe, T.; Kohgo, Y. Precursor processing of human defensin-5 is essential to the multiple functions in vitro and in vivo. *J Innate Immun* **2010**, 2, 66-76.

¹⁰ Shi, J. Defensins and Paneth cells in inflammatory bowel disease. *Inflamm Bowel Dis* **2007**, 13, 1284-1292.

¹¹ Wang, A.; Wang, S.; Shen, M.; Chen, F.; Zou, Z.; Ran, X.; Cheng, T.; Su, Y.; Wang, J. High level expression and purification of bioactive human alpha-

defensin 5 mature peptide in *Pichia pastoris*. *Applied Microbiology and Biotechnology* **2009**, 84, 877-884.

¹² Wanniarachchi, YA.; Kaczmarek, P.; Wan, A.; Nolan, EM. Human defensin 5 disulfide array mutants: disulfide bond deletion attenuates antibacterial activity against *Staphylococcus aureus*. *Biochemistry* **2011**, 50, 8005-8017.

¹³ Wommack, AJ.; Robson, SA.; Wanniarachchi, YA.; Wan, A.; Turner, CJ.; Wagner, G.; Nolan, EM. NMR solution structure and condition-dependent oligomerization of the antimicrobial peptide human defensin 5. *Biochemistry* **2012**, 51, 9624-9637.

¹⁴ Wu, Z.; Ericksen, B.; Tucker, K.; Lubkowski, J.; Lu, W. Synthesis and characterization of human α -defensins 4-6. *J Peptide Res* **2004**, 64, 118-125.

¹⁵ Vila-Perelló, M.; Sánchez-Vallet, A.; García-Olmedo, F.; Molina, A.; Andreu, D. Synthetic and structural studies on *Pyricularia pubera* thionin: a single-residue mutation enhances activity against Gram-negative bacteria. *FEBS Lett* **2003**, 536, 215-219.

¹⁶ Rodrigues, M.; Santos, A.; de la Torre, BG.; Rádis-Baptista, G.; Andreu, D.; Santos, NC. Molecular characterization of the interaction of crotamine-derived nucleolar targeting peptides with lipid membranes. *Biochim Biophys Acta* **2012**, 1818, 2707-2717.

¹⁷ De Leeuw, E.; Burks, SR.; Li, X.; Kao, JP.; Lu, W. Structure-dependent functional properties of human defensin 5. *FEBS Lett* **2007**, 581, 515-520.

¹⁸ García-Ramos, Y.; Paradís-Bas, M.; Tulla-Puche, J.; Albericio, F. ChemMatrix® for complex peptides and combinatorial chemistry. *J Pept Sci* **2010**, 16, 675-678.

¹⁹ Wöhr, T.; Wahl, F.; Nefzi, A.; Rohwedder, B.; Sato, T.; Sun, X.; Mutter, M. Pseudo-prolines as a solubilizing, structure-disrupting protection technique in peptide synthesis. *J Am Chem Soc* **1996**, 118, 9218-9227.

²⁰ Abedini, A.; Raleigh, DP. Incorporation of pseudoproline derivatives allows the facile synthesis of human IAPP, a highly amyloidogenic and aggregation-prone polypeptide. *Org Lett* **2005**, 7, 693-696.

²¹ Ghosh, D.; Porter, E.; Shen, B.; Lee, SK.; Wilk, D.; Drazba, J.; Yadav, SP.; Crabb, JW.; Ganz, T.; Bevins, CL. Paneth cell trypsin is the processing enzyme for human defensin-5. *Nat Immunol* **2002**, 3, 583-590.

²² Wanniarachchi, YA.; Kaczmarek, P.; Wan, A.; Nolan, EM. Human Defensin 5 Disulfide Array Mutants: Disulfide Bond Deletion Attenuates Antibacterial Activity against *Staphylococcus aureus*. *Biochemistry* **2011**, 50, 8005-8017.

²³ Rajabi, M.; de Leeuw, E.; Pazgier, M.; Li, J.; Lubkowski, J.; Lu, W. The conserved salt bridge in human α -defensin 5 is required for its precursor processing and proteolytic stability. *J Biol Chem* **2008**, 283, 21509-21518.